

# UNCLASSIFIED

AD NUMBER
ADB027772
NEW LIMITATION CHANGE
TO Approved for public release, distribution unlimited
FROM Distribution authorized to U.S. Gov't. agencies only; Test and Evaluation; Apr 1978. Other requests shall be referred to Space and Missile Systems Organization, Los Angeles, CA.
AUTHORITY
USAF notice, 17 Oct 1978

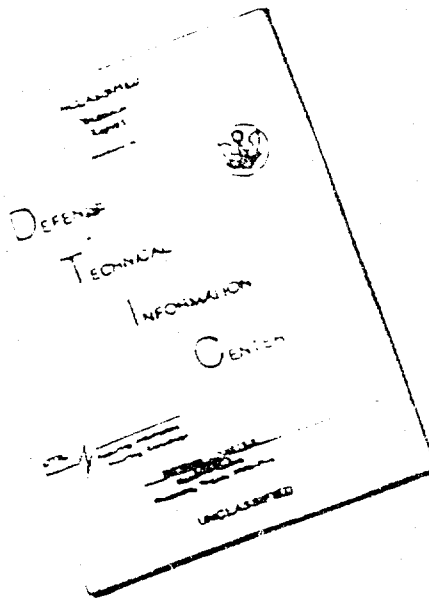
THIS PAGE IS UNCLASSIFIED

THIS REPORT HAS BEEN DELIMITED  
AND CLEARED FOR PUBLIC RELEASE  
UNDER DOD DIRECTIVE 5200.20 AND  
NO RESTRICTIONS ARE IMPOSED UPON  
ITS USE AND DISCLOSURE.

**DISTRIBUTION STATEMENT A**

APPROVED FOR PUBLIC RELEASE;  
DISTRIBUTION UNLIMITED.

# DISCLAIMER NOTICE



THIS DOCUMENT IS BEST  
QUALITY AVAILABLE. THE COPY  
FURNISHED TO DTIC CONTAINED  
A SIGNIFICANT NUMBER OF  
PAGES WHICH DO NOT  
REPRODUCE LEGIBLY.

REPRODUCED FROM  
BEST AVAILABLE COPY

FOR FURTHER TRAN

2

GUIDANCE/NAVIGATION REQUIREMENTS STUDY FINAL REPORT.

VOLUME III: APPENDICES,

Prepared by:

LOGICON, INC.  
255 West Fifth Street  
San Pedro, California 90731

April 1978

Final Report Under Contract F04701-75-C-0112

Period of Performance: May 1975 to April 1978

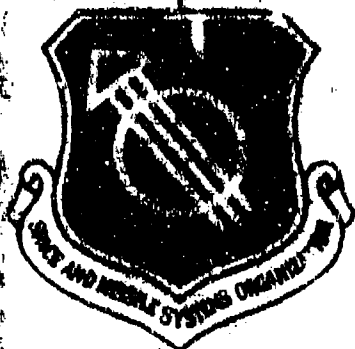
Prepared for:

Hq. Space and Missile Systems Organization  
Air Force Systems Command  
Los Angeles Air Force Station  
Post Office Box 92960, Worldway Postal Center  
Los Angeles, California 90009

Distribution limited to U.S. Government Agencies  
only: Test and Evaluation; April 1978. Other  
requests for this document must be referred to:  
Hq. SAMSO/RSP, Post Office Box 92960, Worldway  
Postal Center, Los Angeles, California 90009.

DDC  
RECEIVED  
JUN 15 1978  
E

Ch



AD No.


DDC FILE COPY


78 06 14 002

This final report was submitted by Logicon, Inc., San Pedro, California, under Contract Number F04701-75-C-0112 with Air Force Systems Command, Space and Missile Systems Organization, Deputy for Reentry Systems, Post Office Box 92980, Worldway Postal Center, Los Angeles, California 90009. The Air Force Project Officer was Major Jack T. Pearson, SAMS0/RSP.

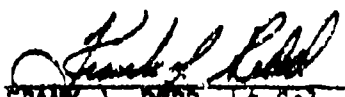
Distribution limited to U.S. Government Agencies only: Test and Evaluation; April 1978. Other requests for this document must be referred to: Hq. SAMS0/RSP, Post Office Box 92980, Worldway Postal Center, Los Angeles, California 90009.

This Technical Report has been reviewed and is approved for release and distribution in accordance with the above distribution statement.

  
JACK T. PEARSON, Major, USAF  
Project Officer  
Systems Plans & Analysis  
Deputy for Reentry Systems

  
FRANK J. REDD, Lt Col, USAF  
Director, System Plans & Analysis  
Deputy for Reentry Systems

FOR THE COMMANDER

  
FRANK J. REDD, Lt Col, USAF  
Director, Program Control  
Deputy for Reentry Systems

**UNCLASSIFIED**

SECURITY CLASSIFICATION OF THIS PAGE (When Data Entered)

REPORT DOCUMENTATION PAGE		READ INSTRUCTIONS BEFORE COMPLETING FORM
1. REPORT NUMBER SAMSQ-TR-78-92	2. GOVT ACCESSION NO.	3. RECIPIENT'S CATALOG NUMBER
4. TITLE (and Subtitle) Guidance/Navigation Requirements Study Final Report, Volume III, Appendices.		5. TYPE OF REPORT & PERIOD COVERED Final 15 May 1975 - 30 April 1978
7. AUTHOR(s) S. M. Archer, C. L. Bowman, E. F. Nicholson, D. D. Sworder, S. B. Vidor		6. PERFORMING ORG. REPORT NUMBER
9. PERFORMING ORGANIZATION NAME AND ADDRESS Logicon, Inc. 255 West Fifth Street San Pedro, California 90731		8. CONTRACT OR GRANT NUMBER(s) F04701-75-C-0112
11. CONTROLLING OFFICE NAME AND ADDRESS Space and Missile Systems Organization, AFSC Post Office Box 92960, Worldway Postal Center Los Angeles, California 90009		10. PROGRAM ELEMENT, PROJECT, TASK AREA & WORK UNIT NUMBERS
14. MONITORING AGENCY NAME & ADDRESS (if different from Controlling Office)		12. REPORT DATE 30 April 1978
		13. NUMBER OF PAGES 250
		15. SECURITY CLASS. (of this report) Unclassified
		16. DECLASSIFICATION/DOWNGRADING SCHEDULE
16. DISTRIBUTION STATEMENT (of this Report) Distribution limited to U. S. Government Agencies only: Test and Evaluation. Other requests for this document must be referred to: Hq. SAMSQ/RSP. APR 1978		
17. DISTRIBUTION STATEMENT (of the abstract entered in Block 20, if different from Report) DDC RECEIVED JUN 15 1978 NY E		
18. SUPPLEMENTARY NOTES		
19. KEY WORDS (Continue on reverse side if necessary and identify by block number) Maneuvering Reentry Vehicle      Guidance      Inflight Calibration Inertial Measurement Unit      Navigation      Deployment Measurements Inertial Navigation System      Modeling      Booster Communication Strapped Down      Accuracy      Trajectory Design Fully Gimballed      Flight Test		
20. ABSTRACT (Continue on reverse side if necessary and identify by block number) This volume of the Guidance/Navigation Requirements Study Final Report contains appendices that describe the analytical techniques employed to estimate the performance of maneuvering reentry vehicle guidance and navigation systems. The seven appendices describe linear error analysis, instrument modeling, system error determination, performance of advanced guidance concepts, test flight trajectory design and freeflight filtering schemes.		

DD FORM 1473 JAN 73 EDITION OF 1 NOV 68 IS OBSOLETE

**UNCLASSIFIED**

SECURITY CLASSIFICATION OF THIS PAGE (When Data Entered)

78 06 14 002

# LOGICON

## FOREWORD

This is the final report on the Guidance/Navigation Requirements Study (G/NRS), which was performed for SAMSO, Air Force Systems Command, USAF, under contract F04701-75-C-0112 by Logicon, Inc. The study was initiated in May of 1975 and completed in April of 1978.

General G/NRS objectives were twofold:

- 1) To develop and maintain performance models for both flight test and operational versions of an Air Force Maneuvering Reentry Vehicle.
- 2) To use these models to assist the Air Force in establishing G/N subsystem requirements and options for a flight test vehicle and investigate the performance of an operational MaRV.

This report is segmented into three volumes. Volume I presents an overview of the reentry system performance analysis problem and summarizes the results of the entire effort. Volume II corroborates the summary presented in Volume I with documentation of the detailed analysis performed during the course of the study. Volume III contains appendices which describe in detail the salient analysis techniques employed during the study.

Logicon wishes to acknowledge valuable technical assistance provided by the principal Air Force and Aerospace participants: Major J. T. Pearson and Capt. J. A. Davis and Messrs. P. Kruh and H. E. Whiteside and Dr. P. O. Rogers. The authors of Volume III are Messrs. S. M. Archer, and E. F. Nicholson, and Drs. C. L. Bowman, D. D. Sworder, and S. B. Vidor. Programming support was provided by Dr. F. A. Rohatsch.

ACCESSION for	
NTIS	White Section <input type="checkbox"/>
DIC	Buff Section <input checked="" type="checkbox"/>
UNANNOUNCED	<input type="checkbox"/>
JUSTIFICATION	
BY	
DISTRIBUTION AVAILABILITY CODES	
DATE AVAIL. and or SPECIAL	
<b>B</b>	

*Eugene F. Nicholson*  
Eugene F. Nicholson  
Project Manager  
Logicon Inc.

TABLE OF CONTENTS :

Appendix (A) - IMU Performance Modeling and Evaluation	A-1
A-1. Navigated State Errors	A-1
A-2. Acceleration Measurement Errors	A-3
A-2.1 Accelerometer Errors	A-3
A-2.2 Gyro Errors	A-5
A-2.3 Structural Compliance	A-8
A-3. Statistical Processing	A-9
Appendix B - Calibration and Alignment Performance Evaluation	
Techniques	B-1
B-1. Introduction	B-1
B-2. SHIP Alignment	B-6
B-3. Dual P5 Calibration	B-7
Appendix C - System Performance Evaluation	C-1
C-1. Introduction	C-1
C-2. Error Propagation	C-1
C-3. Inflight Alignment	C-19
C-4. Reentry Initialization	C-21
C-5. Incorrect System Modeling	C-22
C-6. Computer Program Organization	C-24
C-7. Suboptimal Filter Equations	C-26
Appendix C References	C-38
Appendix D - Linear Regulator Guidance	D-1
D-1. Controllers in the Time Domain	D-2
D-1.1 Time Domain System Description	D-2
D-1.1.1 Trajectory Equations	D-2
D-1.1.2 Approximate Trajectory Model	D-4
D-1.2 Time Domain Controller Definition	D-7
D-1.3 Selection of Weighting Matrices	D-10
D-1.4 An Example	D-21
D-1.5 Summary	D-26
D-2. State Variable as Variable of Evolution	D-29
D-2.1 System Equations	D-30
D-2.2 Vehicle Dynamics in the Perceived Reference Frame	D-33
D-2.3 Quadratic Regulators	D-38
D-2.4 Changes in the Independent Variable	D-41
D-2.5 Introductory Examples	D-44
D-2.6 Selection of the Independent Variable	D-57
D-2.7 An Example	D-69
D-2.8 Conclusion	D-81
D-3. Selection of the Independent Guidance Variable Through a State Dependent Rotation	D-83
D-3.1 Problem Description	D-83
D-3.2 A Locally Best Coordinate System	D-85
Appendix D References	D-97

## TABLE OF CONTENTS

Appendix E - Additional Steering Law Topics . . . . .	E-1
E-1. Influence of Autopilot States on System Performance . . . . .	E-1.
E-1.1 Introduction . . . . .	E-1
E-1.2 Model Reduction . . . . .	E-2
E-1.3 Conclusions . . . . .	E-13
E-2. Influence of Sensor Failures on LQG Regulators . . . . .	E-15
E-2.1 Introduction . . . . .	E-15
E-2.2 Problem Description . . . . .	E-16
E-2.3 Solution Algorithm . . . . .	E-18
E-2.4 Properties of the Optimal Regulator . . . . .	E-20
E-2.5 Conclusion . . . . .	E-21
E-2.6 Proof of Equation E-51 . . . . .	E-22
Appendix E References . . . . .	E-25
Appendix F - Flight Test Trajectory Design by Simplicial Pivoting . . . . .	F-1
F-1. Introduction . . . . .	F-1
F-2. Operational System Description . . . . .	F-3
F-2.1 SHIP Error Model . . . . .	F-3
F-2.2 DINS Error Model . . . . .	F-7
F-2.3 Candidate Operational Trajectory . . . . .	F10
F-3. Identification of Principal Performance Contributors . . . . .	F-12
F-3.1 SHIP Principal Performance Contributors . . . . .	F-14
F-3.2 DINS Principal Performance Contributors . . . . .	F-14
F-4. Flight Test Reentry Trajectory Design . . . . .	F-18
F-4.1 Flight Test System . . . . .	F-18
F-4.2 The Identification Problem . . . . .	F-20
F-4.2.1 Observability of SHIP Error Sources . . . . .	F-20
F-4.2.2 Observability of DINS Error Sources . . . . .	F-22
F-4.3 Input Design Techniques . . . . .	F-24
F-4.4 Trajectory Performance Criterion . . . . .	F-25
F-4.5 The Trajectory Design Problem . . . . .	F-26
F-5. The Simplicial Pivoting Algorithm . . . . .	F-29
F-5.1 Selection of an Optimization Algorithm . . . . .	F-29
F-5.1.1 The Two Classes of Algorithms . . . . .	F-29
F-5.1.2 Trajectory Design Problem Characteristics . . . . .	F-30
F-5.1.3 Direct-Search Algorithms . . . . .	F-31
F-5.1.4 A Comparison of Direct-Search Algorithms . . . . .	F-36
F-5.2 The Simplicial Pivoting Algorithm . . . . .	F-38
F-6. RIMU Parameter Estimation Performance . . . . .	F-40
F-6.1 SHIP Parameter Estimation Performance . . . . .	F-40
F-6.1.1 SHIP Trajectory Design Results . . . . .	F-41
F-6.1.2 SHIP Parameter Estimation Results . . . . .	F-46

## TABLE OF CONTENTS

F-6.2	DINS Parameter Estimation Performance . . . . .	F-48
F-6.2.1	DINS Trajectory Design Results . . . . .	F-48
F-6.2.2	DINS Parameter Estimation Results . . . . .	F-48
F-7.	Summary . . . . .	F-52
Appendix F	References . . . . .	F-53
Appendix G	Free-Flight Filtering . . . . .	G-1
G-1.	Measurement Equations . . . . .	G-1
G-2.	Body Dynamics . . . . .	G-5
G-3.	Computer Organization . . . . .	G-10
DISTRIBUTION LIST	. . . . .	G-12

## APPENDIX A.

## IMU PERFORMANCE MODELING AND EVALUATION

A mathematical description of the errors inherent in utilizing a sensor capable of measuring the non-gravitational acceleration in a navigation system is described in this appendix. The discussion is divided into three segments. The first pertains to the errors in the navigated state produced by a general acceleration measurement error. The second segment discusses the sources of the error in the measured acceleration. The third segment addresses statistical processing of the calculated navigation error to obtain deployment errors, target miss, etc.

A-1. NAVIGATED STATE ERRORS

A linear analysis of the navigation errors associated with inaccurate acceleration measurement considers the following differential equation involving the navigated state:

$$\frac{d^2 \bar{r}}{dt^2} = \ddot{\bar{r}} = \bar{g}(\bar{r}) + \bar{a} \quad (A-1)$$

where

$\bar{a}$  is the acceleration sensed by the navigation system

$\bar{g}(\bar{r})$  is the gravitational acceleration

$\bar{r}$  is the position component of the navigated state.

To obtain an equation relating small errors in the acceleration terms to position errors, let

$$\begin{aligned} \bar{g}(\bar{r}) &= \bar{g}_N(\bar{r}) + \delta \bar{g}(\bar{r}) \\ \bar{r} &= \bar{r}_N + \delta \bar{r} \\ \bar{a} &= \bar{a}_N + \delta \bar{a} \end{aligned} \quad (A-2)$$

where

$$\left. \begin{array}{l} \bar{r}_N, \\ \bar{a}_N, \\ \bar{g}_N(\bar{r}) \end{array} \right\} \text{ are the nominal position and acceleration (measured} \\ \text{and gravitational) along the phase space profile}$$

$$\left. \begin{array}{l} \delta \bar{r}, \\ \delta \bar{a}, \\ \delta \bar{g}(\bar{r}) \end{array} \right\} \text{ are perturbations in position and acceleration.}$$

Substituting (A-2) into (A-1), expanding and rearranging:

$$\left( \ddot{\bar{r}}_N - \bar{g}_N(\bar{r}) - \bar{a}_N \right) + \delta \ddot{\bar{r}} - \delta \bar{r} \cdot \nabla \delta \bar{g}(\bar{r}) = \delta \bar{g}(\bar{r}) + \delta \bar{a} \quad (\text{A-3})$$

Products of perturbations have been ignored. Note that the parenthetical term in Equation A-3 is the differential equation describing the profile, and is therefore zero.

Considering a spherical earth gravitation field for the  $\bar{g}(r)$  term, Equation A-3 becomes

$$\delta \ddot{\bar{r}} + \frac{GM}{|\bar{r}|^3} \left( \delta \bar{r} - \frac{3 \bar{r}_N \cdot \delta \bar{r}}{|\bar{r}_N|^2} \bar{r}_N \right) = \delta \bar{a} + \delta \bar{g}(\bar{r}) \quad (\text{A-4})$$

This differential equation which relates the error in the navigated position to errors in the measured and gravitational acceleration can be numerically solved to obtain the navigation system errors.

The forcing functions ( $\delta \bar{a}$  and  $\delta \bar{g}(\bar{r})$ ) represent the errors inherent in the measurement of the inflight acceleration and the computation of the gravitational acceleration.

The Solution to Equation A-4 yields the position error associated with an acceleration measurement error. If the velocity error is also desired, two first-order equations can be formulated

## LOGICON

from Equation A-4 by the substitution  $\delta \bar{v} = \dot{\delta \bar{r}}$ . The two resulting equations can be solved and  $\delta \bar{v}$  and  $\delta \bar{r}$  determined.

### A-2. ACCELERATION MEASUREMENT ERRORS

The errors in the acceleration measured by the navigation sensing unit are discussed in this section. The section is segmented into three segments, each of which describes a different source of the acceleration measurement error. The first segment discusses the measurement errors associated with the accelerometers, which measure the non-gravitational acceleration along their sensitive axis. The second segment formulates the effect that gyro errors have on determining the orientation of the accelerometer sensitive axes relative to a known computational frame. The third segment demonstrates some of the effects structural compliance has on the transformation of the measured acceleration in accelerometer coordinates to navigation computation coordinates.

#### A-2.1 ACCELEROMETER ERRORS

The errors inherent in the actual measurement of the non-gravitational acceleration are modeled as an acceleration error along each of the accelerometer sensitive axes. This error is then transformed into computational coordinates utilizing the accelerometer to navigation frame transformation which describes the geometry and orientation of the accelerometer cluster. This transformed error can then be handled as described in Section A-1.

The equation performing the above is

$$\delta \bar{a}_N = \delta a_1 [ATN] \begin{pmatrix} \delta_{11} \\ \delta_{21} \\ \delta_{31} \end{pmatrix}$$

where

$\delta \bar{a}_N$  = acceleration error in navigation coordinates

## LOGICON

---

$[ATN]$  = accelerometer to navigation transformation (may be time-varying)

$\delta a_i$  = magnitude of the acceleration error for the  $i$ th accelerometer

$\delta_{ij}$  = Kronecker delta function

The acceleration error magnitude may be from several sources including bias errors, scale factor errors, misalignments and quantization.

For example, if a particular orthogonal accelerometer cluster was inertially held and the accelerometer errors were modeled as bias and scale factor errors, the modeling equations would be:

$$\delta \bar{a}_{N_1} = [ATN] \begin{pmatrix} b_x \\ 0 \\ 0 \end{pmatrix}$$

$$\delta \bar{a}_{N_2} = [ATN] \begin{pmatrix} 0 \\ b_y \\ 0 \end{pmatrix}$$

$$\delta \bar{a}_{N_3} = [ATN] \begin{pmatrix} 0 \\ 0 \\ b_z \end{pmatrix}$$

$$\delta \bar{a}_{N_4} = S_x [ATN] \begin{pmatrix} a_x \\ 0 \\ 0 \end{pmatrix}$$

$$\delta \bar{a}_{N_5} = S_y [ATN] \begin{pmatrix} 0 \\ a_y \\ 0 \end{pmatrix}$$

$$\delta \bar{a}_{N_6} = S_z [ATN] \begin{pmatrix} 0 \\ 0 \\ a_z \end{pmatrix}$$

## LOGICON

where

$b_x, b_y, b_z$  are the bias errors

$S_x, S_y, S_z$  are the scale factor errors

$a_x, a_y, a_z$  are the acceleration components along the accelerometer sensitive axis of the x, y, and z accelerometers

$\delta \bar{a}_{N_i}$  is the  $i$ th error in navigation acceleration.

Each  $\delta \bar{a}_{N_i}$  is treated separately (i.e., a  $\delta \bar{r}_N$  and  $\delta \bar{v}_N$  integrated for each of the six errors) to determine the miss associated with each error source.

### A-2.2 GYRO ERRORS

The error caused by the gyros in the transformation of the acceleration measured by the accelerometer cluster into the navigation frame is discussed in this section. The errors arise due to the drift of the gyro stabilized reference frame, which may either be an actual inertially-stable structure or a computational reference derived from rate (or angle increment) measurements by the gyros. In either case, the acceleration error can be calculated from an accumulated misalignment caused by gyro drift.

The acceleration error associated with gyro drift is represented by:

$$\delta \bar{a}_N = [\phi][ATN] \bar{a}_A - \bar{a}_N$$

where

$[\phi]$  is the gyro derived misalignment matrix

$\bar{a}_A$  is the acceleration measured in accelerometer coordinates

$\bar{a}_N$  is the acceleration computed in navigation coordinates

## LOGICON

The gyro-derived misalignment is the first integral of the gyro drift rate, which is expressed as:

$$\delta\bar{\omega}_N = [GTN] \delta\bar{\omega}_G$$

where

$[GTN]$  is the gyro-to-navigation transformation (either a constant or an integral of the gyro rate)

$\delta\bar{\omega}_G$  is the error in the rate about the gyro input axes

The derivative of  $[\phi]$  is

$$[\dot{\phi}] = [\delta\omega_N] [\phi]$$

where

$$[\delta\omega_N] \text{ is the cross product matrix } \begin{bmatrix} 0 & -\delta\omega_{Nz} & \delta\omega_{Ny} \\ \delta\omega_{Nz} & 0 & -\delta\omega_{Nx} \\ -\delta\omega_{Ny} & \delta\omega_{Nx} & 0 \end{bmatrix}$$

Note that if, initially,  $[\phi(0)] = [I]$ , then

$$[\phi(t)] \text{ is of the form } [I] + [f(\delta\bar{\omega}_N)]$$

where  $[f(\delta\bar{\omega}_N)]$  represents the contribution of the  $\delta\bar{\omega}_N$  to  $[\phi]$  at time  $t$ . However, if products of terms involving  $\delta\bar{\omega}_N$  are ignored

$$[\dot{\phi}] = [\delta\omega_N] ([I] + [f(\delta\bar{\omega}_N)])$$

$$[\dot{\phi}] = [\delta\omega_N] + [0]$$

and

$$[\phi(t)] = \int_0^t [\delta\omega_N(\tau)] d\tau + [\phi(0)]$$

## LOGICON

Thus, the misalignment of the accelerometer-to-navigation transformation can be computed from the drift rate errors associated with the gyros.

For example, consider a constant fixed drift error of an orthogonal triad of initially-stable single degree-of-freedom gyros coincident with the navigation coordinate frame. In this case

$$\dot{\phi}_i = D_i$$

where

$\dot{\phi}_i$  = the drift rate of the  $i$ th gyro

$D_i$  = the fixed drift coefficient of the  $i$ th gyro

Therefore,

$$\delta \bar{\omega}_{N1} = \begin{pmatrix} \dot{\phi}_x \\ 0 \\ 0 \end{pmatrix} = \begin{pmatrix} D_x \\ 0 \\ 0 \end{pmatrix}$$

$$\delta \bar{\omega}_{N2} = \begin{pmatrix} 0 \\ \dot{\phi}_y \\ 0 \end{pmatrix} = \begin{pmatrix} 0 \\ D_y \\ 0 \end{pmatrix}$$

$$\delta \bar{\omega}_{N3} = \begin{pmatrix} 0 \\ 0 \\ \dot{\phi}_z \end{pmatrix} = \begin{pmatrix} 0 \\ 0 \\ D_z \end{pmatrix}$$

and

$$[\phi_1] = \begin{bmatrix} 1 & 0 & 0 \\ 0 & 1 & -D_x t \\ 0 & D_x t & 1 \end{bmatrix}$$

$$[\phi_2] = \begin{bmatrix} 1 & 0 & D_y t \\ 0 & 1 & 0 \\ -D_y t & 0 & 1 \end{bmatrix}$$

$$[\phi_3] = \begin{bmatrix} 1 & -D_z t & 0 \\ D_z t & 1 & 0 \\ 0 & 0 & 1 \end{bmatrix}$$

Finally,

$$\delta \bar{a}_1 = \begin{pmatrix} 0 \\ -a_z \\ a_y \end{pmatrix} D_x t$$

$$\delta \bar{a}_2 = \begin{pmatrix} a_z \\ 0 \\ -a_x \end{pmatrix} D_y t$$

$$\delta \bar{a}_3 = \begin{pmatrix} -a_y \\ a_x \\ 0 \end{pmatrix} D_z t$$

### A-2.3 STRUCTURAL COMPLIANCE

This discussion of the structural compliance is not detailed or involved. Basically, only the effect of the compliance of the accelerometer relative to the navigation frame is considered. It is recognized that this is only one compliance out of many which exist but the ideas presented regarding the treatment of accelerometer bending can be applied to other bending modes as well.

Essentially, all structural compliance of the mounting frame of the platform results in the accelerometer sensitive axes oriented in an unknown direction. The misalignment can be considered small and modeled as follows

$$\delta a_i = C_{ijk} a_j a_k$$

## LOGICON

where

$\delta a_i$  is the error of the  $i$ th accelerometer measurement due to structural compliance

$C_{ijk}$  is the coefficient of bending of the  $i$ th accelerometer sensitive axis toward the  $j$ th direction by acceleration along the  $k$ th direction

$a_j, a_k$  acceleration components.

Depending upon the test data available,  $a_j$  and  $a_k$  above may be platform accelerations or accelerometer accelerations. The acceleration error  $\delta a_i$  is treated in exactly the same way as in Section A-2.1.

### A-3. STATISTICAL PROCESSING

The processing of the position and velocity errors calculated in Section A-1 is discussed in this section. Included will be the propagation of the integrated position and velocity errors into CEP.

The position and velocity errors determined as described in Section A-1 for each of the error sources types discussed in Section A-2 represent a  $6 \times N$  matrix (where  $N$  represents the number of error terms). This matrix will be denoted  $\frac{\partial S}{\partial E_S}$ , as it reflects the sensitivity of state (position and velocity) to unit error source magnitudes, i.e.,

$$\frac{\partial S}{\partial E_S} = \begin{bmatrix} \delta \bar{R}_1 & \delta \bar{R}_2 & \cdots & \delta \bar{R}_N \\ \delta \bar{V}_1 & \delta \bar{V}_2 & \cdots & \delta \bar{V}_N \end{bmatrix}$$

where

$\left. \begin{matrix} \delta \bar{R}_i \\ \delta \bar{V}_i \end{matrix} \right\}$  are the position and velocity errors associated with the  $i$ th error

It is important to note that as a direct result of the linearization of the error equations presented in Section A-1,  $\frac{\partial S}{\partial E_S}$  is linear. That is,

## LOGICON

if a particular error coefficient doubles, the state error associated with that error also doubles. Thus  $\frac{\partial S}{\partial E_S}$  is a linear mapping of error sources into state errors; i.e.,

$$\delta S = \frac{\partial S}{\partial E_S} \delta E_S$$

The differential equation stated in Section A-1 can be solved along any nominal path to produce a  $\frac{\partial S}{\partial E_S}$  at any point along the trajectory. Given this sensitivity, the miss associated with that trajectory point can be calculated from the above equation for  $\delta S$ . For example the covariance of  $\delta S$  is

$$\Lambda_S = E(\delta S \delta S^T) = \frac{\partial S}{\partial E_S} E(\delta E_S \delta E_S^T) \frac{\partial S^T}{\partial E_S}$$

$$\Lambda_S = \frac{\partial S}{\partial E_S} \Lambda_{E_S} \frac{\partial S^T}{\partial E_S}$$

where

$\Lambda_a$  represents covariance of a

$E( )$  represents expectation

Given the covariance of the state errors, statistical quantities such as CEP can be calculated.

For example, if the CEP is desired,  $\frac{\partial S}{\partial E_S}$  must be calculated from navigation initiation to impact. The covariance of the state error is now determined from the covariance of the error sources. The state covariance can now be mapped into a downrange, crossrange time coordinate frame by an orthogonal rotation followed by a projection of the altitude errors along the nominal impact velocity. viz:

# LOGICON

$$\frac{\partial I}{\partial S} = \left[ \begin{array}{ccc|c} 1 & 0 & -\frac{V_D}{V_H} & \\ 0 & 1 & -\frac{V_C}{V_H} & \\ 0 & 0 & \frac{1}{V_H} & \end{array} \right]_{0_3 \times 3} \left[ \begin{array}{c} T \\ 0 \\ 0 \end{array} \right]$$

$$\Lambda_I = \frac{\partial I}{\partial S} \Lambda_S \frac{\partial I}{\partial S}^T$$

where

$\frac{\partial I}{\partial S}$  is the mapping of state errors into impact coordinates (downrange, crossrange, and time)

$V_D, V_C, V_H$  are the nominal velocity components along downrange, crossrange and altitude

$T$  is the orthogonal  $3 \times 3$  rotation of navigation coordinates into downrange, crossrange and altitude.

The CEP can be approximately calculated as

$$CEP = 0.59 \left( \sqrt{\Lambda_{I11}} + \sqrt{\Lambda_{I22}} \right)$$

where

$\Lambda_{Iij}$  is the element of  $\Lambda_I$  in the  $i$ th row of the  $j$ th column.

APPENDIX B  
CALIBRATION AND ALIGNMENT PERFORMANCE  
EVALUATION TECHNIQUES

B-1. INTRODUCTION

The analytic technique that estimates the accuracy of calibration and alignment is described in this appendix. Basically, the lower bound accuracy of a calibration scheme is estimated with optimal Kalman filtering techniques. The deviation of the actual performance of the calibration technique from the optimal Kalman performance is assumed small. This assumption is made because if the optimal technique is substantially more accurate, it is assumed that it, or a sufficiently accurate suboptimal mechanization, would be implemented. With this simplification, the analysis of many calibration techniques can be case in a similar form and quickly performed.

To utilize the Kalman filtering techniques in the analysis of a calibration scheme, the physical process must be described with a linear state space model. Thus the dynamics of the errors must be described by a linear differential equation, and the measurements taken during the calibration sequence must be linearly related to the errors. These two requirements can be written in the form:

$$\dot{x} = Fx + Gw \quad (B-1).$$

$$z = Hx + v \quad (B-2)$$

where

$x$  is the state vector describing the hardware errors  
 $F, G, H$  are model description matrices  
 $v, w$  are random (white noise) disturbances.

The model description matrices ( $F, G$ , and  $H$ ) are generally complicated functions of the orientation of the instrument being calibrated and the

## LOGICON

time derivation of the measurement. However, these matrices can be computed numerically with little difficulty.

Equations B-1 and B-2 describe the system dynamics but do not directly determine the calibration error. However, Kalman filtering can make use of the same model description matrices to perform a covariance analysis of the calibration sequence.

Kalman filtering descriptions are found in many books (see for example, Gelb or Meditch) and it will not be discussed here in any more detail than to write down the discrete covariance equations; viz:

$$\text{Time propagation: } p^k(-) = \phi p^{k-1}(+) \phi^T + Q \quad (B-3)$$

$$\text{Measurement: } p^k(+) = (I - KH)p^k(-) \quad (B-4)$$

where

K is the Kalman gain

$$K = p^k(-)H^T(HP^k(-)H^T + R)^{-1}$$

$\phi$  is the state transition matrix from the  $k-1^{\text{th}}$  measurement to the  $k^{\text{th}}$

$p^k(-)$  is the state covariance prior to the  $k^{\text{th}}$  measurement

$p^k(+)$  is the state covariance after the  $k^{\text{th}}$  measurement

H is the observation sensitivity matrix

R is the observation noise covariance

Q is the system process noise matrix

Equations B-3 and B-4 calculate the covariance of the best estimate of the state errors after each measurement.

The analysis of a calibration sequence is threefold. First, the errors of the hardware (gyro drifts, accelerometer biases, structural

## LOGICON

compliances, gimbal readout errors, etc.) must be identified and error models defined (see Appendix A). This describes the hardware mathematically. In addition to identifying the hardware errors, the initial uncertainties in the model coefficients must also be estimated. These can come from hardware tolerance specifications, previous calibrations or engineering estimates. Finally, the observation sensitivity matrix,  $H$ , the state transition matrix,  $\phi$ , and the system process noise matrix,  $Q$ , can be calculated for the error models defined and the calibration sequence desired. The state covariance matrix can then be calculated for the measurement sequence of the calibration and alignment technique under investigation.

For example, consider the calibration of one accelerometer whose errors are an exponentially correlated bias noise, a bias and a scale factor error. The error equation for the accelerometer would be:

$$\delta a = n + b + sa$$

where

- $\delta a$  is the acceleration error
- $n$  is a time correlated bias
- $b$  is the bias
- $s$  is the scale factor error
- $a$  is the sensitive axis acceleration

Assume also that the initial noise, bias and scale factor uncertainties are  $\sigma_n$ ,  $\sigma_b$  and  $\sigma_s$ , respectively, the available measurement is velocity, and the calibration sequence is the usual up-down accelerometer calibration. For the above system the state variables are:

$$X = \begin{bmatrix} v \\ n \\ s \\ b \end{bmatrix}$$

The initial covariance is therefore

# LOGICON

$$P^0(-) = \begin{bmatrix} 0 & 0 & 0 & 0 \\ 0 & \sigma_n^2 & 0 & 0 \\ 0 & 0 & \sigma_b^2 & 0 \\ 0 & 0 & 0 & \sigma_s^2 \end{bmatrix}$$

The state transition matrix can be calculated from the system differential equation; viz:

$$\dot{X} = FX$$

where

$$F = \begin{bmatrix} 0 & 1 & 1 & a \\ 0 & -1/\tau & 0 & 0 \\ 0 & 0 & 0 & 0 \\ 0 & 0 & 0 & 0 \end{bmatrix}$$

which yields

$$\phi(t,a) = e^{Ft} = \begin{bmatrix} 1 & \tau(1-e^{-t/\tau}) & t & at \\ 0 & e^{-t/\tau} & 0 & 0 \\ 0 & 0 & 1 & 0 \\ 0 & 0 & 0 & 1 \end{bmatrix}$$

The observation sensitivity matrix is

$$H = (1, 0, 0, 0)$$

The measurement noise is

$$R = \sigma_v^2$$

where  $\sigma_v$  is the quantization error of the accelerometer. Finally, the process noise is

$$Q(t) = \int_0^t \phi(t') q \phi^T(t') dt'$$

where

$$q = \begin{bmatrix} 0 & 0 & 0 & 0 \\ 0 & q_n^2 & 0 & 0 \\ 0 & 0 & 0 & 0 \\ 0 & 0 & 0 & 0 \end{bmatrix}$$

which yields

$$Q(t) = \begin{bmatrix} Q_{11} & Q_{12} & 0 & 0 \\ Q_{12} & Q_{22} & 0 & 0 \\ 0 & 0 & 0 & 0 \\ 0 & 0 & 0 & 0 \end{bmatrix}$$

where

$$Q_{11} = q_n^2 \tau^2 \left[ t - 2\tau(1 - e^{-t/\tau}) + \frac{\tau}{2} (1 - e^{-2t/\tau}) \right]$$

$$Q_{12} = q_n^2 \tau^2 \left[ 1 - e^{-t/\tau} - \frac{1}{2} (1 - e^{-2t/\tau}) \right]$$

$$Q_{22} = q_n^2 \frac{\tau}{2} (1 - e^{-2t/\tau})$$

The measurement sequence can be analyzed as follows. First, measure the velocity integrated by the accelerometer after T seconds in the up position. The initial covariance must then be propagated T seconds as:

$$P^1(-) = \phi(T, g) P(-) \phi^T(T, g) + Q(T)$$

The measurement yields an updated state covariance; viz:

$$P^1(+) = \left[ I - P^1(-) H^T (H P^1(-) H^T + R)^{-1} H \right] P^1(-)$$

## LOGICON

The second measurement may be performed in a similar fashion; viz:

$$P^2(-) = \phi(T, -g) P(-) \phi^T(T, -g) + Q(T)$$

$$P^2(+) = [I - P^2(-)H^T(HP^2(-)H^T + R)^{-1}H] P^2(-)$$

and the resulting covariance  $P^2(+)$  yields the statistical information of the calibration procedure.

### B-2. SHIP ALIGNMENT

The analysis of the alignment of the SHIP followed the general procedures outlined in Section B-1. The hardware was modeled with the 87 errors described in the SHIP inflight error analysis. The resulting model description matrices were:

$$\left. \begin{array}{l} F = 0 \\ G = 0 \end{array} \right\} \text{no time dependence}$$

$R$  = measurement noise matrix

$$H = \begin{cases} \left[ \frac{\partial \bar{V}}{\partial E_S} \right]_{3 \times 87} & \text{for Singer Two-Step} \\ \left[ \frac{\partial \dot{\phi}}{\partial E_S} \right]_{1 \times 87} & \text{for gyro compassing} \end{cases}$$

where

$\frac{\partial \bar{V}}{\partial E_S}$  are the sensitivities of velocity sensed by the SHIP to the error models defined for SHIP.

$\frac{\partial \dot{\phi}}{\partial E_S}$  are the sensitivities of the drift of the gyrocompass gyro to the error models defined for SHIP.

In addition, the process noise between measurements consisted of the effect that the gimbal resolver uncertainty had on alignment about up.

## LOGICON

The SHIP was simulated in each of the required alignment positions to calculate H using linear error analysis methods (see Appendix A) and the necessary Kalman processing performed (Equations B-3 and B-4).

The initial covariance for the SHIP alignment analysis was the mature post calibration error budget.

### B-3. DUAL P5 CALIBRATION

The analysis of the calibration of the Litton Dual P5 inertial reference system was abbreviated by considering the calibration of only one of the two platforms. The calibration of the other platform was assumed identical. Thus the gyro and gimbal errors were modeled with 46 error sources. The model description matrices were:

$$\begin{aligned} F &= 0 \\ G &= 0 \end{aligned} \quad \left. \vphantom{\begin{aligned} F &= 0 \\ G &= 0 \end{aligned}} \right\} \text{no time dependence}$$
$$R = \text{gimbal resolver rate error covariance}$$
$$H = \left[ \frac{\partial \dot{\phi}}{\partial H_S} \right]_{2 \times 46}$$

where

$$\left[ \frac{\partial \dot{\phi}}{\partial H_S} \right]$$

are the sensitivities of the inner and outer gimbal resolver rate readouts to the error models defined for the P5.

and the gimbal resolver rate errors were those given by Litton for the P5 platform. The measurement sequence was then simulated and the estimates of the calibration accuracy determined.

APPENDIX C  
SYSTEM PERFORMANCE EVALUATION

C-1. INTRODUCTION

In modeling the accuracy of a maneuvering reentry system, the mission was divided into four phases:

- Prelaunch
- Boost
- Freeflight
- Reentry

The last three phases of flight are illustrated schematically in Figure C-1. The objective is to guide the reentry vehicle to a preselected target. During each phase a particular function is performed to achieve the final objective. In the prelaunch phase, the coarse reentry IMU alignment is determined. During boost, the booster guidance system deploys the reentry vehicle on the trajectory to its reentry point (300,000 ft). In addition, the reentry guidance system is calibrated inflight, (particularly position, velocity and platform alignment). In the free-flight phase the initial reentry state is estimated. During reentry, the reentry guidance system navigates from the initial reentry state to the target. The error analysis program handles each mission phase separately.

C-2. ERROR PROPAGATION

To calculate system accuracy, a linear system error analysis was performed. Since standard linear error analysis was not sufficient for our purpose, estimation theory was used. The standard analysis assumes an error relationship of the form

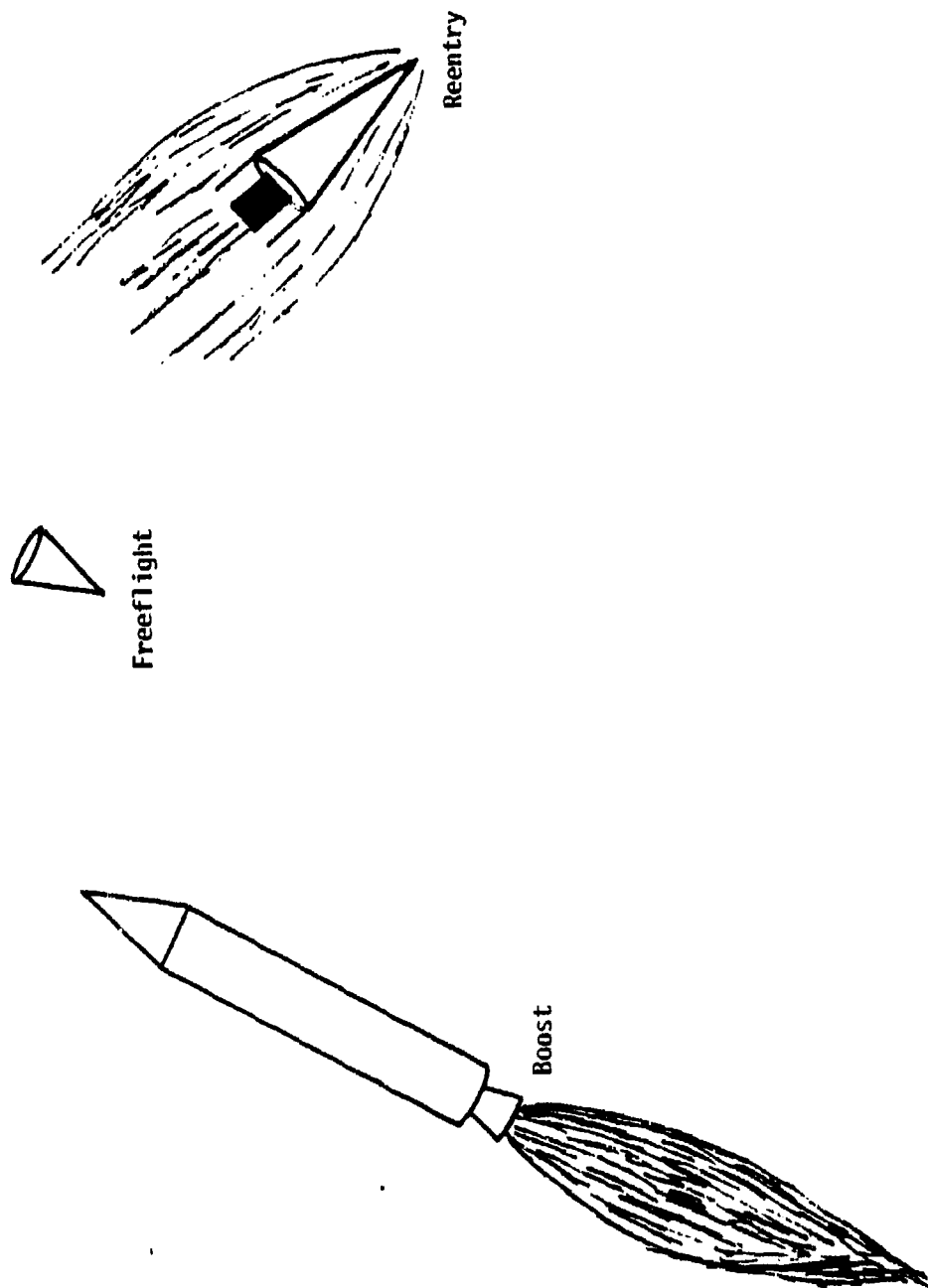


Figure C-1. Mission Phases

$$\Delta \underline{\epsilon} = \frac{\partial \underline{\epsilon}}{\partial \underline{E}} \Delta \underline{E} \quad (C-1)$$

where

$\Delta \underline{\epsilon}$  is the error in the state vector (RIMU position, velocity)

$\Delta \underline{E}$  is the initial error source vector (RIMU platform alignment, accelerometer and gyro errors, etc.)

$\frac{\partial \underline{\epsilon}}{\partial \underline{E}}$  is a matrix determined by integration of error equations on a nominal trajectory

The covariance of the error is given by

$$\text{cov}(\Delta \underline{\epsilon}) = \left( \frac{\partial \underline{\epsilon}}{\partial \underline{E}} \right) \text{cov}(\Delta \underline{E}) \left( \frac{\partial \underline{\epsilon}}{\partial \underline{E}} \right)^T$$

where superscript T indicates matrix transpose. To obtain  $\frac{\partial \underline{\epsilon}}{\partial \underline{E}}$  a simulation of the system is needed. Each error source  $E_i$  is perturbed by  $\Delta E_i$ , and the effects are integrated over the entire trajectory to obtain the sensitivity  $\frac{\partial \underline{\epsilon}}{\partial E_i}$ . Unfortunately, this standard linear error analysis does not easily

accommodate external measurements. Since it is desired to use external measurements, such as a match with the booster IMU (BIMU) or GPS measurements, the technique of linear estimation theory was used. However, the standard linear error analysis method was used to obtain the matrix

$\frac{\partial \underline{\epsilon}}{\partial \underline{E}}$  for incorporation into the analysis by estimation theory.

With linear estimation theory, the system is described by a state vector  $\underline{X}$  which includes all information relevant to the state of the system, such as position, velocity, and error sources which

## LOGICON

---

affect the system. Typical error sources for the case of the BIMU navaid are shown in Table C-1. If GPS is thenavaid, then reentry vehicle clock errors and GPS satellite errors are also included.

The system model assumes that calibrated values of the system parameters are compensated inflight. Therefore, to analyze optimal system performance, the state vector is linearized about the calibrated values of the system parameters. The relevant equation is

$$x_i^A(t) = x_i^C(t) - \delta x_i(t)$$

where

$x_i^A(t)$  is the actual value of the  $i^{\text{th}}$  system parameter at time  $t$

$x_i^C(t)$  is the value of the  $i^{\text{th}}$  system parameter at time  $t$  as stored in the flight computer

$\delta x_i(t)$  is the  $i^{\text{th}}$  system error at time  $t$

For linear error analysis  $\delta \underline{x}(t)$  is used as the state vector. The composition of the state vector for the case of a BIMU navaid is shown in Table C-2. Note that the BIMU and the G&G errors are considered separately from the RIMU errors. This allows separate treatment of each portion of the state vector.

The linearized state vector is assumed to satisfy the linear differential equation

$$\dot{\delta \underline{x}}(t) = F(t)\delta \underline{x}(t) + \Gamma(t)\underline{w}(t) \quad (C-2)$$

Table C-1. System Error Sources

Reentry IMU (RIMU)

- Alignment
- Platform (compliance, gimbals)
- Accelerometers
- Gyros

Booster IMU (BIMU)

- Alignment
- Platform (compliance, gimbals)
- Accelerometers
- Gyros

Geodetic and Geophysical

- Launch and target location
- Earth model (gravity and shape)

Table C-2. System State Vector

$$\underline{\delta X} = \begin{bmatrix} \underline{S} \\ \underline{E_{RIMU}} \\ \underline{E_{BIMU}} \\ \underline{E_{G\&G}} \end{bmatrix}$$

$$\underline{S} = \begin{bmatrix} \underline{P} \\ \underline{V} \end{bmatrix} \quad \begin{array}{l} \text{ECI position error} \\ \text{ECI velocity error} \end{array}$$

$$\underline{E_{RIMU}} = \begin{bmatrix} \underline{\delta\phi^R} \\ \underline{E_p^R} \\ \underline{E_A^R} \\ \underline{E_G^R} \end{bmatrix} \quad \begin{array}{l} \text{RIMU alignment errors} \\ \text{RIMU platform errors} \\ \text{RIMU accelerometer errors} \\ \text{RIMU gyro errors} \end{array}$$

$$\underline{E_{BIMU}} = \begin{bmatrix} \underline{\delta\phi^B} \\ \underline{E_p^B} \\ \underline{E_A^B} \\ \underline{E_G^B} \end{bmatrix} \quad \begin{array}{l} \text{BIMU alignment errors} \\ \text{BIMU platform errors} \\ \text{BIMU accelerometer errors} \\ \text{BIMU gyro errors} \end{array}$$

$$\underline{E_{G\&G}} = \begin{bmatrix} \underline{E_{G\&G}} \end{bmatrix} \quad \text{G\&G errors}$$

## LOGICON

where

$\delta \underline{X}(t)$  = state vector at time  $t$   
 $F(t)$  = process matrix  
 $\underline{w}(t)$  = random disturbance vector  
 $\Gamma(t)$  = disturbance matrix

The covariance of  $\underline{w}(t)$  is given by

$$E[\underline{w}(t)\underline{w}(t')^T] = Q(t)\delta(t-t')$$

where  $E$  symbolizes the expectation operator. The Dirac delta function  $\delta(t-t')$  is nonzero only if  $t = t'$ . The covariance matrix has a delta function dependence since  $\underline{w}(t)$  at time  $t$  is uncorrelated with  $\underline{w}(t')$  at a different time  $t'$ .

Integrating Equation C-2 it is found that the state vector propagates in time by a linear transformation with a superimposed random disturbance:

$$\delta \underline{X}_i = \phi_{i-1} \delta \underline{X}_{i-1} + G_{i-1} \underline{w}_{i-1} \quad (C-3)$$

where

$\delta \underline{X}_{i-1}$  = linearized state vector at time  $i-1$   
 $\phi_{i-1}$  = state transition matrix  
 $\underline{w}_{i-1}$  = random disturbance vector  
 $G_{i-1}$  = disturbance transition matrix

The covariance of  $\underline{w}_i$  is given by

$$E(\underline{w}_i \underline{w}_j^T) = Q_i \delta_{ij}$$

where

$$\delta_{ij} = \begin{cases} 1 & \text{if } i = j \\ 0 & \text{if } i \neq j \end{cases}$$

## LOGICON

The Kronecker delta  $\delta_{ij}$  is used for the discrete time case and indicates that  $\underline{w}_i$  at time  $i$  is uncorrelated with  $\underline{w}_j$  at a different time  $j$ .

The state transition matrix can be shown to satisfy the differential equation

$$\dot{\phi}(t) = F(t)\phi(t) \quad (C-4)$$

where  $F$  is the process matrix of Equation C-2. The initial condition on  $\phi$  is

$$\phi(t_0) = I$$

where  $I$  is the identity matrix. The solution of Equation (C-4) for constant  $F$  is

$$\phi(t, t_0) = e^{F(t - t_0)}$$

where  $\phi(t, t_0)$  is the state transition matrix from time  $t_0$  to  $t$ .

The discrete noise covariance can be expressed in terms of the continuous case as

$$G_{K-1}Q_{K-1}G_{K-1}^T = \int_{t_{K-1}}^{t_K} \phi(t_K, \tau)G(\tau)Q(\tau)G^T(\tau)\phi^T(t_K, \tau)d\tau \quad (C-5)$$

Measurements are taken at discrete time points, and they are assumed to be linearly related to the state vector by

$$\delta \underline{z}_i = H_i \delta \underline{x}_i + \underline{v}_i \quad (C-6)$$

where

$$\delta \underline{z}_i = \text{linearized measurement at time } i$$

## LOGICON

$H_i$  = measurement matrix

$\underline{v}_i$  = random measurement noise

The covariance of  $\underline{v}_i$  is given by

$$E(\underline{v}_i \underline{v}_j) = R_i \delta_{ij}$$

The linearized measurement is related to the actual measurement by

$$\delta \underline{z}_i = \underline{z}_i^C - \underline{z}_i^A$$

where

$\underline{z}_i^A$  = actual measurement

$\underline{z}_i^C$  = nominal measurement expected if state vector  
equaled  $\underline{x}_i^C$

Using the discrete time formulation, the state at time  $i$  is estimated from an earlier estimate at time  $i-1$  by

$$\delta \hat{\underline{x}}_i = \phi_{i-1} \delta \hat{\underline{x}}_{i-1} \quad (C-7)$$

where the symbol  $\hat{\underline{x}}$  indicates the estimate of  $\underline{x}$ . The covariance  $P$  is propagated in time by

$$P_i = \phi_{i-1} P_{i-1} \phi_{i-1}^T + G_{i-1} Q_{i-1} G_{i-1}^T \quad (C-8)$$

The state is updated after a measurement with the standard Kalman filter:

$$\delta \hat{\underline{x}}_i^+ = \delta \hat{\underline{x}}_i^- + K_i [\delta \underline{z}_i - H_i \delta \hat{\underline{x}}_i^-] \quad (C-9)$$

## LOGICON

The corresponding covariance update is

$$P_i^+ = (I - K_i H_i) P_i^- \quad (C-10)$$

where  $K_i = P_i^- H_i^T (H_i P_i^- H_i^T + R_i)^{-1}$  is the Kalman gain and the superscripts + and - indicate before and after a measurement.

The error propagation equations require the calculation of the state transition matrix  $\phi$ . From Equation C-2 it is seen that knowledge of the system dynamics determines the process matrix  $F$ . The process matrix in turn gives rise to the state transition matrix (Equation C-4). Therefore, the first step in calculating the transition matrix is to determine the process matrix from the system dynamics.

The differential equation of motion solved by navigation is

$$\ddot{\underline{p}} = \dot{\underline{v}} = \underline{A}_S - \frac{GM}{|\underline{p}|^3} \underline{p}$$

where

$\underline{p}$  = position vector

$\underline{v}$  = velocity vector

$\underline{A}_S$  = sensed acceleration vector

GM = earth's gravity constant

However,

$$\underline{A}_S = \underline{A}_S^A + \delta \underline{A}_S$$

$$\underline{v} = \underline{v}^A + \delta \underline{v}$$

$$\underline{p} = \underline{p}^A + \delta \underline{p}$$

where superscript A signifies the actual value (assuming no errors) and  $\delta$  represents an error term about the actual value.

## LOGICON

Therefore,

$$\begin{aligned}\dot{\underline{V}}^A + \delta \dot{\underline{V}} &= \underline{A}_S^A + \delta \underline{A}_S - \frac{GM}{|\underline{p}^A|^3} \underline{p}^A - \frac{GM}{|\underline{p}^A|^3} \delta \underline{p} \\ &+ \frac{3GM}{|\underline{p}^A|^5} (\delta \underline{p} \cdot \underline{p}^A) \underline{p}^A - \frac{\delta GM}{|\underline{p}^A|^3} \underline{p}^A\end{aligned}$$

Subtracting out the actual terms,

$$\delta \dot{\underline{V}} = \delta \underline{A}_S - \frac{GM}{|\underline{p}^A|^3} \delta \underline{p} + \frac{3GM}{|\underline{p}^A|^5} (\delta \underline{p} \cdot \underline{p}^A) \underline{p}^A - \frac{\delta GM}{|\underline{p}^A|^3} \underline{p}^A$$

The term  $\delta \underline{A}_S$  is due to alignment, platform and accelerometer errors:

$$\delta \underline{A}_S = \delta \underline{\phi} \times \underline{A}_S + \delta \underline{A}_p + \delta \underline{A}_A$$

where

$\delta \underline{\phi}$  = platform alignment errors

$\delta \underline{A}_p$  = sensed acceleration errors due to platform errors

$\delta \underline{A}_A$  = sensed acceleration errors due to accelerometer errors

The  $\delta \underline{A}_p$  term is modeled as a function of the sensed acceleration and the platform errors:

$$\begin{aligned}(\delta \underline{A}_p)_x &= f_x (\underline{A}_S, \underline{E}_p^R) \\ (\delta \underline{A}_p)_y &= f_y (\underline{A}_S, \underline{E}_p^R) \\ (\delta \underline{A}_p)_z &= f_z (\underline{A}_S, \underline{E}_p^R)\end{aligned}$$

## LOGICON

Similarly,  $\delta \underline{A}_A$  can be written as

$$(\delta A)_X = g_X (\underline{A}_S, \underline{E}_A^R)$$

$$(\delta A)_Y = g_Y (\underline{A}_S, \underline{E}_A^R)$$

$$(\delta A)_Z = g_Z (\underline{A}_S, \underline{E}_A^R)$$

The sensed acceleration errors can therefore be expressed as

$$\delta \underline{A}_S = \delta \phi \times \underline{A}_S + f \underline{E}_p^R + g \underline{E}_A^R$$

where  $f$  and  $g$  are matrices given by

$$f = \frac{\partial \underline{A}_S}{\partial \underline{E}_p^R}$$

$$g = \frac{\partial \underline{A}_S}{\partial \underline{E}_A^R}$$

Writing the previous equation of motion in terms of the individual components, the errors in RIMU position and velocity propagate in time by

$$\delta \dot{P}_X = \delta V_X$$

$$\delta \dot{P}_Y = \delta V_Y$$

$$\delta \dot{P}_Z = \delta V_Z$$

(C-11)

$$\begin{aligned} \delta \dot{V}_X = & (\alpha + \beta P_X^2) \delta P_X + \beta P_X P_Y \delta P_Y + \beta P_X P_Z \delta P_Z \\ & + A_{SZ} \delta \phi_Y - A_{SY} \delta \phi_Z + \sum_j f_{Xj} (E_p^R)_j + \sum_j g_{Xj} (E_A^R)_j \\ & + \gamma P_X \delta(GM) \end{aligned}$$

# LOGICON

$$\begin{aligned}\delta \dot{V}_Y &= \beta P_Y P_X \delta P_X + (\alpha + \beta P_Y^2) \delta P_Y + \beta P_Y P_Z \delta P_Z \\ &+ A_{SX} \delta \phi_Z - A_{SZ} \delta \phi_X + \sum_j f_{Yj} (E_P^R)_j + \sum_j g_{Yj} (E_A^R)_j \\ &+ \gamma P_Y \delta(GM)\end{aligned}$$

$$\begin{aligned}\delta \dot{V}_Z &= \beta P_Z P_X \delta P_X + \beta P_Z P_Y \delta P_Y + (\alpha + \beta P_Z^2) \delta P_Z \\ &+ A_{SY} \delta \phi_X - A_{SX} \delta \phi_Y + \sum_j f_{Zj} (E_P^R)_j + \sum_j g_{Zj} (E_A^R)_j \\ &+ \gamma P_Z \delta(GM)\end{aligned}$$

where

$$\alpha = - \frac{GM}{|\bar{P}|^3}$$

$$\beta = \frac{3GM}{|\bar{P}|^5}$$

$$\gamma = - \frac{1}{|\bar{P}|^3}$$

To keep the equations relatively simple, a spherical earth was assumed for Equation C-11. However, in the actual simulation, higher order spherical harmonic gravity terms were included in addition to the GM term given in Equation C-11. The alignment in the above equations is expressed in the same coordinate system as the position and velocity errors. By means of an orthogonal coordinate transformation, the alignment errors can be easily expressed in platform coordinates even if it differs from the position and velocity coordinates.

## LOGICON

The RIMU platform alignment errors are modeled as functions of the sensed acceleration and the gyro errors:

$$\begin{aligned}\dot{\phi}_X &= h_X (\underline{A}_S, \underline{E}_G^R) \\ \dot{\phi}_Y &= h_Y (\underline{A}_S, \underline{E}_G^R) \\ \dot{\phi}_Z &= h_Z (\underline{A}_S, \underline{E}_G^R)\end{aligned}\tag{C-12}$$

The RIMU platform, accelerometer, and gyro errors are modeled as constants:

$$\begin{aligned}\dot{\underline{E}}_P^R &= 0 \\ \dot{\underline{E}}_A^R &= 0 \\ \dot{\underline{E}}_G^R &= 0\end{aligned}$$

Changes in these quantities are handled by including process noise (Q matrix). Since the BIMU errors are modeled as error sources (i.e. initial values), these errors are also constant in time:

$$\dot{\underline{E}}_{\text{BIMU}} = 0$$

Finally, the G&G errors are modeled as constants:

$$\dot{\underline{E}}_{\text{G\&G}} = 0$$

The F matrix can be determined from the relation

$$\dot{\underline{X}} = \underline{F}\underline{X}$$

Decomposing the state vector into its components

$$\begin{bmatrix} \dot{\underline{S}} \\ \dot{\underline{E}}_{\text{RIMU}} \\ \dot{\underline{E}}_{\text{BIMU}} \\ \dot{\underline{E}}_{\text{G\&G}} \end{bmatrix} = \begin{bmatrix} F_{11} & F_{12} & 0 & F_{14} \\ 0 & F_{22} & 0 & 0 \\ 0 & 0 & 0 & 0 \\ 0 & 0 & 0 & 0 \end{bmatrix} \begin{bmatrix} \underline{S} \\ \underline{E}_{\text{RIMU}} \\ \underline{E}_{\text{BIMU}} \\ \underline{E}_{\text{G\&G}} \end{bmatrix} \quad (\text{C-13})$$

$F_{11}$  and  $F_{12}$  are obtained from Equation C-11 and are given in Figures C-2 and C-3.  $F_{22}$  is obtained from Equation C-12 and is given in Figure C-4. Because G&G errors cancel in a BIMU/RIMU measurement, the  $F_{14}$  term was not included in the calculation. Position and velocity errors due to G&G were added in near the end of the calculation (after all measurement updates) to obtain system performance. Note that for the GPS case, G&G errors can be estimated from pseudo-range measurements. An  $F_{14}$  term was therefore included for the GPS analysis.

To propagate the covariance in time, the standard discrete form is used:

$$P_{K+1} = \phi_K P_K \phi_K^T + G_K Q_K G_K^T$$

where  $\phi_K$  is a solution of

$$\dot{\phi}(t, t_K) = F(t)\phi(t, t_K) ; \phi(t_K, t_K) = I$$

For a constant  $F$ , the solution of the transition matrix equation is

$$\phi = e^{F\Delta t}$$

$$F_{11} = \begin{bmatrix} 0 & 0 & 0 & 1 & 0 & 0 \\ 0 & 0 & 0 & 0 & 1 & 0 \\ 0 & 0 & 0 & 0 & 0 & 1 \\ (\alpha + \beta)P_X^2 & \beta P_X P_Y & \beta P_X P_Z & 0 & 0 & 0 \\ \beta P_X P_Y & (\alpha + \beta)P_Y^2 & \beta P_Y P_Z & 0 & 0 & 0 \\ \beta P_X P_Z & \beta P_Y P_Z & (\alpha + \beta)P_Z^2 & 0 & 0 & 0 \end{bmatrix}$$

$$\alpha = - \frac{GM}{|\bar{P}|^3}$$

$$\beta = \frac{3GM}{|\bar{P}|^5}$$

Figure C-2. System Process Matrix  $F_{11}$

$$F_{12} = \begin{bmatrix} 0 & 0 & 0 & 0 & \cdots & 0 & 0 & \cdots & 0 & 0 & \cdots & 0 \\ 0 & 0 & 0 & 0 & \cdots & 0 & 0 & \cdots & 0 & 0 & \cdots & 0 \\ 0 & 0 & 0 & 0 & \cdots & 0 & 0 & \cdots & 0 & 0 & \cdots & 0 \\ 0 & A_{S_Z} & -A_{S_Y} & f_{11}^P & \cdots & f_{1M}^P & g_{11}^A & \cdots & g_{1N}^A & 0 & \cdots & 0 \\ -A_{S_Z} & 0 & A_{S_X} & f_{21}^P & \cdots & f_{2M}^P & g_{21}^A & \cdots & g_{2N}^A & 0 & \cdots & 0 \\ A_{S_Y} & -A_{S_X} & 0 & f_{31}^P & \cdots & f_{3M}^P & g_{31}^A & \cdots & g_{3N}^A & 0 & \cdots & 0 \end{bmatrix}$$

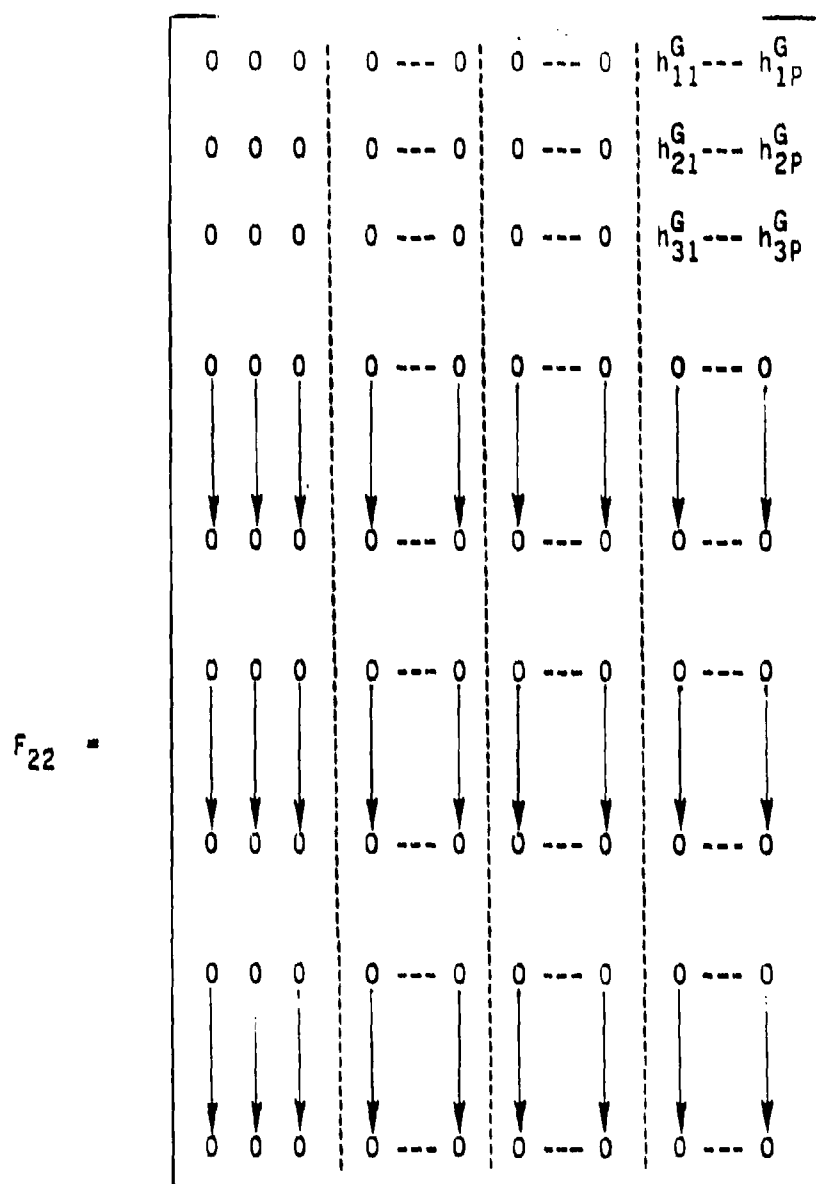
$$f_{ij}^P = \frac{\partial A_{S_i}}{\partial (E_P^R)_j}$$

$$g_{ij}^A = \frac{\partial A_{S_i}}{\partial (E_A^R)_j}$$

$(E_P^R)_j$  represents the  $j^{\text{th}}$  RIMU platform error

$(E_A^R)_j$  represents the  $j^{\text{th}}$  RIMU accelerometer error

Figure C-3. System Process Matrix  $F_{12}$



$$h_{ij}^G = \frac{\partial \phi_i}{\partial (E_G^R)_j}$$

$(E_G^R)_j$  represents the  $j^{\text{th}}$  RIMU gyro error

Figure C-4. System Process Matrix  $F_{22}$

## LOGICON

For variable  $F$ , a small time interval can be chosen during which  $F$  is approximately constant.  $\phi$  is then approximated over the interval  $\Delta t$  as the product

$$\phi = \prod_{i=1}^n e^{F_i \Delta t/n}$$

where  $F_i$  is the average  $F$  over the appropriate subinterval. The exponential can be further approximated as

$$e^{F_i \Delta t/n} = \sum_{j=0}^m \frac{(F_i \frac{\Delta t}{n})^j}{j!}$$

Thus,

$$\phi = \prod_{i=1}^n \left[ \sum_{j=0}^m \frac{(F_i \frac{\Delta t}{n})^j}{j!} \right] \quad (C-14)$$

The quantities  $n$  and  $m$  are chosen to be sufficiently large so that the approximations are adequate.

### C-3. INFLIGHT ALIGNMENT

The Kalman filter (Equation C-10) is used to evaluate the performance of the alignment update. In this appendix, the case of a measurement using the BIMU is described. To take a specific example, a velocity measurement is considered. A similar procedure is used for a position measurement. The velocity measurement is defined by

$$\underline{z} = \underline{v}_{RIMU} - \underline{v}_{BIMU}$$

## LOGICON

The individual velocity terms can be expressed as

$$\underline{V}_{RIMU} = \underline{V}_{ACTUAL} + \delta \underline{V}_{RIMU} + \delta \underline{V}_{QUANT}^R + \delta \underline{V}_{G\&G}$$

$$\underline{V}_{BIMU} = \underline{V}_{ACTUAL} + \delta \underline{V}_{BIMU} + \delta \underline{V}_{QUANT}^B + \delta \underline{V}_{G\&G}$$

where the velocity errors due to G&G and due to quantization are separated from the other velocity errors. The measurement equation is thus:

$$\underline{Z} = \delta \underline{V}_{RIMU} - \delta \underline{V}_{BIMU} + \delta \underline{V}_{QUANT}^R - \delta \underline{V}_{QUANT}^B \quad (C-15)$$

Since all BIMU errors are treated as constant error sources (i.e. as initial values), the BIMU velocity error as a function of time is given by

$$\delta \underline{V}_{BIMU}(t) = \frac{\partial \underline{V}}{\partial \underline{E}_{BIMU}}(t) \underline{E}_{BIMU} \quad (C-16)$$

where the derivative indicates the sensitivity of BIMU velocity error to initial sources. Substituting Equation C-16 into Equation C-15, we arrive at

$$\underline{Z} = \delta \underline{V}_{RIMU}(t) - \frac{\partial \underline{V}}{\partial \underline{E}_{BIMU}}(t) \underline{E}_{BIMU} + \delta \underline{V}_{QUANT}^R - \delta \underline{V}_{QUANT}^B \quad (C-17)$$

where  $t$  is the time of the measurement (thrust termination for this study). From Equation C-17 the measurement matrix is seen to be

$$H = \left[ \begin{array}{cccccc|c|c|c} 0 & 0 & 0 & 1 & 0 & 0 & 0 & -\frac{\partial \underline{V}(t)}{\partial \underline{E}_{BIMU}} & 0 \\ 0 & 0 & 0 & 0 & 1 & 0 & 0 & 0 & 0 \\ 0 & 0 & 0 & 0 & 0 & 1 & 0 & 0 & 0 \end{array} \right]$$

and the noise  $\underline{\gamma}$  is given by

$$\underline{\gamma} = \delta \underline{V}_{QUANT}^R - \delta \underline{V}_{QUANT}^B$$

## LOGICON

---

The covariance R is

$$R = \begin{bmatrix} q & 0 & 0 \\ 0 & q & 0 \\ 0 & 0 & q \end{bmatrix}$$

where

$$q = \text{cov} (\delta \underline{v}_{\text{QUANT}}^R - \delta \underline{v}_{\text{QUANT}}^B)$$

Substituting the measurement and noise covariance matrices into the Kalman filter (Equation C-10), the state is updated, yielding an improved estimate of RIMU platform alignment, position, and velocity.

### C-4. REENTRY INITIALIZATION

After the last measurement has been made, Equation C-8 is used to propagate the covariance matrix to reentry. So far, position and velocity errors due to G&G have not been included for the case of the booster navaid. ( $F_{14}$  of Equation C-13 was not included in the calculation for the BIMU navaid case.) Therefore, at this point position and velocity errors due to G&G are combined with errors due to other sources to obtain the total position and velocity error. The covariance matrix at this point represents the full covariance of the state at reentry for the case of an optimal state propagation method such as a simulation. If other propagation methods are of interest, additional errors due to the particular technique must be included.

C-5. INCORRECT SYSTEM MODELING

The discussion so far has centered on calculating the covariance for the optimal case in which the complete system dynamics and measurements are modeled correctly. Due to computer restrictions or lack of knowledge of the system dynamics, it is not always possible to simulate the system exactly. In this situation it is still necessary to be able to evaluate system performance, although the standard equations for optimal estimation no longer hold. The appropriate equations are given here without proof. A derivation can be found in Section C-7.

The true system dynamics are given by

$$\underline{X}_j = \phi_{j-1} \underline{X}_{j-1} + G_{j-1} \underline{W}_{j-1} \quad (C-18)$$

The true measurement is related to the state by

$$\underline{Z}_j = H_j \underline{X}_j + \underline{v}_j \quad (C-19)$$

The covariance of  $\underline{W}_j$  and  $\underline{v}_j$  are  $Q_j$  and  $R_j$  respectively. The suboptimal filter assumes the model to be

$$\underline{X}_j^* = \phi_{j-1}^* \underline{X}_{j-1}^* + G_{j-1}^* \underline{W}_{j-1}^* \quad (C-20)$$

$$\underline{Z}_j^* = H_j^* \underline{X}_j^* + \underline{v}_j^* \quad (C-21)$$

where the covariance of  $\underline{W}_j^*$  and  $\underline{v}_j^*$  are respectively  $Q_j^*$  and  $R_j^*$ . The starred quantities do not necessarily equal the unstarred quantities modeled in Equations C-18 and C-19. The equations used by the filter to update the state and covariance are

$$\begin{aligned} \hat{\underline{X}}_j^* &= \phi_{j-1}^* \hat{\underline{X}}_{j-1}^* \\ \hat{\underline{X}}_j^{**} &= \hat{\underline{X}}_j^* + K_j^* \left( \underline{Z}_j - H_j^* \hat{\underline{X}}_{j-1}^* \right) \end{aligned} \quad (C-22)$$

$$\begin{aligned}
 P_j^* &= \phi_{j-1}^* P_{j-1}^* \phi_{j-1}^{*T} + G_{j-1}^* Q_{j-1}^* G_{j-1}^{*T} \\
 P_j^{*-} &= (I - K_j^* H_j^*) P_j^{*-} \\
 K_j^* &= P_j^* H_j^{*T} (H_j^* P_j^{*-} H_j^{*T} + R_j^*)^{-1}
 \end{aligned}$$

Since the filter does not model the system correctly, it produces a suboptimal estimate of the state. In addition, the quantity  $P^*$  calculated by the filter does not represent the true covariance of the state. The true covariance is propagated in time by the following set of equations:

$$\begin{aligned}
 P_K &= \phi_{K-1}^* P_{K-1}^* \phi_{K-1}^{*T} + \phi_{K-1}^* V_{K-1}^T \Delta \phi_{K-1}^T + \Delta \phi_{K-1} V_{K-1} \phi_{K-1}^{*T} \\
 &\quad + \Delta \phi_{K-1} U_{K-1} \Delta \phi_{K-1}^T + G_{K-1} Q_{K-1} G_{K-1}^T \quad (C-23) \\
 V_K &= \phi_{K-1} V_{K-1} \phi_{K-1}^{*T} + \phi_{K-1} U_{K-1} \Delta \phi_{K-1}^T - G_{K-1} Q_{K-1} G_{K-1}^T \\
 U_K &= \phi_{K-1} U_{K-1} \phi_{K-1}^T + G_{K-1} Q_{K-1} G_{K-1}^T
 \end{aligned}$$

After a measurement the true covariance is given by

$$\begin{aligned}
 P_K^+ &= (I - K_K^* H_K^*) P_K^- (I - K_K^* H_K^*)^T - (I - K_K^* H_K^*) V_K^{-T} \Delta H_K^T K_K^{*T} \\
 &\quad - K_K^* \Delta H_K V_K^- (I - K_K^* H_K^*)^T + K_K^* \Delta H_K U_K^- \Delta H_K^T K_K^{*T} + K_K^* R_K K_K^{*T} \\
 V_K^+ &= V_K^- (I - K_K^* H_K^*)^T - U_K^- \Delta H_K^T K_K^{*T} \quad (C-24) \\
 U_K^+ &= U_K^-
 \end{aligned}$$

## LOGICON

where

$$\Delta\phi = \phi^* - \phi$$

$$\Delta H = H^* - H$$

$$P = E \left[ (\underline{X} - \hat{\underline{X}}^*) (\underline{X} - \hat{\underline{X}}^*)^T \right] = \text{cov} (\underline{X})$$

$$U = E \left[ \underline{X} \underline{X}^T \right]$$

$$V = -E \left[ \underline{X} (\underline{X} - \hat{\underline{X}}^*)^T \right]$$

In the above equations, E indicates the expectation operator. Using the above equations, the true covariance of the state can be propagated. This technique was used to estimate the accuracy of the state at reentry for the case in which a suboptimal filter was used to process GPS measurements.

### C-6. COMPUTER PROGRAM ORGANIZATION

A flow diagram indicating the computer programs used in the system performance evaluation is shown in Figure C-5. The linear error analysis program (Appendix A) generates the RIMU transition matrices ( $F_{11}$ ,  $F_{12}$ ,  $F_{14}$ , and  $F_{22}$ ) for the boost and reentry portions of the trajectory. For the GPS case, it also generates transition matrices of the navaid (satellite) position and velocity error due to G&G. GEM represents several programs which generate a magnetic tape consisting of the navaid transition and measurement matrices and the RIMU measurement matrix. For the case of the BIMU navaid, the navaid transition matrix and the RIMU measurement matrix are the identity matrix. The system error analysis program (SEAP) uses the Kalman filter formulation to evaluate performance. The RIMU free-flight transition matrices are generated internally by SEAP. Effects due to disturbance noise (Q matrix) for both the RIMU and the navaid are calculated by SEAP. Covariance matrices at the points of interest are output

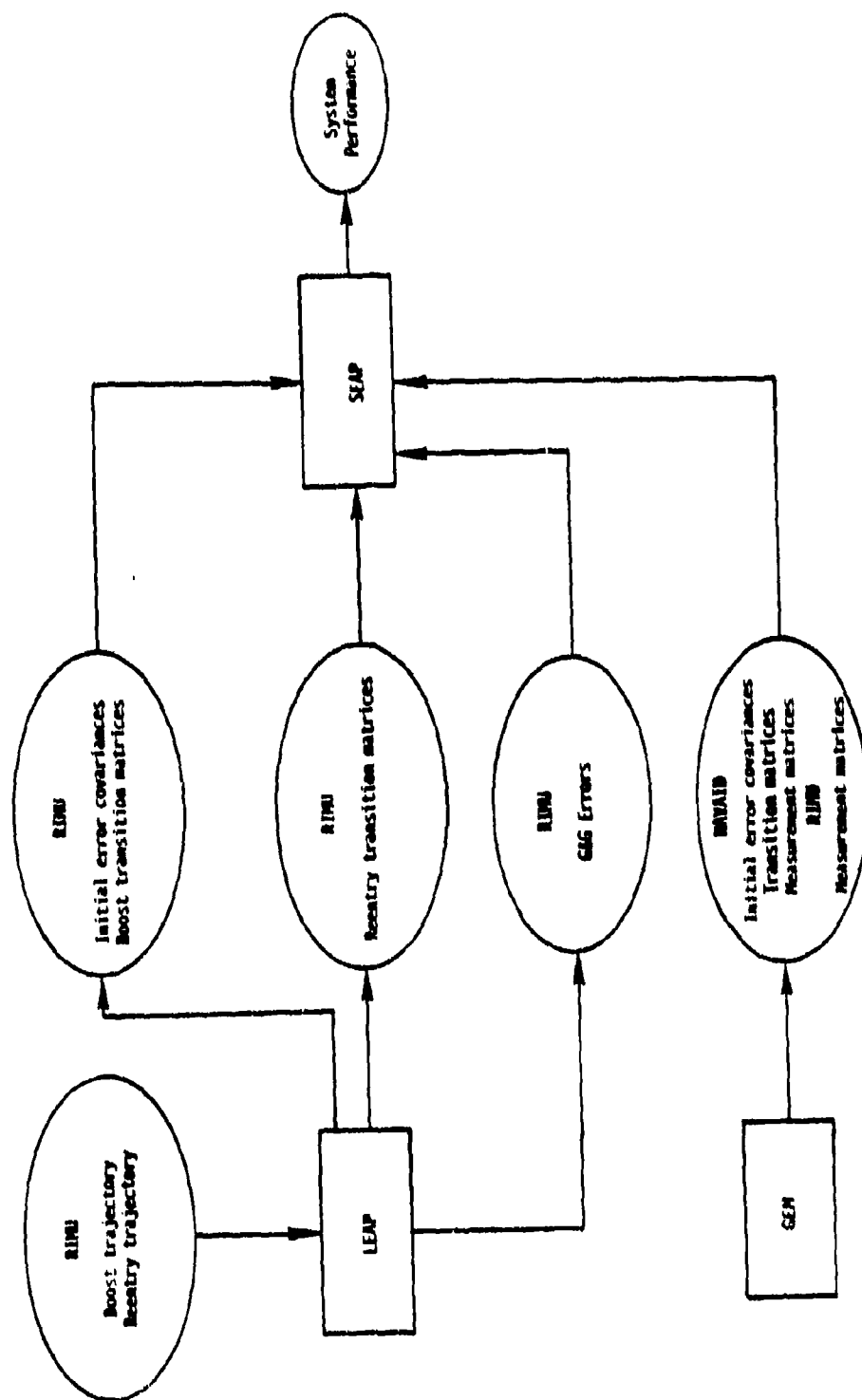


Figure C-7. Computer Program Organization

## LOGICON

---

by SEAP in several coordinate systems: ECI, downrange - crossrange - altitude. or downrange - crossrange - time. These covariance matrices describe the system performance.

### C-7. SUBOPTIMAL FILTER EQUATIONS

This section presents equations which calculate the true covariance of a state as estimated by a suboptimal filter. They may be applied to the linear discrete case in which the suboptimal filter employs incorrect transition and measurement matrices, suboptimal gains, and a reduced order state vector. Analogous equations can be found in Reference C-1 for the special case of the suboptimal filter employing the full size (truth model) state vector.

A linear system is assumed for the system model. Thus, state vector dynamics is given by:

$$x_k = \phi_{k-1} x_{k-1} + G_{k-1} w_{k-1} \quad (C-25)$$

where

$x_{k-1}$  = state vector at time k-1

$\phi_{k-1}$  = state transition matrix

$w_{k-1}$  = zero mean random disturbance vector at time k-1

$G_{k-1}$  = disturbance transition matrix

A measurement of the state at time k is given by:

$$z_k = H_k x_k + v_k \quad (C-26)$$

where

$z_k$  = measurement vector at time k

$H_k$  = measurement matrix

## LOGICON

$v_k$  = zero mean random measurement noise vector  
at time k

$x$  is an  $n$  vector;  $w$  is an  $p$  vector;  $z$  is an  $m$  vector; all other quantities are assumed to be dimensionally compatible.  $x$  is assumed to be a zero mean variable. In addition, the covariance of  $w_{k-1}$  is given by  $Q_{k-1}$ , and the covariance of  $v_k$  is given by  $R_k$ :

$$E(w_k w_j^T) = Q_k \delta_{jk}$$

$$E(v_k v_j^T) = R_k \delta_{jk}$$

$$E(v_k w_j) = 0$$

Note that  $w_k$  and  $v_k$  at time  $k$  are each uncorrelated with  $w_j$  and  $v_j$  at a different time  $j$ , and that  $w_k$  and  $v_k$  are uncorrelated with each other.

The suboptimal filter assumes the following system model:

$$x_k^* = \phi_{k-1}^* x_{k-1}^* + G_{k-1}^* w_{k-1}^* \quad (C-27)$$

$$z_k^* = H_k^* x_k^* + v_k^* \quad (C-28)$$

where  $x^*$  is an  $\ell$  vector.  $w^*$  and  $v^*$  are described statistically by

$$E(w_k^* w_j^*) = Q_k^* \delta_{jk}$$

$$E(v_k^* v_j^*) = R_k^* \delta_{jk}$$

$$E(w_k^* v_j^*) = 0$$

The filter can therefore assume incorrect system dynamics. In addition, the filter does not necessarily account for all elements of the state vector since  $x^*$  can have a smaller dimension than  $x$ .

The relation between  $x^*$  and  $x$  is given by

$$x^* = Wx \quad (C-29)$$

## LOGICON

where  $W$  is an  $L \times n$  matrix. If  $x^*$  is formed by deleting bias states from  $x$ , then  $W$  takes the form

$$W = (I \mid 0)$$

In this case the state vector  $x$  is partitioned as

$$x = \begin{pmatrix} -\frac{s}{b} \end{pmatrix}$$

and the filter uses only the states

$$x^* = (s)$$

Thus,

$$x^* = (s) = (I \mid 0) \begin{pmatrix} -\frac{s}{b} \end{pmatrix} = Wx$$

The covariance equations can be derived from the above by letting  $W^{-1}$  be defined by

$$WW^{-1} = I \quad (C-30)$$

If  $x^*$  is formed by deleting bias states from  $x$ , then  $W^{-1}$  has the form

$$W^{-1} = \begin{pmatrix} -I \\ 0 \end{pmatrix} \quad (C-31)$$

(Actually, any quantity can replace the 0 in the above equation and still satisfy Equation C-30. However, for Equation C-30 to be correct,  $W^{-1}$  is uniquely given by Equation C-31 for the case of deleting bias states from the state vector.) Let  $\hat{x}_{k-1}^*$  be the suboptimal filter's estimate of  $x$  at time  $k-1$ . The error  $x_{k-1}$  in the filter's estimate of the state vector is given by

$$\hat{x}_k = W^{-1} \hat{x}_k^* - x_k \quad (C-32a)$$

The filter estimate of the state is propagated in time by

$$\hat{x}_k^* = \phi_{k-1}^* \hat{x}_{k-1}^* \quad (C-32b)$$

## LOGICON

Substituting Equations C-25 and C-27 into Equation C-32a and doing some algebraic manipulation we get

$$\begin{aligned}\bar{x}_k &= W^{-1} \phi_{k-1}^* \hat{x}_{k-1}^* - (\phi_{k-1} x_{k-1} + G_{k-1} w_{k-1}) \\ \bar{x}_k &= W^{-1} \phi_{k-1}^* W W^{-1} \hat{x}_{k-1}^* - W^{-1} \phi_{k-1}^* W x_{k-1} \\ &\quad + W^{-1} \phi_{k-1}^* W x_{k-1} - \phi_{k-1} x_{k-1} - G_{k-1} w_{k-1}\end{aligned}$$

The resulting equation is

$$\bar{x}_k = \phi_{w_{k-1}}^* \bar{x}_{k-1} + \Delta \phi_{k-1} x_{k-1} - G_{k-1} w_{k-1} \quad (C-33)$$

where

$$\begin{aligned}\phi_{w_{k-1}}^* &= W^{-1} \phi_{k-1}^* W \\ \Delta \phi_{k-1} &= \phi_{w_{k-1}}^* - \phi_{k-1}\end{aligned}$$

Let us define a new vector  $X$  by the relation

$$X = \begin{pmatrix} \bar{x} \\ x \end{pmatrix}$$

$X$  is propagated in time by

$$x_k = \begin{pmatrix} \bar{x}_k \\ x_k \end{pmatrix} = \begin{pmatrix} \phi_{w_{k-1}}^* & \Delta \phi_{k-1} \\ 0 & \phi_{k-1} \end{pmatrix} \begin{pmatrix} \bar{x}_{k-1} \\ x_{k-1} \end{pmatrix} + G_{k-1} \begin{pmatrix} -w_{k-1} \\ w_{k-1} \end{pmatrix} \quad (C-34)$$

The equation for the mean square value of  $X$  is given by

$$\begin{aligned}P &= E(XX^T) \\ &= E \begin{pmatrix} \bar{x}\bar{x}^T & \bar{x}x^T \\ x\bar{x}^T & xx^T \end{pmatrix} \quad (C-35)\end{aligned}$$

# LOGICON

Substituting Equation C-34 into Equation C-35, we find that  $\mathcal{P}$  propagates in time by

$$\begin{aligned} \mathcal{P}_k = & \begin{pmatrix} \phi_{w_{k-1}}^* & \Delta\phi_{k-1} \\ 0 & \phi_{k-1} \end{pmatrix} \mathcal{P}_{k-1} \begin{pmatrix} \phi_{w_{k-1}}^* & \Delta\phi_{k-1} \\ 0 & \phi_{k-1} \end{pmatrix}^T \\ & + E \left[ G_{k-1} \begin{pmatrix} w_{k-1}w_{k-1}^T & -w_{k-1}w_{k-1}^T \\ -w_{k-1}w_{k-1}^T & w_{k-1}w_{k-1}^T \end{pmatrix} G_{k-1}^T \right] \end{aligned} \quad (C-36)$$

Defining the quantities  $P$ ,  $U$ ,  $V$  by

$$P = E(\bar{x}\bar{x}^T)$$

$$U = E(xx^T)$$

$$V = E(x\bar{x}^T)$$

the quantity  $\mathcal{P}$  is seen to be given by

$$\mathcal{P} = \begin{pmatrix} P & V^T \\ V & U \end{pmatrix} \quad (C-37)$$

$P$  is the covariance of the filter estimate of  $x$  and is the quantity we are trying to calculate.  $U$  is the mean square value of the state vector  $x$ , with no estimate of the state subtracted off. If the initial covariance of  $x$  before the first measurement (i.e., before the estimate of  $x$  is updated from zero) is given by  $P_0$ , then the initial conditions are:

$$U_0 = P_0 \quad (C-38)$$

$$V_0 = -P_0$$

Multiplying out the matrices in Equation C-36 and comparing with Equation C-37, we find that the covariance is propagated in time by

$$\begin{aligned} U_k &= \phi_{k-1} U_{k-1} \phi_{k-1}^T + G_{k-1} Q_{k-1} G_{k-1}^T \\ V_k &= \phi_{k-1} V_{k-1} \phi_{k-1}^{*T} + \phi_{k-1} U_{k-1} \Delta \phi_{k-1}^T - G_{k-1} Q_{k-1} G_{k-1}^T \\ P_k &= \phi_{k-1}^* P_{k-1} \phi_{k-1}^{*T} + \Delta \phi_{k-1} V_{k-1} \phi_{k-1}^{*T} \\ &\quad + \phi_{k-1}^* V_{k-1}^T \Delta \phi_{k-1}^T + \Delta \phi_{k-1} U_{k-1} \Delta \phi_{k-1}^T \\ &\quad + G_{k-1} Q_{k-1} G_{k-1}^T \end{aligned} \quad (C-39)$$

Note that the propagation of the true covariance  $P$  does not explicitly depend on  $Q^*$ . By contrast, the covariance as calculated by the filter (computed covariance) is given by

$$P_k^* = \phi_{k-1}^* P_{k-1}^* \phi_{k-1}^{*T} + G_{k-1}^* Q_{k-1}^* G_{k-1}^{*T}$$

The computed covariance is therefore a function of  $Q^*$ .

Similar equations can be derived for a measurement update. The estimate of  $x^*$  after a measurement is given by

$$\hat{x}_k^{**} = \hat{x}_k^{*-} + K_k^* [z_k - H_k^* \hat{x}_k^{*-}]$$

where  $K_k^*$  is the gain used by the filter. The error in the estimate is given by

$$\tilde{x}_k^+ = W^{-1} \hat{x}_k^{**} - x_k$$

$$\tilde{x}_k^+ = W^{-1} \hat{x}_k^{*-} + W^{-1} K_k^* [z_k - H_k^* \hat{x}_k^{*-}] - x_k$$

$$\begin{aligned}
 \hat{x}_k^+ &= W^{-1} \hat{x}_k^{*-} - x_k - W^{-1} K_k^* H_k^* W W^{-1} \hat{x}_k^{*-} \\
 &+ W^{-1} K_k^* H_k^* W x_k - W^{-1} K_k^* H_k^* W x_k \\
 &+ W^{-1} K_k^* H_k^* x_k + W^{-1} K_k^* v_k \\
 \hat{x}_k^+ &= \hat{x}_k^- - K_{W_k}^* H_{W_k}^* \hat{x}_k^- - K_{W_k}^* \Delta H_k x_k + K_{W_k}^* v_k
 \end{aligned} \tag{C-40}$$

where

$$\begin{aligned}
 H_{W_k}^* &= H_k^* W \\
 K_{W_k}^* &= W^{-1} K_k^* \\
 \Delta H_k &= H_{W_k}^* - H_k
 \end{aligned}$$

Augmenting the state vector as before

$$x_k^+ = \begin{pmatrix} \hat{x}_k^+ \\ x_k \end{pmatrix}$$

and taking the mean square value of  $x_k^+$ , we can use Equations C-26, C-28, C-37, and C-40 to obtain

$$\begin{aligned}
 U_k^+ &= U_k^- \\
 V_k^+ &= V_k^- (I - K_{W_k}^* H_{W_k}^*)^T - U_k^- \Delta H_k^T K_{W_k}^{*T} \\
 P_k^+ &= (I - K_{W_k}^* H_{W_k}^*) P_k^- (I - K_{W_k}^* H_{W_k}^*)^T \\
 &- (I - K_{W_k}^* H_{W_k}^*) V_k^{-T} \Delta H_k^T K_{W_k}^{*T} \\
 &- K_{W_k}^* \Delta H_k V_k^- (I - K_{W_k}^* H_{W_k}^*)^T
 \end{aligned} \tag{C-41}$$

$$\begin{aligned}
 &+ K_{W_k}^* \Delta H_k U_k^- \Delta H_k^T K_{W_k}^{*T} \\
 &+ K_{W_k}^* R_k K_{W_k}^{*T}
 \end{aligned}$$

Note that the measurement update of  $P$  does not explicitly depend upon  $R^*$ . However, Equation C-41 does implicitly involve  $R^*$  and  $Q^*$  if the gain  $K^*$  is chosen to be a function of these quantities. Note that if  $x^* = x$  (i.e.,  $W = I$ ) and the correct dynamics are implemented ( $\Delta H = \Delta \phi = 0$ ), then Equations C-39 and C-41 reduce to the standard form for the optimal Kalman filter.

If the filter state  $x^*$  is formed by deleting states from the full state vector  $x$ , then the covariance  $P$  can be expressed in terms of the retained states  $s$  and the deleted states  $b$ :

$$\begin{aligned}
 P &= E \{ \tilde{x} \tilde{x}^T \} = E \left\{ \begin{bmatrix} \tilde{x}^* \\ -\tilde{s} \end{bmatrix} \begin{bmatrix} \tilde{x}^* \\ -\tilde{s} \end{bmatrix}^T \right\} \\
 P &= \begin{pmatrix} E \left[ (\tilde{x}^* - s)(\tilde{x}^* - s)^T \right] & E \left[ -(\tilde{x}^* - s)b^T \right] \\ E \left[ -b(\tilde{x}^* - s)^T \right] & E \left[ bb^T \right] \end{pmatrix}
 \end{aligned}$$

Defining  $P_1, P_2, P_3$  by

$$\begin{aligned}
 P_1 &= E \left[ (\tilde{x}^* - s)(\tilde{x}^* - s)^T \right] \\
 P_2 &= E \left[ -b(\tilde{x}^* - s)^T \right] \\
 P_3 &= E \left[ bb^T \right]
 \end{aligned}$$

# LOGICON

the covariance P is seen to be given by

$$P = \begin{pmatrix} P_1 & P_2^T \\ P_2 & P_3 \end{pmatrix}$$

Equations C-39 and C-41 provide the full covariance matrix P and are equivalent to propagating a  $2n \times 2n$  matrix. For large n this can require excessive computer time and memory. Often one is interested only in the quantity  $P_1$ . In this case, it is possible to formulate equations which require propagation of an  $(n + \ell) \times (n + \ell)$  matrix where  $\ell$  is the order of  $x^*$ . This can result in significant savings if most states in the state vector are to be deleted.

Define the following:

$$G_{W_k} = W G_k$$

$$\bar{x}_k' = \bar{x}_k^* - W x_k$$

$$\Delta \phi_k' = \phi_k^* W - W \phi_k$$

$$\Delta H_k' = H_k^* W - H_k = \Delta H_k$$

$$P' = E(\bar{x}' \bar{x}'^T)$$

$$V' = E(x \bar{x}'^T)$$

$$U' = E(x x^T) = U$$

$$\phi = \begin{pmatrix} P' & V'^T \\ V' & U' \end{pmatrix}$$

## LOGICON

The covariance of the retained states can be derived as before. Since the method has already been presented, only the results are given here.

The initial condition, before an estimate of the state is performed, is given by

$$V_0' = -U_0' W^T$$

$$P_0' = W U_0' W^T$$

The covariance is propagated in time by

$$U_k' = \phi_{k-1} U_{k-1}' \phi_{k-1}^T + G_{k-1} Q_{k-1} G_{k-1}^T \quad (C-42)$$

$$V_k' = \phi_{k-1} V_{k-1}' \phi_{k-1}^{*T} + \phi_{k-1} U_{k-1}' \Delta \phi_{k-1}'^T - G_{k-1} Q_{k-1} G_{W_{k-1}}^T$$

$$\begin{aligned} P_k' &= \phi_{k-1}^* P_{k-1}' \phi_{k-1}^{*T} + \Delta \phi_{k-1}' V_{k-1}' \phi_{k-1}^{*T} \\ &\quad + \phi_{k-1}^* V_{k-1}'^T \Delta \phi_{k-1}'^T + \Delta \phi_{k-1}' U_{k-1}' \Delta \phi_{k-1}'^T \\ &\quad + G_{W_{k-1}} Q_{k-1} G_{W_{k-1}}^T \end{aligned}$$

The measurement update is given by

$$U_k'^+ = U_k'^-$$

$$V_k'^+ = V_k'^- (I - K_k^* H_k^*)^T - U_k' \Delta H_k'^T K_k^{*T}$$

$$\begin{aligned} P_k'^+ &= (I - K_k^* H_k^*) P_k'^- (I - K_k^* H_k^*)^T \\ &\quad - (I - K_k^* H_k^*) V_k'^-{}^T \Delta H_k'^T K_k^{*T} \\ &\quad - K_k^* \Delta H_k' V_k'^- (I - K_k^* H_k^*)^T \end{aligned}$$

# LOGICON

$$+ K_k^* \Delta H_k^T U_k - \Delta H_k^T K_k^{*T} \\ + K_k^* R_k K_k^{*T}$$

In summary, the following equations can be used to propagate the full suboptimal filter covariance:

Initialize with

$$U_0 = P_0$$

$$V_0 = -P_0$$

(The initialization assumes no prior estimate of the state.)

Propagate in time by

$$U_k = \phi_{k-1} U_{k-1} \phi_{k-1}^T + G_{k-1} Q_{k-1} G_{k-1}^T \\ V_k = \phi_{k-1} V_{k-1} \phi_{k-1}^{*T} + \phi_{k-1} U_{k-1} \Delta \phi_{k-1}^T - G_{k-1} Q_{k-1} G_{k-1}^T \\ P_k = \phi_{k-1}^* P_{k-1} \phi_{k-1}^{*T} + \Delta \phi_{k-1} V_{k-1} \phi_{k-1}^{*T} \\ + \phi_{k-1}^* V_{k-1}^T \Delta \phi_{k-1}^T + \Delta \phi_{k-1} U_{k-1} \Delta \phi_{k-1}^T \\ + G_{k-1} Q_{k-1} G_{k-1}^T$$

Update after a measurement by

$$U_k^+ = U_k^-$$

$$V_k^+ = V_k^- (1 - K_{W_k}^* H_{W_k}^{*T})^T - U_k^- \Delta H_k^T K_{W_k}^{*T}$$

# LOGICON

$$\begin{aligned}
 P_k^+ &= (I - K_{W_k}^* H_{W_k}^*) P_k^- (I - K_{W_k}^* H_{W_k}^*)^T \\
 &\quad - (I - K_{W_k}^* H_{W_k}^*) V_k^- T \Delta H_k^T K_{W_k}^{*T} \\
 &\quad - K_{W_k}^* \Delta H_k V_k^- (I - K_{W_k}^* H_{W_k}^*)^T \\
 &\quad + K_{W_k}^* \Delta H_k U_k^- \Delta H_k^T K_{W_k}^{*T} \\
 &\quad + K_{W_k}^* R_k K_{W_k}^{*T}
 \end{aligned}$$

Similar equations can be used to propagate the covariance of the states retained by the filter.

**APPENDIX C  
REFERENCE**

- C-1.     Gelb, Arthur, "Applied Optimal Estimation," MIT Press,  
          Cambridge, 1974.

APPENDIX D  
LINEAR REGULATOR GUIDANCE

In this appendix the results of the analysis of the application of Linear Regulator theory to the problem of steering an aerodynamically controlled maneuvering re-entry vehicle are described.

In Section D-1 a steering law and a methodology for the selection of the associated weighting matrices are derived using time as the system variable of evolution.

In Section D-2 the use of a state variable as the variable of evolution is investigated. A steering law formulation for this case is derived and simulation results presented.

In Section D-3 the use of transformations depending on the instantaneous vehicle state to define the evolutionary variable are considered and the mathematical theory of Appendix D-2 modified to incorporate this case.

## D-1. CONTROLLERS IN THE TIME DOMAIN

In this section controllers operating in the time domain are considered. A controller based on the Linear Quadratic Regulator is derived and the stability and controllability properties are examined. The analysis of these properties leads to a methodology based on these properties for the selection of the weighting matrices associated with the regulator formulation.

### D-1.1 Time Domain System Description

For the present studies the vehicle is assumed to be a bank-to-turn vehicle which orients the acceleration vector by changing the vehicle bank angle. The target centered coordinate system and the trajectory and vehicle orientation angles are as shown in Figure D-1.

#### D-1.1.1 Trajectory Equations

The nonlinear dynamic equations of motion for the vehicle are:

$$\begin{aligned}
 \dot{x} &= V \cos \gamma \cos \psi \\
 \dot{y} &= V \cos \gamma \sin \psi \\
 \dot{z} &= V \sin \gamma \\
 \dot{\gamma} &= \frac{A \cos \phi}{V} + \frac{g \cos \gamma}{V} \\
 \dot{\psi} &= \frac{A \sin \phi}{V \cos \gamma} \\
 \dot{V} &= -\frac{D}{m} + g \sin \gamma \\
 \dot{A} &= -a A + a A_c \\
 \dot{\phi} &= -b \phi + b \phi_c
 \end{aligned}
 \tag{D-1}$$

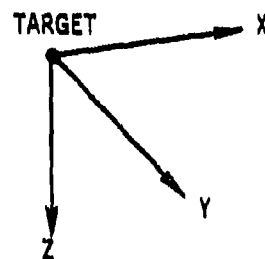
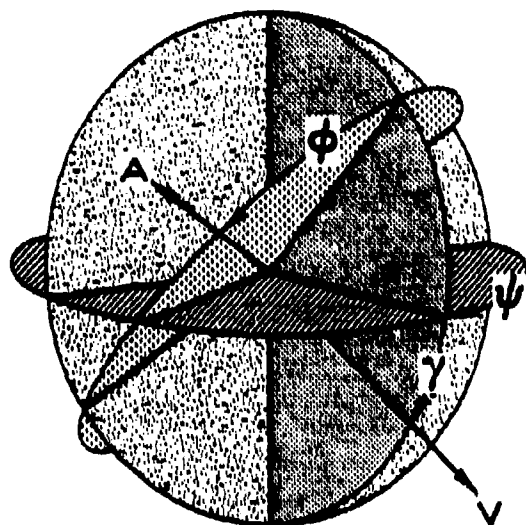


Figure D-1. Definition of Coordinate Systems

where  $A_c$  is the commanded acceleration and  $A$  is the actual acceleration, and where  $\varphi$  is the actual bank angle and  $\varphi_c$  is the commanded bank angle.  $a$  and  $b$  are the autopilot corner frequencies.

The assumptions in (D-1) are constant gravity ( $g$ ) and flat, nonrotating earth. The drag force  $D$  is a function of angle of attack, Mach number, and altitude.

#### D-1.1.2 Approximate Trajectory Model

In previous studies it has been found that the velocity,  $V$ , behaves in such a manner that the difference between it and the nominal velocity can be ignored. So in the approximate model the  $\dot{V}$  equation will not be used, and whenever  $V$  is needed in the other equations, it will be replaced by the nominal velocity,  $V_N$ . This approximation follows since  $V$  is a slowly varying monotonically decreasing variable, and the PGRV has no direct control over velocity magnitude (i.e., no thrust or braking). Also it is assumed that the gravity force is negligible in comparison to the lateral acceleration force for the PGRV maneuvers. These approximations reduce Equations (D-1) to the following equation set:

$$\begin{aligned}
 \dot{x} &= V_N \cos \gamma \cos \psi \\
 \dot{y} &= V_N \cos \gamma \sin \psi \\
 \dot{z} &= V_N \sin \gamma \\
 \dot{\gamma} &= \frac{A \cos \phi}{V_N} \\
 \dot{\psi} &= \frac{A \sin \phi}{V_N \cos \gamma} \\
 \dot{A} &= -aA + aA_c \\
 \dot{\phi} &= -b\phi + b\phi_c
 \end{aligned}
 \tag{D-2}$$

For convenience, let us denote (D-2) by

$$\begin{aligned}\dot{\xi}(t) &= f(\xi(t), u(t)) \quad ; \quad t_0 \leq t \leq t_f \\ \xi(t_0) &= \xi_0\end{aligned}\tag{D-3}$$

where  $\xi$  is a vector of seven components given in (D-2) and  $u(t)$  is the vector actuating signal given by

$$u(t) = \begin{bmatrix} A_c(t) \\ \phi_c(t) \end{bmatrix}\tag{D-4}$$

The vector function  $f$  can be identified from (D-2).

Corresponding to a nominal value for  $u$ , say  $u_n$ , there is a solution to (D-3) which gives the associated nominal trajectory. Denote by  $(x_n, u_n)$  the nominal vehicle trajectory and control, with  $x_n(t)$ ;  $t_0 \leq t \leq t_f$  the solution to (D-3) corresponding to the open-loop control  $u_n(t)$ ;  $t_0 \leq t \leq t_f$ . We will suppose that  $u_n$  satisfies all the constraints placed upon the input and that  $x_n$  satisfies both the path and terminal constraints placed upon the vehicle trajectory.

The actual trajectory of the vehicle will deviate from the nominal for an assortment of reasons. The controller output may be  $u_p$  instead of  $u_n$ ; the trajectory may begin at a point not equal to  $\xi_0$ ; the differential equation of describing the vehicle motion may differ from (D-3) in some way; etc. Denote the actual vehicle motion by  $x_p$  and the actual control signal by  $u_p$ . The deviation in trajectory and control is given by the pair  $(x, u)$  where

$$\begin{aligned}x &= x_p - x_n \\ u &= u_p - u_n\end{aligned}\tag{D-5}$$

## LOGICON

Since  $x$  and  $u$  represent deviations from the ideal trajectories given by  $(x_n, u_n)$ , it is natural to try to make them as small as possible. Unfortunately,  $(x, u)$  is a vector time function and pointwise minimization is impossible. Furthermore, since  $(x, u)$  represent all of the vehicle characteristics unmodeled by (D-3), the dynamics of the perturbation variables are difficult to quantify.

Certain assumptions and approximations make the problem simpler to solve. It will be assumed that (D-3) represents the vehicle dynamics and there is an error in the starting point of the trajectory; i.e., the initial condition on  $x_p$  differs from  $x_n$ .

$$x_p(t_0) \neq x_n(t_0)$$

Further  $(x, u)$  will be assumed to be small enough that the dynamical equations of the perturbation variables are given to an adequate degree of closeness by

$$\begin{aligned} \dot{x} &= Fx + Gu & t_0 \leq t \leq t_f \\ x(t_0) &= x_p(t_0) - x_n(t_0) \end{aligned} \tag{D-6}$$

where

$$F = \left. \frac{\partial f}{\partial x} \right|_{(x_n, u_n)} ; \quad G = \left. \frac{\partial f}{\partial u} \right|_{(x_n, u_n)} \tag{D-7}$$

For the system described in (D-2) F and G are given by \*

$$F = \begin{bmatrix} 0 & F_{12} \\ 0 & F_{22} \end{bmatrix} \quad , \quad G = \begin{bmatrix} 0 & 0 \\ \vdots & \vdots \\ a & 0 \\ 0 & b \end{bmatrix} \quad (D-8)$$

where

$$F_{12} = \begin{bmatrix} -V \sin \gamma \cos \psi & -V \cos \gamma \sin \psi & 0 & 0 \\ -V \sin \gamma \sin \psi & V \cos \gamma \cos \psi & 0 & 0 \\ V \cos \gamma & 0 & 0 & 0 \end{bmatrix} \quad (D-9)$$

$$F_{22} = \begin{bmatrix} 0 & 0 & -V^{-1} \cos \phi & V^{-1} A \sin \phi \\ \frac{A \sin \phi \sin \gamma}{V \cos^2 \gamma} & 0 & \frac{\sin \phi}{V \cos \gamma} & \frac{A \cos \phi}{V \cos \gamma} \\ 0 & 0 & -a & 0 \\ 0 & 0 & 0 & -b \end{bmatrix} \quad (D-10)$$

All of the control and trajectory variables are evaluated on the nominal trajectory. The matrix F is time variable on the trajectories of interest, but the accelerations are such that the variation is "slow".

#### D-1.2 Time Domain Controller Definition

There are several properties which the controller should possess. First, it should be a full state feedback policy. Further the control algorithm must have a simple structure. Linear control rules provide a large class of easy to mechanize controllers and attention will be restricted to this class. The closed-loop system must be asymptotically stable about the nominal trajectory and must follow the nominal with small errors. In

\*To simplify notation the dimensions of null and identity matrices will not be given if obvious from the context.

addition it is desirable that the controller be robust in the sense that if the dynamic equation of perturbation variables differs from that given in (D-6), the closed-loop system response will still be satisfactory.

To produce a suitable controller, an index of controller performance will be introduced. Since  $x_p$  should track  $x_n$  as closely as possible,  $x$  should be minimized. To measure the closeness in tracking at time  $t$  a quadratic weighting will be used;  $x(t)'Q(t)x(t)$ ; where  $Q$  is positive semidefinite symmetric ( $Q \geq 0$ ). To minimize the deviation in control from that required on the nominal trajectory a quadratic measure will also be used;  $u(t)'R(t)u(t)$  with  $R > 0$  (the specific value of  $R$  is given in Reference D-1). Finally terminal miss will also be weighted in the performance index with a quadratic term;  $x(t_f)'P_f x(t_f)$  with  $P_f \geq 0$ . The full performance index is the generalized sum of the weightings at all of the time points along the trajectory;

$$J = x(t)'P_f x(t) + \int_{t_0}^{t_f} [x'(t)Q(t)x(t) + u'(t)R(t)u(t)] dt \quad (D-11)$$

It is well known from linear regulator theory that the control policy which is best with respect to the indicated measure of performance is given by

$$u = -R^{-1}G'Px \quad (D-12)$$

with

$$\begin{aligned} \dot{P} &= -F'P - PF + PGR^{-1}G'P - Q \\ P(t_f) &= P_f \end{aligned} \quad (D-13)$$

The control policy given by (D-11) has many of the properties considered to be desirable in this application. It is linear with time variable gains. Furthermore, the system is stable if the model (D-6) satisfies

## LOGICON

---

certain technical conditions which will be considered in detail in later sections of this appendix.

Furthermore, (D-12) is robust control. Suppose that the true representation for  $x$  should satisfy an equation of the form

$$\begin{aligned}\dot{x} &= \tilde{F}x + \tilde{G}u + w \\ x(t_0) &= x_p(t_0) - x_n(t_0)\end{aligned}\tag{D-14}$$

where  $w$  is a high frequency random disturbance and the coefficient matrices  $(\tilde{F}, \tilde{G})$  differ slightly from  $(F, G)$  given by (D-7). The random forcing term  $w$  could represent the influence of turbulence, atmospheric inhomogeneities, unmodeled high frequency vehicle dynamics, etc. The elements in the coefficient matrix may change because of changes in the lift and drag coefficients, etc. It is well known that even in the presence of unmodeled high frequency disturbances, the linear feedback control given by (D-12) performs the path following and stabilization functions in the best possible way. In addition, this controller gives the closed loop system the property of having a uniformly smaller sensitivity to parameter variations than that exhibited by the open-loop system.

The control policy given by (D-12) has many favorable attributes in the application under study. The general form given by (D-12) and (D-13) is broad enough to include all of the controllers which might reasonably be studied at this stage in the investigation. The fundamental problem in design is the selection of the appropriate weighting matrices in the performance index. This choice must be made judiciously in order to simultaneously provide adequate path following performance and a terminal miss within specified bounds.

D-1.3 Selection of Weighting Matrices

Although the controller given by (D-11) has all of the previously listed attributes for any permissible choice of (P,Q,R), system performance may still be unsatisfactory. For example, although the closed-loop system is asymptotically stable, it may be inadequately damped. Effecting changes in the closed-loop damping is accomplished by modifying the weighting matrices of (D-11), but unfortunately it is not immediately evident how (P,Q,R) should be changed.

For some purposes it is more convenient to study vehicle motion in a rotated coordinate system. Let T be the coordinate transformation given by

$$T = \begin{pmatrix} T_{11} & 0 \\ 0 & I \end{pmatrix} \quad (D-15)$$

where

$$T_{11} = \begin{pmatrix} \cos \gamma \cos \psi & \cos \gamma \sin \psi & \sin \gamma \\ -\sin \psi & \cos \psi & 0 \\ -\sin \gamma \cos \psi & -\sin \gamma \sin \psi & \cos \gamma \end{pmatrix}$$

It can easily be shown that if we let z represent the perturbed state in the rotated coordinate system; i.e.,

$$z = Tx \quad (D-16)$$

then (see Reference D-3, (A-3) and Reference D-3)

$$\dot{z} = F_z z + Gu \quad (D-17)$$

where

$$F_z = \begin{bmatrix} 0 & \dot{\psi} \cos \gamma & \dot{\gamma} & 0 & 0 & 0 & 0 \\ -\dot{\psi} \cos \gamma & 0 & \dot{\psi} \sin \gamma & 0 & V \cos \gamma & 0 & 0 \\ -\dot{\gamma} & -\dot{\psi} \sin \gamma & 0 & V & 0 & 0 & 0 \\ 0 & 0 & 0 & 0 & 0 & -V^{-1} \cos \psi & -VA \sin \psi \\ 0 & 0 & 0 & \frac{A \sin \psi \sin \gamma}{V \cos^2 \gamma} & 0 & \frac{\sin \psi}{V \cos \gamma} & \frac{A \cos \psi}{V \cos \gamma} \\ 0 & 0 & 0 & 0 & 0 & -a & 0 \\ 0 & 0 & 0 & 0 & 0 & 0 & -b \end{bmatrix}$$

This change in state variable representation resolves the vehicle motion into a component along the velocity vector\*  $z_1$ , an orthogonal component in the plane of the motion  $z_3$ , and third component perpendicular to the plane of vehicle motion  $z_2$ .

The uncontrolled system given by (D-17) has anomalous stability properties. To illustrate these, consider the case in which the coefficients in  $(F_z, G)$  are slowly varying, i.e.,

$\dot{\gamma}, \dot{\psi}, \dot{\phi}$  are small

$A, V$  are constant.

The stability of the open-loop system is partially characterized by the open-loop poles which are in turn given by the eigenvalues of  $F_z$ . Direct calculation (see Reference D-2, (23)) shows that these eigenvalues  $\{\lambda_i\}$  are located at points given by

$$\{\lambda_i\} = \{0, 0, 0, \pm j \sqrt{\dot{\psi}^2 + \dot{\gamma}^2}, -a, -b\} \quad (D-18)$$

\* If  $z$  is a vector,  $z_i$  is its  $i$ th component. The vector  $\bar{z}_i$  is a unit vector in the  $i$ th direction.

Only those poles attributable to the autopilot are in the left half plane. The poles of the vehicle are all on the imaginary axis and indeed there are five poles very near the origin. While a system with poles given by (D-18) could, under very unusual conditions be stable, it could never be asymptotically stable. Only through feedback can the system be made asymptotically stable.

Because of the lack of open-loop damping, the existence of a feedback controller which will stabilize the closed-loop system depends upon the satisfaction of a technical condition on  $[F_z, G]$ . The condition is called controllability. A controllable system is one in which any initial error can be eliminated with a linear feedback control law in an arbitrarily short time\*. The property of a controllable system of relevance here is that if  $[F_z, G]$  is controllable then the closed-loop system given by (D-6) and (D-12) is asymptotically stable.

Under the assumption that the coefficient matrices are sufficiently smooth, an algebraic condition for controllability can be deduced. Define the matrix sequence  $\{M_k(t)\}$  by

$$M_0(t) = G(t) \tag{D-19}$$

$$M_{k+1}(t) = -F(t)M_k(t) + \dot{M}_k(t); k = 0, 1, \dots$$

Then let

$$C_j(t) = [M_0, M_1, \dots, M_{j-1}] \tag{D-20}$$

\* This is actually a strong form of controllability, but this definition will suffice for the system under study here.

## LOGICON

The system described by (D-6) is instantaneously controllable if  $\text{rank } C_n(t) = n$ .

The matrix  $C_n(t)$  given by (D-20) bears striking resemblance to the controllability matrix  $\bar{C}_n$  for a time invariant system. Indeed it is easy to see that

$$\text{rank } C_n(t) = \text{rank } [G, F_z G, \dots, F_z^{n-1} G]$$

if  $[F_z, G]$  is a constant matrix.

In Reference D-2 both  $\bar{C}_n$  and  $C_n$  were studied and it was shown that

$$\text{rank } \bar{C}_n = 6 \quad (\text{D-21a})$$

$$\text{rank } C_n(t) = 7 \quad (\text{D-21b})$$

The implication of (D-21) is important in this application. Equation (D-21b) is sufficient to guarantee that closed-loop system guidance law displayed in (D-12) is asymptotically stable for appropriately restricted weightings in (D-11). Equation (D-21a) indicates that the degree of stability may be inadequate. To see why this is so, a careful study of the implications of uncontrollability is required. The state space of linear system may always be decomposed into a set of states or modes that are controllable and a residual set which are uncontrollable. These former modes are always stabilizable by linear feedback while the latter are unaffected by linear feedback. If the uncontrolled modes are not asymptotically stable the closed-loop system will not be asymptotically stable either.

The system in question is controllable but for any fixed time say  $t^*$  the matrices  $[F_z(t^*), G(t^*)]$  do not satisfy the conditions for time invariant controllability. The system could be described as being locally

uncontrollable mode which rotates with time. Detailed analysis shows that the locally uncontrollable direction in state space rotates among the eigenvectors of  $F_z(t)$  which have zero damping. The system is then said to be locally nonstabilizable in the sense that for every fixed  $t$ , the constant matrix  $[F_z, G]$  is not stabilizable. If  $[F_z, G]$  were a rapidly varying function of time, no adverse effect would be expected from these local properties. Unfortunately, the nominal trajectory considered for this vehicle results in very slowly varying dynamic matrices in (D-6). It is to be expected, therefore, that the closed-loop system will exhibit peculiarities normally associated with uncontrollable systems.

The above qualitative discussion can be made more precise by reference to  $C_j(t)$ . Denote by  $\mathcal{N}_j$  the set of vectors in  $R^7$  orthogonal to both columns of  $M_j$ ; i.e.

$$\mathcal{N}_j(t) = \{z: z \in R^7, z'M_j(t) = [0, 0]\}$$

and let  $\bar{\mathcal{N}}_j(t)$  be its complement. Define the positive definite matrix  $W(t_1, t_2)$  by

$$W(t_1, t_2) = \int_{t_1}^{t_2} \phi_z(t_1, \tau) G(\tau) R^{-1}(\tau) G'(\tau) \phi_z'(t_1, \tau) d\tau$$

where  $\phi_z$  is the transition matrix of  $F_z$ . It can be shown (Reference D-3) that if  $z(t_1)$  is an eigenvector of  $W(t_1, t_1 + \Delta)$  and if

$$z(t_1) \in \bigcup_{R=0}^{i-1} \mathcal{N}_R \cap \bar{\mathcal{N}}_i, \text{ then for small } \Delta, z(t_1) \text{ can be transferred to the}$$

origin with control energy proportional to  $\Delta^{-(1+2i)}$ . The implication of this result is important. For example, if  $z(t_0)$  is a linear combination of columns of  $G$ , the error can be eliminated by direct action of  $u$  and the energy is proportional to  $\Delta^{-1}$ . Moreover, if  $z_\alpha$  and  $z_\beta$  are orthogonal eigenvectors of  $W(t_0, t_0 + \Delta)$  and if  $z_\alpha' M_j(t_0) = [w_1, 0]$ ,

## LOGICON

$z_B^{M_j}(t_0) = [0, w_2]$ , then the energy required to transfer  $z_\alpha$  to the origin is, for small  $\Delta$ ,  $\left(\frac{w_2}{w_1}\right)^2$  times that required to cause a similar

transfer of  $z_\beta$  to the origin. The direction  $z_\beta$  is said to be more controllable than  $z_\alpha$  by the factor  $\left|\frac{w_2}{w_1}\right|$ . Clearly if  $z(t) \in \eta_j(t)$  for all  $(j, t)$ , it can not be transferred to the origin at all.

Applying these considerations to the system described by (D-17) some rather interesting system properties can be deduced. Assuming that the system coefficient matrices are slowly varying, that  $\dot{\psi} \ll \dot{\gamma}$ , that  $a=b$  and that  $\psi_{nom} = 180^\circ$  it is shown in Reference D-3 that to first order

- C1.  $(\bar{z}_6, \bar{z}_7) \in \bar{\eta}_0$  and  $\bar{z}_6$  and  $\bar{z}_7$  are equally controllable
- C2.  $(\bar{z}_5, \bar{z}_4) \in \bar{\eta}_1 \cap \eta_0$  and  $\bar{z}_5$  is more controllable than  $\bar{z}_4$  by the factor  $A(\cos \gamma)^{-1}$
- C3.  $(\bar{z}_3, \bar{z}_2) \in \bar{\eta}_2 \cap \eta_0 \cap \eta_1$  and  $\bar{z}_2$  is more controllable than  $\bar{z}_3$  by the factor  $A$
- C4.  $\bar{z}_1 \in \eta_3 \cap \eta_2 \cup \eta_1 \cup \eta_1$  and the energy required to eliminate errors in  $\bar{z}_1$  is proportional to  $\dot{\gamma}^{-2}$

Relations C1 through C4 provide measures of the relative controllability of pairs of modes of the system. They are based upon  $u(t)'u(t)$  as the power measure. The components of  $u$  are actually related to different physical quantities and a better weighting for power would probably be  $u'Ru$ . Such a power weighting measures not only the magnitude of the components of the actuating signal but also minimizes them with respect

## LOGICON

to their permissible size.

Since  $R > 0$ , (D-6) can be written in the form

$$\dot{x} = Fx + GR^{-\frac{1}{2}} (R^{\frac{1}{2}}u) \quad (D-22)$$

As (D-22) makes clear, the controllability indices given in C1-C4 can be modified to provide controllability with respect to  $u^T R u$  if  $GR^{-\frac{1}{2}}$  is used in (D-19) instead of  $G$ . This is easily done when  $R$  is given by

$$R = \text{diag} \left( \frac{1}{\Delta A_{\max}^2}, \frac{1}{\Delta \phi_{\max}^2} \right) \quad (D-126)$$

where  $\Delta A_{\max}$  and  $\Delta \phi_{\max}$  are the maximum permissible magnitude variations in the actuating signals.

It can be shown that C1-C4 become

C1'.  $\bar{z}_6$  and  $\bar{z}_7$  are equally controllable

C2'.  $\bar{z}_5$  is more controllable than  $\bar{z}_4$  by the factor

$$\frac{A \Delta \phi_{\max}}{\Delta A_{\max} \cos \gamma} = \lambda_1$$

C3'.  $\bar{z}_2$  is more controllable than  $\bar{z}_3$  by the factor

$$\frac{A \Delta \phi_{\max}}{\Delta A_{\max}} = \lambda_2^{-1}$$

C4'. The energy required to eliminate errors in  $\bar{z}_1$  is proportional to  $\dot{\gamma}^{-2}$

## LOGICON

With the relation given in C1' -C4' we are in a position to make a judicious choice of the state weighting matrices P and Q. Since the conditions are stated in the z-coordinate system, the weighting matrices  $P_z$  and  $Q_z$  corresponding to this coordinate system will be found first.

The states  $z_6$  and  $z_7$  are autopilot states and there are no penalties associated with their variation. Consequently a reasonable choice for their weighting would be

$$(Q_z)_{66} = (Q_z)_{77} = 0 \quad (D-24)$$

The states  $z_4$  and  $z_5$  are flight path and azimuth errors, respectively. Suppose these errors are required to stay within nominal bounds given by  $q_2$ ; i.e.,

$$\max_t \left( z_4^2 + z_5^2 \right) \leq \frac{2}{q_2^2} \quad (D-25)$$

The usual rule-of-thumb for selecting  $(Q_z)_{44}$  and  $(Q_z)_{55}$  would be

$$(Q_z)_{44} = (Q_z)_{55} = q_2^2$$

Suppose  $\lambda_1 > 1$ . Then  $z_5$  is easier to control than  $z_4$  by the factor  $\lambda_1$ . For equal initial errors, the residual error in  $z_4$  at times greater than  $t_0$  will tend to dominate that in  $z_5$  because of the difficulty in applying effort to  $z_4$ . To cause the closed-loop damping in these two modes to be more nearly the same, a heavier weight should be assigned to  $z_4$ . The weighting of  $z_4$  will be increased by the factor  $\lambda_1$  while maintaining the same overall angular deviation; i.e.,

$$(Q_z)_{44}^2 + (Q_z)_{55}^2 = 2 q_2^2 ; \quad \frac{(Q_z)_{44}}{(Q_z)_{55}} = \lambda_1^2$$

This yields

(D-26)

$$(Q_z)_{44} = \frac{2 \lambda_1^2}{1 + \lambda_1^2} q_2^2 ; \quad (Q_z)_{55} = \frac{2}{1 + \lambda_1^2} q_2^2$$

It is readily apparent that (D-26) provides suitable weightings when  $\lambda_1 \leq 1$  as well.

The important trajectory variables are  $z_2$  and  $z_3$  which measure errors orthogonal to the nominal trajectory. Reasoning as we did in the previous paragraph if

$$\max_t (z_2^2 + z_3^2) \leq \frac{2}{q_1^2} \quad (D-27)$$

then

$$(Q_z)_{22} = \frac{2 \lambda_2^2}{1 + \lambda_2^2} q_1^2 ; \quad (Q_z)_{33} = \frac{2}{1 + \lambda_2^2} q_1^2 \quad (D-28)$$

The final state variable measures motion along the nominal velocity vector. As C4' indicates errors in this direction are quite difficult to control. Errors in  $z_1$  require energy proportional to  $\dot{Y}^{-2}$  to correct and  $\dot{Y}$  is fairly small in this problem. It is easy to see the physical cause of the difficulty in controlling  $z_1$ . Neither normal acceleration nor bank angle commands create any first order change in tangential velocity. If the flight path angle were constant ( $\dot{Y} = 0$ ) errors along the velocity vector could not be eliminated (the system is not stabilizable). Since  $\dot{Y} \neq 0$  we have some control over  $z_1$ . This is accomplished by shortening or lengthening the turning radius of the vehicle. To

## LOGICON

accomplish regulation of path length, sizable amounts of control force are required to produce small variations in  $z_1$ . Because of this very weak coupling between  $u$  and  $z_1$ , if  $z_1$  has a weighting in  $Q_z$ ,  $u$  will have a tendency to give excessive attention to this error.

If the absolute time of evolution along the trajectory is of little concern, the system can be made insensitive to tangential errors by making  $(Q_z)_{11} = 0$ . In this specific application this is a reasonable choice since terminal impact performance is of primary concern.

The final form of  $Q_z$  is then:

$$Q_z = \text{diag} \left( 0, \frac{2\lambda_2^2}{1+\lambda_2^2} q_1^2, \frac{2}{1+\lambda_2^2} q_1^2, \frac{2\lambda_1^2}{1+\lambda_1^2} q_2^2, \frac{2q_2^2}{1+\lambda_1^2}, 0, 0 \right) \quad (D-29)$$

where  $\{\lambda_i\}$  are given in C2' and C4' and  $q_i^2$  are given in (D-25) and (D-28)

For the reasons outlined above, the only terminal errors are those associated with errors perpendicular to the flight path. If

$$z_2(t_f)^2 + z_3^2(t_f) \leq \frac{2}{q_3} \quad (D-30)$$

a reasonable choice of  $P_f$  would be

$$P_{z,f} = \text{diag} \left( 0, \frac{2\lambda_2^2}{1+\lambda_2^2} q_3^2, \frac{2q_3^2}{1+\lambda_2^2}, 0, 0, 0, 0 \right) \quad (D-31)$$

Equations (D-23), (D-29), and (D-31) give the weighting matrices in the z-coordinate system. The actual observations and calculations take place in the x-coordinate system. It is shown in Reference D-2 that an optimization problem in the z-coordinate system with respect to the weighting  $(P_z, Q_z, R_z)$  is equivalent to the optimization problem in the x-coordinate system parameterized by  $(T'P_zT, T'Q_zT, R_z)$ . Using the value of T given in (D-15), it follows that

$$P_f = T'P_{z,f}T$$

$$= \begin{pmatrix} (P_f)_{11} & 0 \\ 0 & (P_f)_{22} \end{pmatrix} \quad (D-32)$$

where  $(P_f)_{11} =$

$$\begin{bmatrix} \frac{2 q_3^3}{1+\lambda_2^2} (\lambda_2^2 \sin^2 \psi + \sin^2 \gamma \cos^2 \psi) & \dots & \dots \\ \frac{2 q_3^2}{1+\lambda_2^2} (-\lambda_2^2 \cos \psi \sin \psi + \sin^2 \gamma \sin \psi \cos \psi) & \frac{2 q_3^2}{1+\lambda_2^2} (\lambda_2^2 \cos^2 \psi + \sin^2 \gamma \sin^2 \psi) & \dots \\ -\frac{2 q_3^3}{1+\lambda_2^2} (\sin \gamma \cos \gamma \cos \psi) & -\frac{2 q_3^2}{1+\lambda_2^2} \sin \gamma \cos \gamma \sin \psi & \frac{2 q_2}{1+\lambda_2^2} \cos^2 \gamma \end{bmatrix} \quad (D-33)$$

$$(P_f)_{22} = 0 \quad (D-34)$$

Similarly,

$$Q = T'Q_zT$$

$$= \begin{pmatrix} Q_{11} & 0 \\ 0 & Q_{22} \end{pmatrix} \quad (D-35)$$

where

$$Q_{11} = \frac{q_2^2}{q_3^2} (P_f)_{11} \quad (D-36)$$

$$Q_{22} = \text{diag} \left( \frac{2 \lambda_1^2}{1 + \lambda_1^2} q_2^2, \frac{2 q_2^2}{1 + \lambda_1^2}, 0, 0 \right) \quad (D-37)$$

Equations (D-23), (D-33), (D-34), (D-36), and (D-37) give the final system weighting matrices for this design problem.

#### D-1.4 An Example

The previous section provides a procedure for selecting the weighting matrices to be used in the synthesis of a vehicle guidance law. To illustrate the utility of these weighting matrices a simple example is useful. In this example two controllers will be compared. The first  $u_1$  will use a modification of the techniques presented above while the second will use weighting matrices which might have been chosen after viewing the open-loop simulation.

To isolate the influence of the coordinate transformations,  $(P, Q, R)$  have been kept as close as possible for the two controllers. Denote the weighting matrices associated with control  $i$  by  $(P_i, Q_i, R_i)$ . Then

$$R_1 = R_2 = \text{diag}(r_1, r_2) \quad (D-38)$$

The scalar  $r_1$  measures the perturbed acceleration along the nominal trajectory. Its calculation is detailed in Reference D-5. Suffice it to say that

$$r_1(t_0) \approx (10)^{-5} ; r_1(t_f) \approx (10)^{-7} \quad (D-39)$$

## LOGICON

with a smooth monotonic variation in between. The perturbation in bank angle was restricted to about  $10^\circ$  and

$$r_2(t) = (.2)^{-2} = 25 \quad (D-40)$$

Equations (D-39) and (D-49) give R for this problem.

The nominal trajectory used

$$\psi(t) = 0 ; A(t) \equiv 1600, 25^\circ \leq \gamma \leq 65^\circ \quad (D-41)$$

From (D-142) - (D-144) we see that

$$\lambda_2 \approx \frac{\Delta A_{\max}}{1.6 \times 10^3 (.2)} \in [1, 8] \quad (D-42)$$

$$\lambda_1 \approx \frac{1.6 \times 10^3 (.2)}{\Delta A_{\max} \cos} \in [1, 2.5] \quad (D-43)$$

Because it is believed that the method of computing  $\Delta A_{\max}$  gives rise to excessively large values, it has been decided to approximate  $\lambda_2$  and  $\lambda_1$  by

$$\lambda_2 = \lambda_1 = 1 \quad (D-44)$$

The choice of  $q_1$  is based upon an allowable position deviation from the nominal of  $6 \times 10^3'$  at  $t_0$  and  $10'$  at  $t_f$ .

$$q_1 = \left[ 6000 - 5990 \frac{(t - t_0)}{(t_f - t_0)} \right]^{-1} \quad (D-45)$$

The weighting on  $x_4$  and  $x_5$  is deduced from permitting  $1^\circ$  of angular deviation in flight; i.e.,

$$q_2 = 57.3$$

Substituting (D-41), (D-44), (D-45), and (D-46) into (D-36)

$$Q_1 = \begin{bmatrix} q_1^2 \sin^2 \gamma & 0 & -q_1^2 \sin \gamma \cos \gamma & 0 & 0 & 0 \\ 0 & q_1^2 & 0 & 0 & 0 & 0 \\ -q_1^2 \sin \gamma \cos \gamma & 0 & q_1^2 \cos^2 \gamma & 0 & 0 & 0 \\ 0 & 0 & 0 & q_2^2 & 0 & 0 \\ 0 & 0 & 0 & 0 & q_3^2 & 0 \\ 0 & 0 & 0 & 0 & 0 & 0 \end{bmatrix} \quad (D-47)$$

Although there is no importance attached to terminal deviations in  $x_4$  and  $x_5$ , for reasons of computational simplicity  $P_1$  was chosen as

$$P_1 = Q_1(t_f) \quad (D-48)$$

Equations (D-38), (D-47), and (D-48) give  $(P_1, Q_1, R_1)$ .

The second controller  $u_2$  is parameterized by the weighting matrices  $(P_2, Q_2, R_2)$ . The matrices  $(P_2, Q_2)$  differ from  $(P_1, Q_1)$  only in that they are not rotated to conform to the z-coordinate system and no penalty is accorded to deviations in the altitude coordinate z. As was observed in Reference D-3, for the trajectory of interest, no penalty on deviations in the altitude yields a zero gain for altitude perturbations.

To compare system performance with the two guidance laws, the results of a simple example are instructive. For the guidance law  $u_1$ , the weightings  $(P_1, Q_1, R_1)$  are given in (D-38), (D-47), and (D-48). For guidance law  $u_2$

$$Q_2 = \begin{bmatrix} q_1^2 & 0 & 0 & 0 & 0 & 0 \\ 0 & q_1^2 & 0 & 0 & 0 & 0 \\ 0 & 0 & 0 & 0 & 0 & 0 \\ 0 & 0 & 0 & q_2^2 & 0 & 0 \\ 0 & 0 & 0 & 0 & q_3^2 & 0 \\ 0 & 0 & 0 & 0 & 0 & 0 \end{bmatrix} \quad (D-49)$$

$$P_2 = Q_2(t_f) ; R_2 = R_1$$

A simple trajectory contained in the  $(x_1, x_3)$  plane was examined;

$$\begin{aligned} x_1(t_0) &= 6 \times 10^3 & x(t_0) &= \text{order } 10^5 \\ x_1(t_0) &= 0 ; i \neq 1 & z(t_0) &= \text{order } 10^5 \\ t_0 &= 0 , t_f = 8 \end{aligned}$$

Some important qualitative features of the system response are shown in Figure D-2. The trajectory associated with control  $u$ , is denoted by  $x_{p1}$ . This figure is not drawn to scale in order that effects attributable to the difference in controllers can be made more apparent.

All of the trajectories begin at the same point but  $x_{p2}$  crosses  $x_n$  and terminates below it. The trajectories have the properties which would be expected from their respective performance indices. The guidance law  $u_1$  reduces the magnitude of the error and rotates its direction so that it is aligned with the velocity vector. The guidance law  $u_2$  on the other hand rotates the error essentially into elevation.

The character of  $x_{p2}$  has one anomaly deserving comment. The matrices  $(P_2, Q_2)$  attach no penalty to shifts in elevation and so it is to be

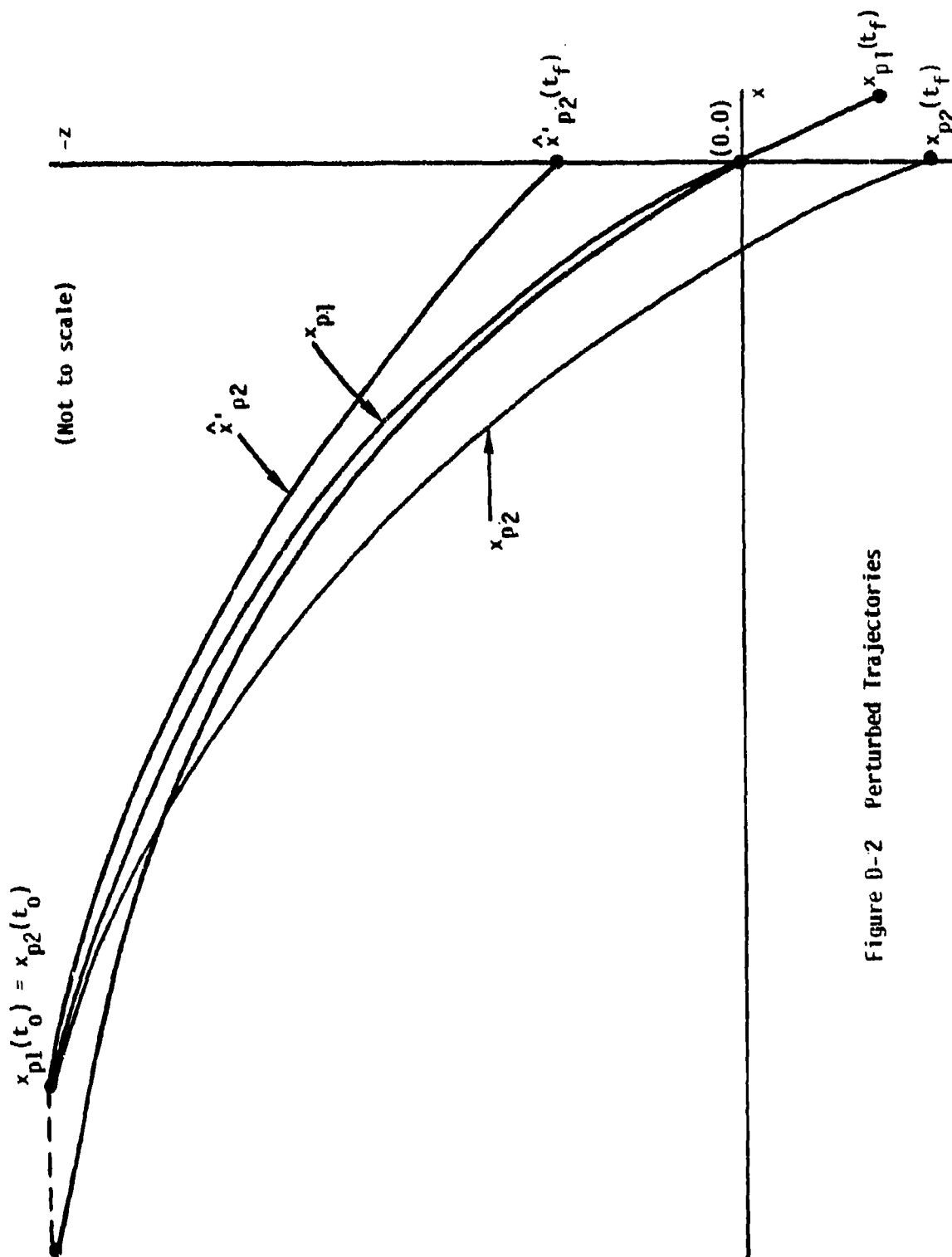


Figure D-2 Perturbed Trajectories

expected that  $x_{p2}$  would take the form of a motion "parallel" to  $x_n$ ; i.e., a motion having the same direction but vertically shifted. On this basis another trajectory denoted by  $\hat{x}_{p2}$  appears to be a more likely candidate for the trajectory because it is "parallel" and presumably takes less energy to accomplish. The flaw in this line of reasoning is that more than "parallel" motion is required if the penalty accorded by  $(P_2, Q_2)$  is to approach zero. "Parallel" motions with time translation give rise to positive penalties because of a perceived error in  $x$ . Observe that  $u_2$  must "slow" the system before moving into a "parallel" path. This slowing is accomplished by having  $x_{p2}$  cross  $x_n$ , and producing an increase in path length thereby. For reasons discussed earlier, this leads to a considerable increase in the energy required from the guidance law. To "slow" the vehicle, the weakly controllable mode must be excited and this necessitates an increase in the size of the actuating signal. For the specific sample trajectory  $x_{p2}$  requires roughly twice the energy required by  $x_{p1}$ .

Table D-1 gives relative performance of  $u_1$  and  $u_2$  at impact for various initial errors and parameter variations. In every case  $u_1$  provided superior performance. Though it is probably true that  $u_2$  is inferior to other controllers that could have been selected empirically, this example illustrates that the system designer ignores the relative stability of the system modes at his great risk. Only by explicitly modifying the performance penalties can the available guidance energy be allocated in the most appropriate way.

#### D-1.5 Summary

In this section a methodology for synthesizing a guidance law, based on the Linear Quadratic Regulator theory, and the associated weighting matrices has been developed. In this formulation the relative controllability of the different system modes enters directly into the system penalty function. The point of view espoused here differs from

Table D-1. Guidance Law Comparison \*

Perturbations	Guidance Law	Impact Deviations			
		$\Delta X$ (ft)	$\Delta y$ (deg)	$\Delta t$ (sec)	$\Delta \text{Mach}$ (-)
Initial downrange error	$u_2$	652.	3.8	.11	.21
	$u_1$	-10.	0.9	.09	.16
Initial altitude error	$u_2$	-2773.	-6.9	-.36	.09
	$u_1$	-151.	-2.9	-.33	.19
Density perturbation	$u_2$	377.	-2.0	.06	-.50
	$u_1$	-3.	0.1	.05	-.50

\* Comparison by analysis of the linear response

that typically used in that  $P$  and  $Q$  are usually constrained to be diagonal and equal weightings are assigned to states that are intended to have equal deviations. It is the fundamental point of this discussion that equal penalties do not cause "equal" responses. Indeed, just the opposite is true. Equal weighting on states will tend to preserve relative responses in closed-loop that the states had in open-loop. Weightings modified by the relative controllability properties of the states will tend to counteract this. Though the problem is conceptually simpler than that studied by Skelton, Reference D-4, this procedure is similar in effect to that of Skelton in that the difficult-to-control directions are identified and greater emphasis is placed upon them. The closed-loop controller is expected to display more uniformity in its response to initial errors in different directions than would one not employing the controllability factors.

In addition, the analysis of the controllability illustrates the difficulties associated with any guidance law for this system, and for systems with similar characteristics, which is based upon the use of time as the system variable of evolution.

## D-2. STATE VARIABLE AS VARIABLE OF EVOLUTION

In this section the use of a state variable rather than time as the variable of evolution of the system is considered. The motivation for this approach is manifold. Historically it was observed that a reduction in the number of states carried in the solution of the matrix Riccati equation reduces significantly the time requirements for targeting the optimal control guidance law. Another concern in the case of a maneuvering reentry vehicle is the uncertainty in the time to begin the process. Clearly, the use of a state variable for the independent variable provides benefits in the above areas. Previous studies, primarily motivated by the above considerations, found that performance was improved through the use of a state variable rather than time. The reason for the improvement is that when time is used for the variable of evolution the controller not only tries to control the state variables to follow a space curve but also tries to control the rate at which the space curve is traversed. Such control applies some of the resources to the control of the least important part of the problem, in this case the time, rather than concentrating on the most important part of the problem, the steering of the vehicle along the desired space curve. For example, suppose

$$x_p(t_0) = \xi_1 \text{ where } \xi_1 \text{ satisfies}$$

$$x_n(t_1) = \xi_1 ; t_1 > t_0$$

i.e. because of clock errors in the vehicle, the control process begins on the desired trajectory but with a time error of  $(t_1 - t_0)$  seconds. The LQ controller using D-6 and D-12, however, perceives this time error as a state error and tries to remove it. It thus overcontrols the vehicle trying to eliminate errors that are of no importance. Similar behavior occurs if the aerodynamic drag is greater than the nominal.

D-2.1 System Equations

The basic problem of order reduction by change of independent variable can be posed in the following way. Let the system dynamics be described by the nonlinear differential equation (D-3) with the perturbation variables defined as in (D-5).

Suppose that  $x_n$  and  $x_p$  are both such that their first component is monotone increasing; i.e.,

$$x_{p1}(t_1) < x_{p1}(t_2)$$

$$x_{n1}(t_1) < x_{n1}(t_2) \quad \text{for} \quad t_2 > t_1$$

Since  $x_n$  and  $x_p$  are continuously differentiable, either one could be used in place of time as an independent variable.

Consider first  $x_{n1}$ . From Equation D-3

$$\frac{d x_n}{d x_{n1}} = \frac{f(x_n, u_n)}{f_1(x_n, u_{n1})} = f_r(x_n, u_n) \quad (D-50)$$

The linear variational model is obtained from (D-50) by perturbing  $x_n$  and  $u_n$  slightly and equating first order terms. Note that only the numerator of  $f_r$  is perturbed and not the denominator. Because this does not yield the gradient of  $f_r$ , the associated variational equation is non-degenerate; i.e., even though

$$f_{r1} = 1 \quad (D-51)$$

it is still true that

$$\frac{d x_2}{d x_{n2}} \neq 0$$

Carrying out the usual variational arguments on (D-50), a linear evolutionary equation for  $x$  as a function of  $x_{n1}$  can be obtained and the standard control problems solved. Note, however, this design problem takes place in  $n$ -space if  $n$  is the dimension of  $x_p$ .

By contrast if  $x_{p1}$  is used as an independent variable, the problem becomes conceptually more complicated. There is an ensemble of functions  $\{x_p\}$ , the elements of which are parametrically dependent upon the perturbations from nominal of the system dynamics. If the specific  $x_p$  realized by the vehicle were known a priori, this would create no essential difficulty. Unfortunately, this knowledge would violate system causality and may be ruled out immediately. Furthermore, the one rationale for using  $x_{p1}$  as an independent variable is to eliminate the explicit time dependence of the perturbed trajectory and the control. With no measure of absolute time, there is no way to calculate  $x_n$  from  $x_p$  and consequently no way to compute  $x$ .

One way to avoid the problem of loss of time information is to generate a pseudo time variable. Suppose at time  $t_1$ ,  $x_{p1}(t_1)$  is observed. From this information alone  $t_1$  can not be computed because  $x_1(t_1)$  and hence  $x_{n1}(t_1)$  are not known. It is possible, however, to estimate  $t_1$  by  $t_1^*$  where  $t_1^*$  satisfies

$$x_{n1}(t_1^*) = x_{p1}(t_1)$$

That is, the first state variable is posited to be observed without error, and the nominal values of the other variables inferred from this

observation.

If  $|t_1^* - t_1|$  is small

$$x_{n1}(t_1^*) = x_{n1}(t_1) + (t_1^* - t_1) f_1(x_n(t_1), u_n(t_1)) \quad (D-53)$$

From (D-5), (D-52), and (D-53)

$$x_{n1}(t_1) + (t_1^* - t_1) f_1(x_n(t_1), u_n(t_1)) = x_{n1}(t_1) + x_1(t_1) \quad (D-54)$$

or

$$(t_1^* - t_1) = \frac{x_1(t_1)}{f_1(x_n(t_1), u_n(t_1))}$$

The time shift inherent in making the identification shown in (D-54) is proportional to the unacknowledged error in the first component in the state vector. Thus, trajectory errors become time errors under (D-54). The time anomaly influences the perceived vehicle dynamics. The vehicle controller using  $x_{p1}$  as an independent variable observes errors in a new coordinate frame  $x_r$  where

$$x_r(t_1) = x_p(t_1) - x_n(t_1^*) \quad (D-55)$$

Obviously

$$x_{r1} \approx 0$$

as the controller can not identify first component errors. If only first order terms are retained, it follows that

$$\begin{aligned}
 x_r(t_1) &= x_p(t_1) - (x_n(t_1) + (t_1^* - t_1)f(x_n, u_n)) \\
 &= x_p(t_1) - x_n(t_1) - \frac{x_1(t_1)}{f_1(t_1)} f(x_n, u_n) \\
 &= x(t_1) - \frac{x_1}{f_1} f(x_n, u_n)
 \end{aligned}
 \tag{D-56}$$

Equation (D-56) shows the aliasing of time errors into state errors in  $x_r$ . Errors in the first state component of the system are unmeasurable, but they are reflected in the perceived errors in the other components at the state vector.

#### D-2.2 Vehicle Dynamics in the Perceived Reference Frame

The vector  $x_r$  in (D-56) is the perceived error state of the system. To provide adequate regulation of this error, its equation of evolution must be derived. From (D-3) it follows that

$$\begin{aligned}
 d(x_p(t)) &= (f(x_n, u_n) + \frac{\partial f}{\partial x} x + \frac{\partial f}{\partial u} u)dt \\
 d(x_{p1}(t)) &= (f_1 + \frac{\partial f_1}{\partial x} x + \frac{\partial f_1}{\partial u} u)dt
 \end{aligned}
 \tag{D-57}$$

Consequently

$$\frac{dx_n(t)}{dx_{p1}(t)} + \frac{dx(t)}{dx_{p1}(t)} = \frac{(f + \frac{\partial f}{\partial x} x + \frac{\partial f}{\partial u} u) \frac{1}{f_1}}{(1 - \frac{1}{f_1} \frac{\partial f_1}{\partial x} x - \frac{1}{f_1} \frac{\partial f_1}{\partial u} u)}$$

where terms of order  $x^2$  and  $u^2$  and  $xu$  have been neglected. So

$$\begin{aligned} \frac{dx(t)}{dx_{p1}(t)} = & \left( \frac{1}{f_1} \frac{\partial f}{\partial x} - \frac{f}{f_1^2} \frac{\partial f_1}{\partial x} \right) x + \left( \frac{1}{f_1} \frac{\partial f}{\partial u} - \frac{f}{f_1^2} \frac{\partial f_1}{\partial u} \right) u \\ & + f_r - \frac{dx_n}{dx_{p1}} \end{aligned} \quad (D-58)$$

Denote

$$\frac{\partial f_r}{\partial x} = F_r ; \quad \frac{\partial f_r}{\partial u} = G_r$$

From their definition it follows that

$$F_r = \frac{1}{f_1} \frac{\partial f}{\partial x} - \frac{f}{f_1^2} \frac{\partial f_1}{\partial x}$$

$$G_r = \frac{1}{f_1} \frac{\partial f}{\partial u} - \frac{f}{f_1^2} \frac{\partial f_1}{\partial u}$$

and thus

$$\frac{dx(t)}{dx_{p1}(t)} = F_r x + G_r u + f_r - \frac{dx_n}{dx_{p1}} \quad (D-59)$$

The last term in (D-59) can be simplified;

$$\frac{dx_n}{dx_{p1}} = \frac{f(x_n, u_n)}{f_1(x_p, u_p)} = \frac{f}{f_1} \left( 1 - \frac{1}{f_1} \frac{\partial f_1}{\partial x} x - \frac{1}{f_1} \frac{\partial f_1}{\partial u} u \right)$$

# LOGICON

and

$$\frac{dx}{dx_{p1}} = F_r x + G_r u - \frac{f}{f_1^2} \left( \frac{\partial f_1}{\partial x} x - \frac{\partial f_1}{\partial u} u \right) \quad (D-60)$$

Now consider the change of variable indicated in (D-56)

$$\frac{dx_r}{dx_{p1}} = \frac{dx}{dx_{p1}} - \frac{d}{dx_{p1}} (x_1 f_r) \quad (D-61)$$

The first term of (D-61) is given in (D-60). The second term can be found by observing

$$\begin{aligned} \frac{d}{dt} f_r &= F_r \frac{dx_n}{dt} + G_r \frac{du_n}{dt} \\ &= F_r f + G_r \dot{u}_n \end{aligned} \quad (D-62)$$

$$\frac{d x_{p1}}{dt} = f_1 \quad (D-63)$$

where only zero'th order terms in the expansions have been retained in (D-62) and (D-63). Thus

$$\frac{d}{d x_{p1}} (x_1 f_r) = f_r \frac{dx_1}{dx_{p1}} + \frac{x_1}{f_1} (F_r f + G_r \dot{u}_n) \quad (D-64)$$

Substituting (D-64) and D-60) into (D-61)

$$\begin{aligned} \frac{dx_r}{d x_{p1}} &= F_r (x - x_1 f_r) + G_r (u - \dot{u}_n \frac{x_1}{f_1}) - \frac{f_r}{f_1} \left( \frac{\partial f_1}{\partial x} x - \frac{\partial f_1}{\partial u} u \right) - f_r \frac{dx_1}{dx_{p1}} \\ & \quad (D-65) \end{aligned}$$

## LOGICON

From its defining equation it is apparent that the first row of  $F_r$  and the first row of  $G_r$  are zero. From (D-60)

$$\frac{d x_1}{d x_{p1}} = -\frac{1}{f_1} \left( \frac{\partial f_1}{\partial x} x + \frac{\partial f_1}{\partial u} u \right)$$

Substituting this into (D-65)

$$\frac{dx_r}{d x_{p1}} = F_r x_r + G_r u_r \quad (D-66)$$

where

$$u_r = u - \dot{u}_n \frac{x_1}{f_1} \quad (D-67)$$

Note that the system equation given by (D-66) is degenerate because  $x_{r1} = 0$ .

The interpretation of  $(x_r, u_r)$  is evident from Figure D-3. The controller has no measurement of absolute time. By assuming that  $x_{p1} = x_{n1}$ , it concludes that  $t = t^*$ . Actually

$$t^* - t = \frac{x_1}{f_1}$$

Not realizing this error means that at time  $t$

$$u_n \Big|_{x_p(t)} = u_n(t^*) = u_n + \frac{x_1}{f_1} \dot{u}_n$$

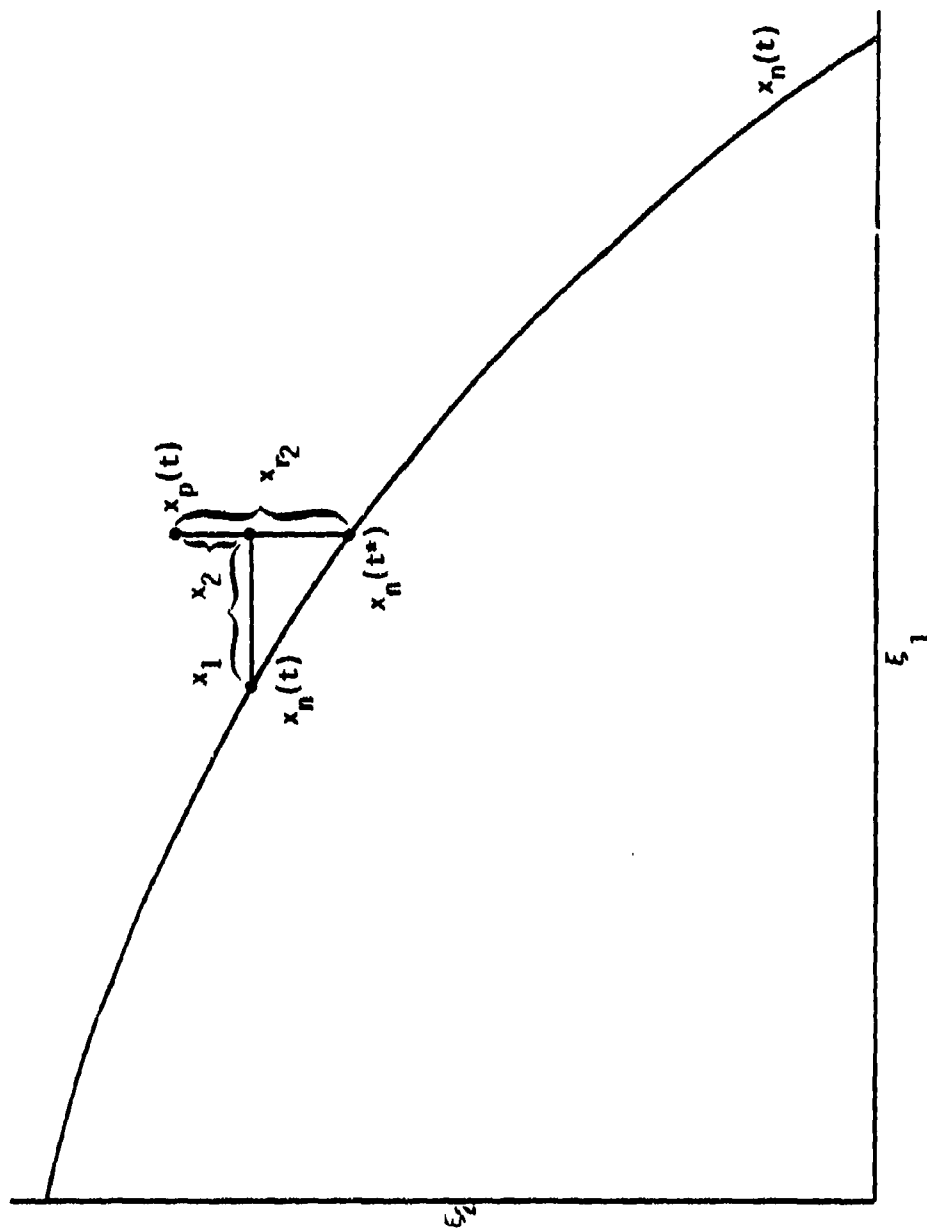


Figure D-3. Errors in Perceived Coordinate System

Note that even if

$$x_p(t) \equiv x_n(t^*)$$

$$u_p(t) \neq u_n(t)$$

To avoid penalizing control deviations that are due only to absolute time translations in the trajectory variables, define  $u_r$  as a perturbation from  $u_n(t^*)$ ; i.e.,

$$\begin{aligned} u_r(t) &= u_p(t) - u_n(t^*) \\ &= u_n(t) + u - u_n(t) - \frac{x_1}{T_1} \dot{u}_n \\ &= u - \frac{x_1}{T_1} \dot{u}_n \end{aligned}$$

This is identical with (D-67)

In the perceived coordinate system the error is  $x_r$  and the actuating signal is  $u_r$ . With (D-66) we are now in a position to pose to a quadratic regulator problem.

g

### D-2.3 Quadratic Regulators

Using (D-66) as the dynamic model, a quadratic regulation problem can be delineated. Define

$$J = x_r(t_f)' P_r x_r(t_f) + \int_{x_{p1}(t_0)}^{x_{p1}(t_f)} (x_r' Q_r x_r + u_r' R_r u_r) dx_{p1} \quad (D-68)$$

## LOGICON

The cost function  $J$  measures errors in the perceived coordinate system. The error vector  $x_r$  can be considered to evolve in  $R^{n-1}$  since  $x_{r1} \equiv 0$ . To facilitate comparison with the original coordinate system,  $x_r$  will be treated as an  $n$ -dimensional vector. Thus  $Q_r$  is  $n \times n$ .

From (D-56)

$$x_r = T_r x \quad (D-69)$$

where

$$T_r = \begin{bmatrix} 0 & 0 & \cdots & 0 \\ \frac{f_2}{f_1} & & & \\ \vdots & & I & \\ \frac{f_n}{f_1} & & & \\ -\frac{f_1}{f_1} & & & \end{bmatrix}$$

As was pointed out in Reference D-2 (pg 5); the problem of minimizing  $J$  in (D-68) is identical to that of minimizing

$$J = x(t_f)' P x(t_f) + \int_{x_{p1}(t_0)}^{x_{p1}(t_f)} (x' Q x + u_r' R u_r) dx_{p1} \quad (D-70)$$

where

$$P = T_r' P_r T_r, \quad Q = T_r' Q_r T_r$$

It is interesting to observe that  $T_r$  is singular. Indeed

$$T_r f_r = 0$$

Hence

$$f_r' P f_r = f_r' Q f_r = 0$$

The control system which minimizes (D-68) or (D-70) will try to resolve the residual error into the  $f_r$  direction. This result is not surprising when the motivation for selecting  $x_{p1}$  is recalled.

Since

$$d x_{p1} = f_1(x_n, u_n) dt$$

it follows that

$$J = x_r' P_r x_r + \int_{t_0}^{t_1} (x_r' (Q_r f_1) x_r + u_r' (R_r f_1) u_r) dt$$

From (D-67)

$$u_r' R_r u_r = (u - \frac{\dot{u}_n}{f_1} x_1)' R_r (u - \frac{\dot{u}_n}{f_1} x_1)$$

(D-71)

Thus

$$J = x_r' P_r x_r + \int_{t_0}^{t_1} \left[ x' \left( f_1' T_r' Q_r T_r + \frac{1}{f_1} (T_1' u_n' R_r u_n T_1) \right) x \right. \\ \left. - 2 u' R_r u_n T_1 x + f_1 u' R_r u \right] dt$$

where  $T_1 = (1, 0, \dots, 0)$ .

In the time domain the regulator problem becomes somewhat nonclassical because of the inclusion of cross product terms in the integrand.

In the problem under study here,  $u_r' R_r u_r$  is a more reasonable measure of control power than  $u' R_r u$  and so we will say that (D-68) is equivalent to a regulator problem in the time domain parameterized by matrices.

$$(P, Q, R) = (T_r' P_r T_r, f_1' T_r' Q_r T_r, f_1' R_r) \quad (D-72)$$

#### D-2.4 Changes in the Independent Variable

It may happen that  $x_{p1}$  is absolutely continuous and monotone increasing for only a portion of the trajectory. It would then be advantageous to change independent variables at discrete points on the trajectory to make use of a different trajectory variable with preferable properties. Let  $\{t_i; i=1, \dots, n\}$  be an increasing sequence of points in  $[t_0, t_f]$  and suppose that the independent variable is changed at these time points.\*

The simplest class of such changes simply involves renumbering the states in  $x_n$ ; e.g.  $x_{n1}$  becomes  $x_{n2}$  and conversely;  $f_2$  becomes  $f_1$  and conversely. Thus, while  $x_{p1}$  is the generic label for the independent variable,  $x_{p1}$  may correspond to different state variables along the trajectory. A change in independent variables creates a new matrix  $T_r(t)$  at  $\{x_{p1}(t_i)\}$  and consequently  $x_r(t)$  changes discretely at these same time points:

$$x_r(t_i^-) = T_r(t_i^-) x \neq T_r(t_i^+) x = x_r(t_i^+) \quad (D-73)$$

\* Second order errors are introduced by assuming the change of variable is time based rather than being based on the perceived independent variable.

# LOGICON

Although  $T_r$  is singular, (D-73) can be used with an additional hypothesis to find the change in  $x_r$ . The vector  $x$  can be decomposed into a component along  $f$  and a component orthogonal to  $f$

$$x(t) = \alpha(t)f + x_s(t)$$

Let

$$\tilde{x}_r(t) = \begin{bmatrix} x_{r2}(t) \\ \vdots \\ x_{rn}(t) \end{bmatrix} ; \tilde{x}_s(t) = \begin{bmatrix} x_{s2}(t) \\ \vdots \\ x_{sn}(t) \end{bmatrix} ; \text{etc}$$

Clearly

$$x_r(t^+) = T_r(t^+)x_s(t^+) \quad (D-74)$$

subject to

$$f'x_s(t^+) = 0. \quad (D-75)$$

Equation (D-73) can be written

$$\tilde{x}_r(t_1^+) = \tilde{T}_r(t_1^+)\tilde{x}_s(t_1^+) \quad (D-76)$$

where

$$\tilde{T}_r = \begin{bmatrix} (1 + \frac{f_2^2}{f_1^2}) & \frac{f_2 f_3}{f_1} & \dots & \frac{f_2 f_n}{f_1} \\ & \ddots & & \\ & & (1 + \frac{f_n^2}{f_1^2}) & \end{bmatrix} \quad (D-77)$$

If it assumed that  $T_r$  is nonsingular, then

$$x_s(t_i^+) = \tilde{T}_r^{-1}(t_i^+) \tilde{x}_r(t_i^+) \quad (D-78)$$

Combining (D-75) and (D-78)

$$x_s(t_i^+) = T_r^\#(t_i^+) x_r(t_i^+) \quad (D-79)$$

where

$$T_r^\#(t_i^+) = \begin{bmatrix} 0 & (-\frac{f_2}{f_1}, \dots, -\frac{f_m}{f_1}) \tilde{T}_r^{-1}(t_i^+) \\ 0 & \tilde{T}_r^{-1}(t_i^+) \\ 0 & \end{bmatrix} \quad (D-80)$$

The matrix  $T_r^\#$  is the correct pseudoinverse of  $T_r$  in this problem because

$$\begin{aligned} x_r(t_i^-) &= T_r(t_i^-) T_r^\#(t_i^+) x_r(t_i^+) \\ &= T(t_i) x_r(t_i^+) \end{aligned} \quad (D-81)$$

The formalism of dynamic programming can now be used to produce the control which minimizes subject to (D-67) and (D-81). The development is routine and only the result is of interest:

$$u_r(x_{p1}) = R_r^{-1} G_r' K_r x_r \quad (D-82)$$

$$\frac{dK_r}{dx_{n1}} = -F_r' K_r - K_r F_r + K_r G_r R_r^{-1} G_r' K_r - Q_r; x_{n1} \neq x_{n1}(t_i) \quad i=1, \dots, N$$

$$-K_r(x_{n1}(t_i^-)) + K_r(x_{n1}(t_i^+)) = \Gamma(t_i)' K_r(x_{n1}(t_i^+)) \Gamma(t_i); i=1, \dots, N$$

$$K_r(x_{n1}(T)) = P_r$$

Note that  $F_r$  and  $G_r$  change discretely at the same points that  $T_r$  does because the form of  $f_r$  changes at these points.

#### D-2.5 Introductory Examples

To explore the implications of the results presented thus far, and to illustrate the mechanics of the indicated transformations, two simple examples are useful. As the first consider the uncontrolled motion in the plane given by

$$\begin{pmatrix} \dot{x} \\ \dot{z} \end{pmatrix} = \begin{pmatrix} V \cos \gamma \\ V \sin \gamma \end{pmatrix} = \dot{\xi} \quad (D-83)$$

where  $V$  is constant and  $\gamma$  is a given function of time, monotonically increasing and  $0 < \gamma < \pi/2$  over the time interval of interest. For suitable initial conditions both components of  $\xi$  are monotonic and we will suppose that the motion given by (D-83) is as shown in Figure D-4.

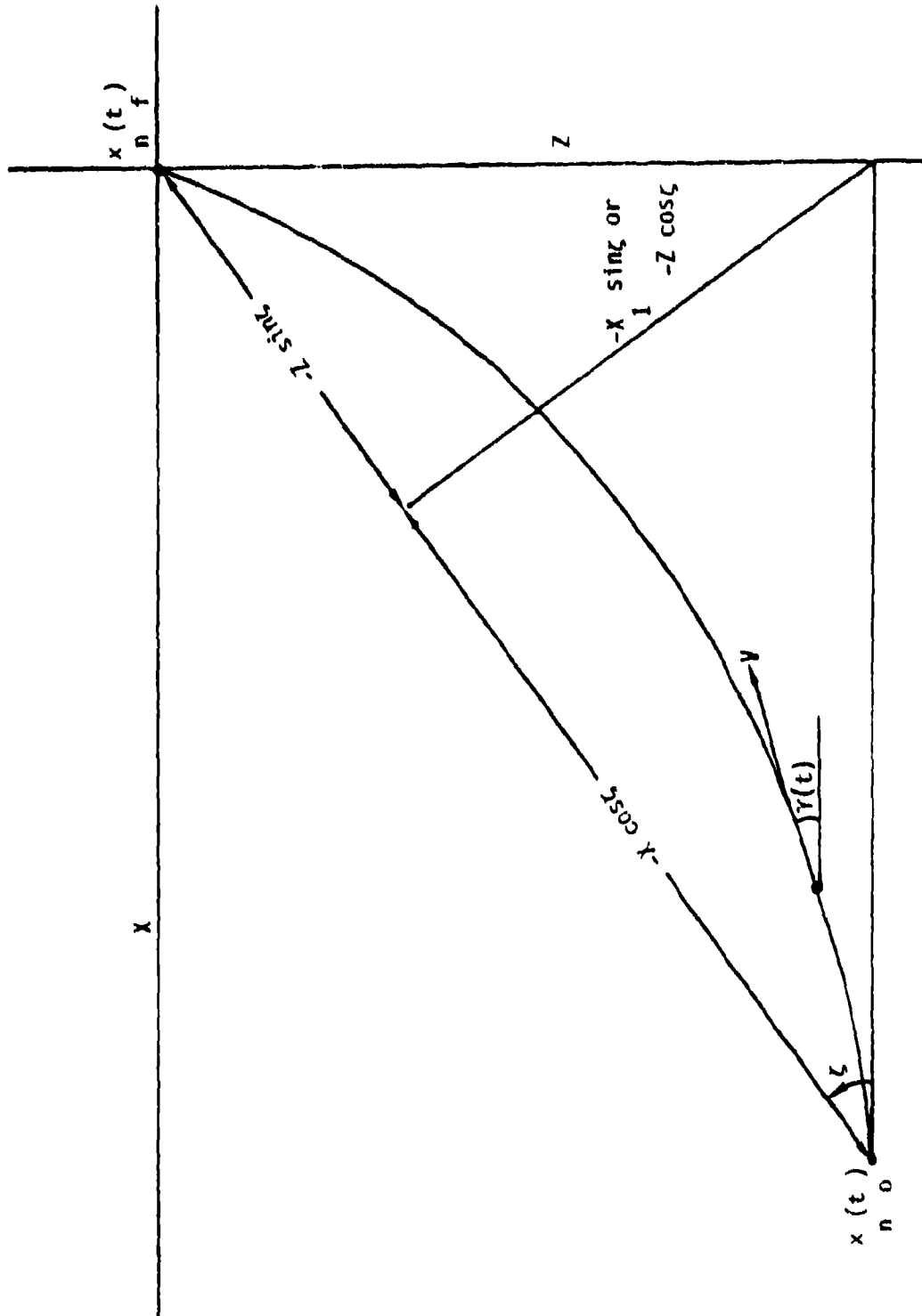


Figure D-4. Independent Variable Geometry

Suppose  $X$  is used as the independent variable. Then

$$\begin{aligned} f_r &= \begin{pmatrix} 1 \\ \tan \gamma \end{pmatrix} \\ F_r &= 0 \\ T_r &= \begin{bmatrix} 0 & 0 \\ -\tan \gamma & 1 \end{bmatrix} \end{aligned} \tag{D-84}$$

Suppose

$$Q_r = \text{diag} (0, q_2^2), \quad P_r = \text{diag} (0, p_2^2)$$

Then (see (D-72))

$$\begin{aligned} P &= p_2^2 \begin{bmatrix} \tan^2 \gamma & \tan \gamma \\ \tan \gamma & 1 \end{bmatrix} \\ Q &= q_2^2 \cos \gamma \begin{bmatrix} \tan \gamma \sin \gamma & \sin \gamma \\ \sin \gamma & \cos \gamma \end{bmatrix} \end{aligned} \tag{D-85}$$

Note that  $(V \cos \gamma, V \sin \gamma)$  is in the null space of both  $P$  and  $Q$  and hence any errors along  $f$  will not be penalized by either  $P$  or  $Q$ .

The method of selection proposed in Appendix D-1.2 attempted to achieve this same effect by use of the transformation

$$T = \begin{pmatrix} \cos \gamma & \sin \gamma \\ -\sin \gamma & \cos \gamma \end{pmatrix} \tag{D-86}$$

As shown in Appendix D-1.2, Equations D-26 and D-27, this gives normalized values for P and Q of

$$P_w = p_2^2 \begin{bmatrix} 1 & -\cot\gamma \\ -\cot\gamma & \cot^2\gamma \end{bmatrix}$$

$$Q_w = q_2^2 \begin{bmatrix} \sin^2\gamma & -\sin\gamma \cos\gamma \\ -\sin\gamma \cos\gamma & \cos^2\gamma \end{bmatrix}$$

Comparing (D-85) and (D-87)

$$P = P_w \tan^2\gamma(t_f)$$

$$Q = Q_w$$

(D-88)

Thus the two methods provide essentially the same weightings. The difference in P and  $P_w$  is attributable to the difference in the way maximum error at impact is computed.

A more interesting example is the control problem in the plane with no autopilot dynamics. Let

$$\begin{pmatrix} \dot{X} \\ \dot{Z} \\ \dot{Y} \end{pmatrix} = \begin{pmatrix} V \cos\gamma \\ V \sin\gamma \\ A/V \end{pmatrix} = \xi$$

(D-89)

the control is exercised through the acceleration A. It will be assumed that A/V is small in magnitude and that X and Z are both monotone increasing (See Figure D-4)

The problem is perhaps more easily studied in a rotated coordinate system. Let  $T_R$  be a rotation in the plane; i.e.,

$$T_R = \begin{pmatrix} T_{11} & 0 \\ 0 & 1 \end{pmatrix} \quad (D-90)$$

$$T_{11} = \begin{pmatrix} \cos \zeta & \sin \zeta \\ -\sin \zeta & \cos \zeta \end{pmatrix}$$

where  $\zeta$  is the angle of rotation. Clearly

$$\text{Det } |T_R| = 1; T_R^{-1} = T_R'$$

Further if  $\zeta$  is a differentiable function of time, then

$$\dot{T}_R = \dot{\zeta} \begin{pmatrix} -\sin \zeta & \cos \zeta & 0 \\ -\cos \zeta & -\sin \zeta & 0 \\ 0 & 0 & 0 \end{pmatrix} \quad (D-91)$$

$$\dot{T}_R T_R^{-1} = \begin{bmatrix} 0 & \dot{\zeta} & 0 \\ -\dot{\zeta} & 0 & 0 \\ 0 & 0 & 0 \end{bmatrix} \quad (D-92)$$

Let  $x_{nT}$  be the nominal trajectory in the new coordinate system; i.e.,

$$x_{nT} = T_R x_n \quad (D-93)$$

Then

$$\begin{aligned}
 \dot{x}_{nT} &= \dot{T}_R x_n + T_R \dot{x}_n \\
 &= \dot{T}_R T_R^{-1} x_{nT} + T_R f(T_R^{-1} x_{nT}) \\
 &= f_T(x_{nT}, u_n)
 \end{aligned}
 \tag{D-94}$$

From (D-92) and (D-94)

$$T^{-1} x_{nT} = \begin{pmatrix} x_{nT1} \cos \gamma - x_{nT2} \sin \gamma \\ x_{nT1} \sin \gamma + x_{nT2} \cos \gamma \\ A/V \end{pmatrix}
 \tag{D-95a}$$

$$f(T^{-1} x_{nT}, u) = \begin{pmatrix} V \cos \gamma \\ V \sin \gamma \\ A/V \end{pmatrix}
 \tag{D-95b}$$

$$f_T = \begin{pmatrix} \dot{\zeta}_2 x_{nT} + V \cos(\zeta - \gamma) \\ -\dot{\zeta}_1 x_{nT} - V \sin(\zeta - \gamma) \\ A/V \end{pmatrix}
 \tag{D-96}$$

Equation (D-96) gives the dynamics in the new coordinate system. If  $\zeta = 0$ , then  $f_T = f$ . If  $\zeta = 90$ , then  $x_{nT1} = Z$ . By selecting the correct rotation variable, one is able to choose either of the original position variables in (D-89) as the independent variable for the problem. Furthermore, time variable choices for  $\zeta$  permit still more flexibility. Unfortunately, analysis of (D-96) is fairly difficult. To gain insight into the properties of the system, some interesting special cases will

be investigated.

Suppose that  $\zeta = 0$ . Using the first component of  $x_{nT}$  as the independent variable yields.

$$f_r = \begin{pmatrix} 1 \\ \tan \gamma \\ AV^{-2} \sec \gamma \end{pmatrix} \quad (D-97)$$

From (D-97),  $F_r$  and  $G_r$  are easily derived.

$$F_r = \begin{bmatrix} 0 & 0 & 0 \\ 0 & 0 & \sec^2 \gamma \\ 0 & 0 & AV^{-2} \tan \gamma \sec \gamma \end{bmatrix}$$

$$G_r = \begin{bmatrix} 0 \\ 0 \\ V^{-2} \sec \gamma \end{bmatrix}$$

Suppose the nominal values for A and V are nearly constant. Then (D-19) becomes

$$M_0 = \begin{bmatrix} 0 \\ 0 \\ V^{-2} \sec \gamma \end{bmatrix}$$

$$M_1 = \begin{bmatrix} 0 \\ V^{-2} \sec^3 \gamma \\ AV^{-4} \tan \gamma \sec^2 \gamma \end{bmatrix} - \begin{bmatrix} 0 \\ 0 \\ \gamma V^{-2} \tan \gamma \sec \gamma \end{bmatrix} \quad (D-99)$$

$$= \begin{bmatrix} 0 \\ V^{-2} \sec^3 \gamma \\ AV^{-3} \tan \gamma \sec \gamma (V^{-1} \sec \gamma - 1) \end{bmatrix}$$

# LOGICON

and

$$Q = \begin{bmatrix} 0 & 0 \\ 0 & V^{-2} \sec^3 \gamma \\ V^{-2} \sec \gamma & AV^{-3} \tan \gamma \sec \gamma (V^{-1} \sec \gamma - 1) \end{bmatrix} \text{ if } \zeta \equiv 0$$

Clearly states 2 and 3 are controllable while state 1 is not.

Suppose next that  $\zeta = 90$ . From (D-96)

$$f_T = \begin{pmatrix} V \sin \gamma \\ -V \cos \gamma \\ AV^{-1} \end{pmatrix}, \quad f_r = \begin{pmatrix} 1 \\ -\cot \gamma \\ AV^{-2} \csc \gamma \end{pmatrix} \quad (D-100)$$

Consequently,

$$F_r = \begin{bmatrix} 0 & 0 & 0 \\ 0 & 0 & -\csc^2 \gamma \\ 0 & 0 & -AV^{-2} \cot \gamma \csc \gamma \end{bmatrix}; \quad G_r = \begin{bmatrix} 0 \\ 0 \\ V^{-2} \csc \gamma \end{bmatrix} \quad (D-101)$$

As before

$$M_0 = \begin{bmatrix} 0 \\ 0 \\ V^{-2} \csc \gamma \end{bmatrix}$$

$$M_1 = \begin{bmatrix} 0 \\ -V^{-2} \csc^3 \gamma \\ -AV^{-4} \cot \gamma \csc^2 \gamma \end{bmatrix} - \begin{bmatrix} 0 \\ 0 \\ -\dot{\gamma} V^{-2} \cot \gamma \csc \gamma \end{bmatrix} \quad (D-102)$$

$$= \begin{bmatrix} 0 \\ -V^{-2} \csc^3 \gamma \\ -AV^{-3} \cot \gamma \csc \gamma (V^{-1} \csc \gamma - 1) \end{bmatrix}$$

and

$$Q = \begin{bmatrix} 0 & 0 \\ 0 & -V^{-2} \csc^3 \gamma \\ V^{-2} \csc \gamma & -AV^{-3} \cot \gamma \csc \gamma (V^{-1} \csc \gamma - 1) \end{bmatrix} \text{ if } \zeta \equiv 90$$

The first two transformations are of obvious interest. Let us turn now to some time variable relations. Suppose that  $\zeta = \gamma$ . From (D-96)

$$f_T = \begin{pmatrix} AV^{-1} x_{nT2} + V \\ -AV^{-1} x_{nT2} \\ AV^{-1} \end{pmatrix}, \quad f_r = \begin{pmatrix} 0 \\ -x_{nT1} (x_{nT2} + A^{-1}V^2)^{-1} \\ (x_{nT2} + A^{-1}V^2)^{-1} \end{pmatrix} \quad (D-103)$$

Let

$$x_{nT2} + A^{-1}V^2 = \Delta$$

Then

$$\frac{\partial \Delta^{-1}}{\partial x_{nT2}} = -\Delta^{-2} \quad ; \quad \frac{\partial \Delta^{-1}}{\partial A} = V^2 A^{-2} \Delta^{-2}$$

Consequently

$$F_r = \begin{bmatrix} 0 & 0 & 0 \\ -\Delta^{-1} & x_{nT1} \Delta^{-2} & 0 \\ 0 & -\Delta^{-2} & 0 \end{bmatrix} ; \quad G_r = \begin{bmatrix} 0 \\ -V^2 A^{-2} x_{nT1} \Delta^{-2} \\ V^2 A^{-2} \Delta^{-2} \end{bmatrix} \quad (D-104)$$

# LOGICON

It then follows that

$$M_0 = \begin{bmatrix} 0 & \\ -V^2 A^{-2} x_{nT1} \Delta^{-2} & \\ V^2 A^{-2} \Delta^{-2} & \end{bmatrix};$$

$$M_1 = \begin{bmatrix} 0 & \\ -V^2 A^{-2} x_{nT1}^2 \Delta^{-4} & \\ V^2 A^{-2} \Delta^{-4} x_{nT1} & \end{bmatrix} - V^2 A^{-2} \begin{bmatrix} 0 & \\ -x_{nT1} \Delta^{-2} - x_{nT1} \frac{d}{dt} \Delta^{-2} & \\ \frac{d}{dt} \Delta^{-2} & \end{bmatrix}$$

and

$$Q = \begin{bmatrix} 0 & 0 & \\ -V^2 A^{-2} x_{nT1} \Delta^{-2} & -V^2 A^{-2} x_{nT1}^2 \Delta^{-4} + V^2 A^{-2} (x_{nT1} \Delta^{-2} + x_{nT1} \frac{d}{dt} \Delta^{-2}) & 1 \text{ if } \epsilon = \gamma \\ V^2 A^{-2} \Delta^{-2} & V^2 A^{-2} \Delta^{-4} x_{nT1} - V^2 A^{-2} \frac{d}{dt} \Delta^{-2} & \end{bmatrix}$$

(D-105)

Observe that Q has the form

$$Q = \begin{pmatrix} 0 \\ Q_2 \end{pmatrix}$$

## LOGICON

where  $Q_2$  is  $2 \times 2$ . From (D-105)

$$\begin{aligned} \det Q_2 &= V^4 A^{-4} \Delta^{-4} x_{nT1} \\ &= V^3 A^{-3} \Delta^{-3} \end{aligned} \quad (D-106)$$

From this we see that states 2 and 3 are controllable, but only barely so. If the nominal trajectory were constant ( $\dot{x}_{nT2} = 0$ )  $Q_2$  would have rank 1.

As a final example, consider the rotation

$$\zeta = \tan^{-1} \frac{x_{n2}}{x_{n1}} \quad (D-107)$$

The angle  $\zeta$  is simply the look angle toward the target.

From (D-90) and (D-93) we observe that (see Figure D-4)

$$x_{nT1} = x_{n1} \cos \zeta + x_{n2} \sin \zeta = \sqrt{x_{n1}^2 + x_{n2}^2} \quad (D-108)$$

$$x_{nT2} = -x_{n1} \sin \zeta + x_{n2} \cos \zeta \equiv 0 \quad (D-109)$$

From (D-109) and (D-96) it then follows that

$$\dot{\zeta} = - \frac{V \sin (\zeta - \gamma)}{x_{nT1}} \quad (D-110)$$

$$\dot{x}_{nT1} = V(\cos (\zeta - \gamma) - \frac{x_{n2}}{x_{n1}} \sin (\zeta - \gamma)) \quad (D-111)$$

$$= \Delta$$

Thus

$$f_r = \begin{pmatrix} 1 \\ 0 \\ AV^{-1}\Delta^{-1} \end{pmatrix} \quad (D-112)$$

$$F_r = \begin{bmatrix} 0 & 0 & 0 \\ 0 & 0 & 0 \\ AV^{-1} \frac{\partial \Delta^{-1}}{\partial x_{nT1}} & AV^{-1} \frac{\partial \Delta^{-1}}{\partial x_{nT2}} & AV^{-1} \frac{\partial \Delta^{-1}}{\partial \gamma} \end{bmatrix} \quad (D-113)$$

$$G_r = \begin{bmatrix} 0 \\ 0 \\ V^{-1}\Delta^{-1} \end{bmatrix}$$

Direct substitution yields

$$Q = \begin{bmatrix} 0 & 0 \\ 0 & 0 \\ Q_{31} & Q_{32} \end{bmatrix} \quad (D-114)$$

The system given by (D-113) has only one controllable direction.

The loss of controllability evidenced by (D-114) is due to the fact that one position component is always zero in the rotated coordinate system. Only range and flight path angle are measured and these variables are not enough to control the system. Suppose we augment the state by including  $\zeta$  as a state variable. Since  $x_{nT2} = 0$ , we find that

$$\dot{x}_{nT1} = V \cos (\zeta - \gamma) \quad (D-115)$$

$$\dot{\zeta} = \frac{-V}{x_{nT1}} \sin (\zeta - \gamma)$$

$$\dot{\gamma} = \frac{A}{V}$$

If we use  $x_{nT1}$  as an independent variable

$$f_r = \begin{pmatrix} 1 \\ -x_{nT1} \tan(\zeta - \gamma) \\ AV^{-2} \sec(\zeta - \gamma) \end{pmatrix} \quad (D-116)$$

Direct calculation yields

$$F_r = \begin{bmatrix} 0 & 0 & 0 \\ x_{nT1}^{-2} \tan(\zeta - \gamma) & -x_{nT1}^{-1} \sec^2(\zeta - \gamma) & +x_{nT1}^{-1} \sec^2(\zeta - \gamma) \\ 0 & AV^{-2} \tan(\zeta - \gamma) \sec(\zeta - \gamma) & AV^{-2} \tan(\zeta - \gamma) \sec(\zeta - \gamma) \end{bmatrix}$$

$$G_r = \begin{bmatrix} 0 \\ 0 \\ V^{-2} \sec(\zeta - \gamma) \end{bmatrix} \quad (D-117)$$

From this we see that

$$M_0 = \begin{bmatrix} 0 \\ 0 \\ V^{-2} \sec(\zeta - \gamma) \end{bmatrix} \quad (D-118)$$

$$M_1 = \begin{bmatrix} 0 \\ V^{-2} x_{nT1}^{-1} \sec^3(\zeta - \gamma) \\ AV^{-4} \tan(\zeta - \gamma) \sec^2(\zeta - \gamma) \end{bmatrix} \dot{G}_r$$

If  $\dot{G}_r$  is small,  $(F_r, G_r)$  is controllable in the two coordinates  $\zeta$  and  $\gamma$ .

D-2.6 Selection of the Independent Variable

In the previous selections the use of a state variable as the independent variable is shown to ameliorate the undesired characteristics of the time based controller. The analysis thus far has not addressed the issue of selecting the independent variable when in fact several candidates possess the requisite properties. In this section a means of performing the selection is of interest.

Restricting attention to the class of transformations given by (D-90) and to those values of  $\zeta$  for which

$$x_{p1}(\zeta) = (T_T(\zeta)x_{p1})_1 \text{ is monotone}$$

and

$$\frac{dx_p(\zeta)}{dx_{p1}(\zeta)} = f_r(x_p, u_p; \zeta) \quad (D-119)$$

Corresponding to a specific value of  $\zeta$  there is a dynamic equation of the re-entry vehicle, Equation D-119. To synthesize the best regulator, the analyst must select a permissible value of  $\zeta$  in such a way as to make the closed-loop system perform in the best possible way. Observe that different system representations are being compared and a germane "docility" index which would expedite this comparison would be useful.

Before defining a docility index for this system, a few observations are apropos. Consider the nonlinear system of Equation (D-3) with its perturbation equation characterized by the  $[F, G]$  matrix of Equation D-7. If the perturbation equation is controllable at time  $t_1$ , it is well known that any observed error  $x(t_1)$  can be eliminated at time  $t_2 > t_1$  with

minimum expenditure of control energy E given by (See Reference D-6)\*

$$E(x(t_1); t_1, t_2) = (t_2 - t_1)^{-1} \int_{t_1}^{t_2} u^2(\tau) d\tau \quad (D-120)$$

$$= (t_2 - t_1)^{-1} x'(t_1) W^{-1}(t_1, t_2) x(t_1)$$

where

$$W(t_1, t_2) = \int_{t_1}^{t_2} \Phi(t_1, \tau) G(\tau) G'(\tau) \Phi'(t_1, \tau) d\tau \quad (D-121)$$

And  $\Phi$  is the transition matrix associated with F. Let  $\{\lambda_i(t_1, t_2)\}$  be the positive eigenvalues of W arrayed in decending order and let  $\{n_i(t_1, t_2)\}$  be the associated set of eigenvectors ordered in conformity with  $\{\lambda_i(t_1, t_2)\}$ . Let

$$n_i = \lim_{t_2 \rightarrow t_1} n_i(t_1, t_2) \quad (D-122)$$

Recall the definition of the controllability matrix  $C_n$  as

$$C_n = [M_0, M_1, \dots, M_{n-1}]$$

$$M_0 = G \quad (D-123)$$

$$M_{k+1} = -FM_k + \dot{M}_k; k=1, \dots$$

\* To call E as defined by Equation D-120 the control energy is something of a misnomer in so far as the  $(t_2 - t_1)^{-1}$  factor gives E units more akin to power. Still, in this application it is useful to think of E as an energy figure with an implicit normalization with respect to the time increment.

## LOGICON

The system  $(F, G)$  is completely controllable if the rank of  $C_n$  is  $n$ . In this circumstance  $W$  (see D-121) is positive and the minimum energy transfer from any initial state to the origin in the interval  $[t_1, t_2]$  is that given by Equation (D-120) (See Reference D-6)

It was shown in Reference D-7 that  $W$  can be expressed as the sum

$$W(t_0, t_1) = \sum_{i,j=0}^{\infty} \frac{(t_1 - t_0)^{i+j+1}}{(i+j+1)!} M_i(t_0) M_j'(t_0) \quad (D-124)$$

If  $x_0$  is a unit eigenvector of  $W(t_0, t_1)$  with associated eigenvalue  $\lambda$ , then the energy required to drive  $x_0$  to the origin is  $\lambda^{-1}$ .

Suppose  $(t_1 - t_0)$  is small. In the system of interest  $u$  is scalar and  $M_i$  are column vectors. Retaining only third order terms

$$\begin{aligned} W(t_0, t_1) &= (t_1 - t_0) M_0 M_0' + \frac{(t_1 - t_0)^2}{2} (M_0 M_1' + M_1 M_0') + \\ &\quad \frac{(t_1 - t_0)^3}{3} \left[ \frac{M_0 M_2'}{2} + \frac{M_2 M_0'}{2} + M_1 M_1' \right] + o(t_1 - t_0)^3 \end{aligned} \quad (D-125)$$

The eigenvectors  $\{n_i(t_0, t_1)\}$  of the positive matrix  $W$  span  $R^n$  and can be found from the algorithm

$$\begin{aligned} n_1' W n_1 &= \max_n n' W n ; n' n = 1 \\ n_2' W n_2 &= \max_n n' W n ; \begin{cases} n' n = 1 \\ n' n_1 = 0 \end{cases} \\ &\vdots \end{aligned}$$

Let the associated eigenvalues be labeled  $\lambda_1, \lambda_2, \dots$ . From Equation (D-125) it is clear that for small  $(t_1 - t_0)$

$$\eta_1 \approx M_0 \|M_0\|^{-1}, \lambda_1 = (t_1 - t_0) \|M_0\|^2$$

$$E(\eta_1, dt) = \|M_0\|^{-2} dt^{-2} \quad (D-126)$$

The energy associated with the next eigenvector  $\eta_2$  can be similarly computed

$$\eta_2 \approx C(M_1 - M_1' M_0 (M_0' M_0)^{-1} M_0)$$

$$E(\eta_2, dt) = \frac{1}{3} (\eta_2' M_1 M_1' \eta_2)^{-1} dt^{-4} \quad (D-127)$$

Where  $C$  is a normalization constant.

This procedure can be continued, but Equations (D-126) and (D-127) will suffice for this problem. The directions  $\eta_1$  and  $\eta_2$  can be thought of as "easy" and "hard" directions to control, respectively. Since  $M_0 = G$ , the fact that  $\eta_1 = CM_0$  simply expresses the fact that the first order influence of  $u$  is in the direction  $G$ . It is more difficult to cause the system to move in the  $\eta_2$  direction as evidenced by the fact that  $E(\eta_2, dt)$  is proportional to  $dt^{-4}$ . The energy figure for this latter direction depends upon  $FG$  as well as the time variation of  $G$ .

The problem of using these energy figures to compare different independent variables is made difficult by structural degeneracies in the  $(F_r, G_r)$  system (see D-66). Indeed, since  $x_{r1} = 0$ ,  $(F_r, G_r)$  can not be controllable in the usual sense. Consider the system described by (D-66). Mimicking the development leading to (D-123),  $(F_r, G_r)$  will be said to be controllable if  $\text{rank } C_{n-1} = n-1$ ;

$$C_{n-1} = \begin{bmatrix} 0 & \dots & 0 \\ \tilde{C}_{n-1} \end{bmatrix}$$

The controllability subspace would be all  $x_p$  orthogonal to  $(1, 0, \dots, 0)$ . The energy content in the directions  $n_1$  and  $n_2$  in the  $(x_p, u_p)$  coordinate system follow directly from (D-126) and (D-127)

$$E(n_1; dx_{p1}(\xi)) = \|M_0\|^{-2} \|n_1\|^2 |dx_{p1}(\xi)|^{-2} \quad (D-128)$$

$$E(n_2; dx_{p1}(\xi)) = \frac{(\eta_2' M_1 M_1' \eta_2)^{-1}}{3 \|n_2\|^2} \|n_2\|^2 |dx_{p1}(\xi)|^{-4} \quad (D-129)$$

From (D-128) and (D-129) the energy content is the product of three types of factors. The first factor is the energy associated with a unit perturbation in the  $n_1$  direction. The second factor  $\|n_1\|^2$  scales the error with respect to the actual perturbation expected in the indicated direction. The final factor scales the energy with respect to the increment in the independent variable.

As written, (D-128) and (D-129) are not in a form which facilitates comparison of different values of  $\xi$ . Each of the factors in these equations depends on  $\xi$  and simple scale changes in  $x_{p1}$  are translated into apparent changes in energy content. To form a valid basis for comparison, (D-128) and (D-129) must be expressed as a function of the same error in the time domain. From (D-3) it is clear that

$$dx_{p1}(\xi) = (T_R(\xi) f(x_p, u_p))_1 dt \quad (D-130)$$

(D-130) provides the factor required to normalize the time interval over which control is accomplished.

## LOGICON

The normalization of the eigenvectors  $n_i$  is somewhat more subtle. A given initial error in the  $x_n$  coordinate system is transformed into a different apparent error in the  $x_p(\zeta)$ -plane. Suppose there is an initial error  $x$  in the  $x_n$ -plane. This error becomes  $x(\zeta)$  under the transformation  $T_R(\zeta)$ :

$$x(\zeta) = T_R(\zeta)x$$

It was shown in Reference D-8 that the perceived error when  $x_{p1}(\zeta)$  is used as the variable of evolution is

$$x_p(\zeta) = T_p(x_{p1}(\zeta))T_R(\zeta)x \quad (D-131)$$

where

$$T_R = \begin{pmatrix} 0 & 0 & 0 \\ -f_{r2} & & \\ -f_{r3} & & I \\ \vdots & & \end{pmatrix} \quad (D-132)$$

An initial error  $x$  gives rise to an indicated error  $x_p(\zeta)$  of the following form

$$x_p(\zeta) = \sum_{i=1}^{n-1} \frac{n_i^T T_R T_R x}{\|n_i\|^2} n_i \quad (D-133)$$

The coefficients of the decomposition of the error vector given above measure the relative size of sensed errors in the different coordinate

## LOGICON

systems. In the problem under study here  $x$  is not known a priori and will be considered to be a random variable. In this case the relative sizes of the initial errors in the  $x_r$  coordinate system will be

$$\|n_i\| = \|\beta_i' T_r(x_{p1}(\zeta)) T_R(\zeta) x\|; i=1, \dots, n-1 \quad (D-134)$$

where  $\beta_i$  is a unit vector in the  $n_i$  direction.

Combining Equations (D-128), (D-129), (D-130) and (D-134)

$$E(n_1; dx_{p1}) = \|M_0\|^{-2} \left[ (T_R^f)_1 \right]^{-2} \|\beta_1' T_r T_R x\|^2 dt^{-2} \quad (D-135)$$

$$E(n_2; dx_{p1}) = \frac{1}{3} (\beta_2' M_1 M_1' \beta_2)^{-1} \left[ (T_R^f)_1 \right]^{-4} \|\beta_2 T_r T_R x\|^2 dt^{-4}$$

•  
•  
•

For convenience let  $E(n_i; dx_{p1}) = \alpha_i dt^{-2i+2}$  where  $\alpha_i$  is defined above. With the energy content of errors in the  $n_i$  directions given by (D-135), a scalar valued measure of system docility would be a useful intermediary for comparing the relative merits of different values of  $\zeta$ . Obviously if there existed a value of  $\zeta$  say  $\zeta^*$  which minimized  $\alpha_i$  uniformly;

$$\alpha_i(\zeta^*) \equiv \min_{\zeta} \alpha_i(\zeta); i=1, \dots, n-1$$

then  $\zeta^*$  would yield the best possible choice for  $x_{p1}(\zeta)$ . Unfortunately, a uniformly best value of  $\zeta$  will seldom exist, and the analyst must be content with something less.

The docility index found most suitable for this class of problem is given by  $H$ ;

$$H(\zeta) = E \left\{ \prod_{i=1}^{n-1} \alpha_i(\zeta) \right\} \quad (D-136)$$

where  $E \{ \}$  denotes mathematical expectation. That value of  $\zeta$  which minimizes  $H(\zeta)$  is said to be locally best choice of  $\zeta$ :

$$H(\zeta^*) = \inf_{\zeta} H(\zeta) \quad (D-137)$$

Since  $\alpha_i$  cannot be made uniformly small by selection of  $\zeta$ , the expectation of the product of the  $\alpha$ 's is made small. Note that for  $\zeta = \zeta_0$  the controllability subspace of  $(F_r, G_r)$  is of dimension less than  $n-1$ , and  $H(\zeta = \zeta_0) = \infty$ . It is interesting to note that  $H(\zeta)$  bears close kinship with measures of controllability proposed in References D-9 and D-10 which use  $\det W^{-1}$  to induce a controllability ordering on the set of admissible controllers. Of course, the normalizations involved in deriving (D-136) makes the final criterion somewhat different.

It has been shown above that, if  $|t_2 - t_1|$  is small and  $u$  is scalar valued,

$$E(\eta_i; t_1, t_2) = \alpha_i |t_2 - t_1|^{2(1-i)} + \text{higher order terms};$$

$$i=1, \dots, n \quad (D-137)$$

The equations for the individual  $\alpha_i$  are given in the Appendix (see D-135).

(D-137) indicates that there is a natural decomposition of the state space into a set of orthogonal directions characterized by the difficulty with which initial errors along each of the directions can be eliminated. For example an error in the 'easy' direction,  $\eta_1$ , can be eradicated by an actuating signal expending energy proportional to  $|t_2 - t_1|^{-2}$ . Observe that as the time interval over which control is accomplished decreases, the amplitude of the actuating signal is increased. The asymptotic

## LOGICON

behavior of E represents the confluence of these antithetical limits.

In (D-137) the time factor  $|t_2 - t_1|^k$  is a fixed scaling, but the set  $\{\alpha_i\}$  gives a local indication of the systems ability to steer out errors. Because only local energy figures have been derived, the relative merits of different systems would be expected to vary with time. The way in which these sets are used to form a performance index depends upon the specific objective envisioned for the vehicle. An example of such an index is given in the following section.

Different independent variables, or equivalently different choices of  $\zeta$ , give rise to different behavioral characteristics for the vehicle in the coordinate system associated with the regulator. To put the problem of selecting the best value of  $\zeta$  on a rational basis, some criterion of choice is required. In the Appendix, one such criterion is discussed. In lieu of trying to minimize the individual values of the  $\alpha_i$  in (D-137) a function H is defined as follows:\*

$$H(\zeta) = \prod_{i=1}^{n-1} \alpha_i(\zeta) \quad (D-138)$$

This function orders the set of permissible independent variables. The value of  $\zeta$  is sought which minimizes H;

$$H(\zeta^*) = \inf_{\zeta} H(\zeta) \quad (D-139)$$

---

\*As indicated earlier  $E\{\prod \alpha_i(\zeta)\}$  is used when  $x(t_1)$  is random.

Note the  $\{\alpha_i\}$  are coefficients which characterize the energy content of a class of errors in  $(n-1)$  orthogonal directions. In the unlikely event that there is a value of  $\zeta$  which minimizes these energy coefficients uniformly, this value of  $\zeta$  would be that indicated by (D-139). A more typical situation would be one in which improvement in performance in one direction carries with it a concomitant degradation in performance in one or more of the other directions. The index H provides an ordering of possible independent variables in this more common circumstance satisfying some but not all of the desiderata used by Muller and Weber in Reference D-9 to delineate a measure of the quality of controllability.

To illustrate these notions consider the dynamics model of a re-entry vehicle whose primary motion is confined to the X-Z plane as in (D-89). Observe that (D-89) is a very simple representation of the actual equation of motion for the vehicle. Neglected are the nonlinearities, samplers, autopilot dynamics, and exogenous influences which affect actual vehicle motion. The simplification implicit in (D-89) is intentional since one of the objectives of this study is to determine the degree to which simple analysis models can be used to derive controllers for a complicated dynamic system.

The class of transformations of interest in this study are fixed rotations in the X-Z plane; i.e.  $\dot{\zeta} \equiv 0$ .

Direct calculation leads to the conclusion that

$$\dot{x}_p(\zeta) = \begin{pmatrix} V \cos(\gamma - \zeta) \\ V \sin(\gamma - \zeta) \\ AV^{-2} \end{pmatrix} ; \quad f_r = \begin{pmatrix} 1 \\ \tan(\gamma - \zeta_0) \\ AV^{-2} \sec(\gamma - \zeta_0) \end{pmatrix} \quad (D-140)$$

where it has been assumed that  $x_p$  is such that  $x_{p1}(\zeta)$  is monotone.

## LOGICON

To find  $\{a_i\}$ , the system controllability matrix must first be found. This matrix is given in (D-123).

$$C_2 = (M_0, M_1)$$

where (see Equation (A-4))

$$M_0 = \begin{pmatrix} 0 \\ 0 \\ V^{-2} \sec(\gamma - \zeta) \end{pmatrix} ; M_1 = \begin{pmatrix} 0 \\ V^{-2} \sec^3(\gamma - \zeta_0) \\ \dots \end{pmatrix} \quad (D-141)$$

Using (D-141) it follows that

$$\eta_1 = ||\eta_1|| \begin{pmatrix} 0 \\ 0 \\ 1 \end{pmatrix} ; \eta_2 = ||\eta_2|| \begin{pmatrix} 0 \\ 1 \\ 0 \end{pmatrix} \quad (D-142)$$

(D-142) requires careful interpretation. The controllable subspace of the perturbation equation associated with (D-140) can be decomposed into an "easy" direction,  $\eta_1$ , and a "hard" direction  $\eta_2$ . From D-89 it is evident that the easy direction is associated with an angular error and the hard direction with a position error. This result is intuitively appealing since the acceleration acts directly on  $\gamma$  and only indirectly on position errors.

To compute the docility index given by Equation D-138 using the result given in (D-135) only the appropriate amplitude normalization is yet to be determined. (D-131) provides an equation relating the time based error,  $x$ , and the error perceived by the controller  $x_p(\zeta)$ . Substituting the required quantities into this equation

$$x_p(\zeta) = \begin{pmatrix} 0 & 0 & 0 \\ -\sin \gamma \sec(\gamma - \zeta) & \cos \gamma \sec(\gamma - \zeta) & 0 \\ -AV^{-2} \cos \zeta \sec(\gamma - \zeta) & -AV^{-2} \sin \zeta \sec(\gamma - \zeta) & 1 \end{pmatrix} x \quad (D-143)$$

In the application of interest, the primary initial errors are in position since the angular orientation of the vehicle is controlled quite accurately during boost and freeflight. Suppose, therefore, that the initial error in the  $(x_n, u_n)$  coordinate system is given by

$$x = \begin{pmatrix} \delta X \\ \delta Z \\ \delta Y \end{pmatrix} = \begin{pmatrix} \cos \lambda \\ \sin \lambda \\ 0 \end{pmatrix} \quad (D-144)$$

The parameter  $\lambda$  gives the direction of the initial error and the size of this error has been normalized. The perceived error resulting is

$$x_r(\zeta) = \begin{pmatrix} 0 \\ \sec(\gamma - \zeta) \sin(\lambda - \gamma) \\ AV^{-2} \sec(\gamma - \zeta) \cos(\lambda - \zeta) \end{pmatrix} \quad (D-145)$$

Assume that the initial error angle  $\lambda$  is uniformly distributed on  $[0, 2\pi]$  and is independent of  $\gamma$ . From (D-134)

$$\begin{aligned} ||\eta_1|| &= |AV^{-1} \sec(\gamma - \zeta) \cos(\lambda - \zeta)| \\ ||\eta_2|| &= |\sec(\gamma - \zeta) \sin(\lambda - \zeta)| \end{aligned} \quad (D-146)$$

Substituting these values into the defining equation for H

$$H(\zeta) = \frac{A^2 V^{-2}}{24} [1 + 2 \sin^2(\gamma - \zeta)] \sec^2(\gamma - \zeta) \quad (D-147)$$

From D-147 it follows that the best choice of  $\zeta$  at time  $t_1$  would be  $\zeta = \gamma(t_1)$

$$\begin{aligned} H(\zeta = \gamma(t_1)) &= \min_{\zeta} H(\zeta) \\ &= \frac{A^2 V^{-2}}{24} \end{aligned} \quad (D-148)$$

From (D-148) it is clear that the locally best coordinate system in which to control the vehicle is one in which the instantaneous position is expressed in the rotated coordinate system shown in Figure D-5. The independent variable  $x_{p1}(\zeta^*)$  can be thought of a range variable and the component of state in which error can be measured can be thought of as a pseudo-miss variable. Although (D-148) would appear to suggest that good performance could be attained by setting  $\zeta(t) = Y(t)$ , time variable rotation is not permitted by the hypotheses which lead to (D-148). The rotation angle must be constant throughout the trajectory and as a consequence a judicious choice for  $\zeta$  would be that which approximates most closely the realized value of  $Y$  for that portion of the trajectory of primary concern. On a mission in which terminal miss is a prime performance contributor,  $\zeta = Y_n(t_f)$  would appear to be a rational choice.

## D-2.7 An Example

To explore some of the nuances of the synthesis procedure presented in the foregoing sections, a simulation study was performed to test some of the guidance laws described above on a sophisticated and relatively complete simulation model of a particular aerodynamically controlled re-entry vehicle. There were a number of questions to which this study gave at least partial answer. Of most concern were the relative merits of a time based guidance law and one which used a trajectory variable as the variable of evolution. Secondly, the correspondence of the docility index given by (D-137) and the observed behavioral qualities of the guidance law were of interest. Finally, the general question of the utility of the analysis model, (D-89), in constructing guidance laws was also under investigation. There are four guidance laws whose behavior has been studied in some detail. They are:

$U_t$ : time is the independent variable

$U_x$ : downrange position is the independent variable ( $\zeta = 0$ )

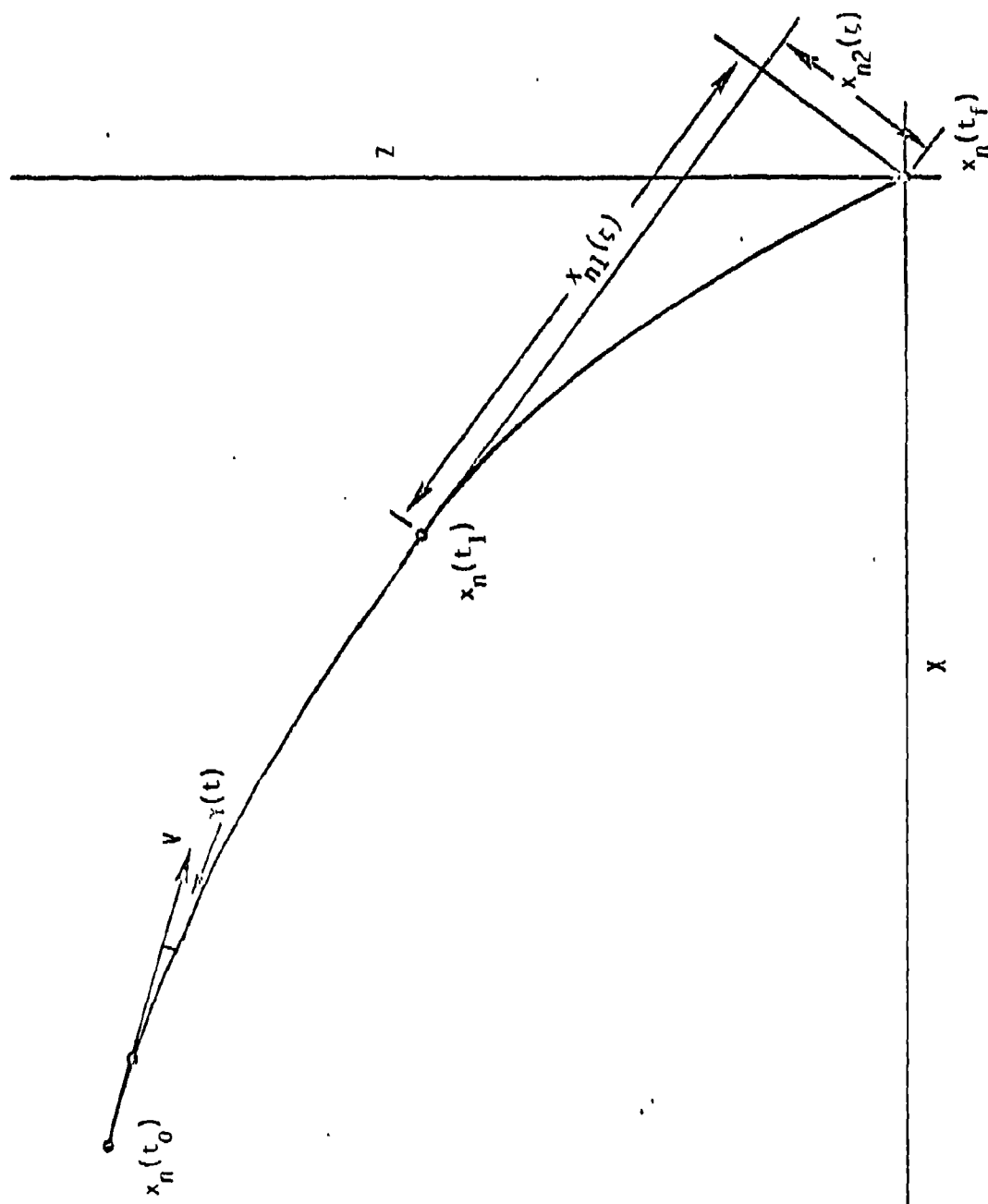


Figure D-5. Trajectory Geometry When  $z = \gamma(t_1)$

## LOGICON

$U_z$ : altitude is the independent variable ( $\zeta = \pi/2$ )

$U_*$ :  $\zeta = \gamma_n(t_f)$

The regulators  $U_x$  and  $U_z$  are of interest because of their implementational simplicity. In both cases a directly measured trajectory variable is used as the independent variable. On the other hand, the independent variable associated with  $U_*$  must be computed from measured quantities. Still  $U_*$  is of significant interest because it locally minimizes  $H$  at the termination of the trajectory. The regulator  $U_t$  is explicitly time dependent and its performance forms a base of comparison for the other regulators.

The weighting matrices in the performance indices for the regulators were selected to penalize each of the regulators similarly for similar errors. First consider  $(P, Q, R)$  in (D-11). The weighting on control was constant and was essentially given by

$$R = \frac{1}{\Delta A_{\max}^2} \quad (D-149)$$

where  $\Delta A_{\max}$  is the maximum permissible magnitude of variation of acceleration from its nominal value. The state error weighting took the form

$$Q(t) = \text{diag}(q_1^2(t), q_2^2(t), q_3^2(t)) \quad (D-150)$$

The state weights were ,

$$q_1^2(t) = \frac{1}{(\Delta x_1^2)_{\max}} \quad (D-151)$$

where the allowable position error decreased monotonically from the order of  $10^4$  feet at re-entry to the order of 10 feet at impact. The

allowable angular deviation was also time variable but was monotonically increasing. The terminal position weight,  $P$ , is given by

$$P = Q(t_f) \quad (D-152)$$

The weighting matrices for  $U_x$ ,  $U_z$ , and  $U_\psi$  were defined similarly. In each case the associated  $Q$  was diagonal. Because of the degeneracy of the state space,  $q_1$  is irrelevant and the complete position error is weighted by  $q_2$ . For this reason

$$Q_\zeta = \left( \frac{dx_{p1}(\zeta)}{dt} \right)^{-1} (0, q_1^2 + q_2^2, q_3^2) \quad (D-153)$$

where  $q_1$  is given by (D-151) and the first factor in  $Q_\zeta$  is time normalization, the other performance weights are

$$R_\zeta = \left( \frac{dx_{p1}(\zeta)}{dt} \right)^{-1} R \quad (D-154)$$

$$P_\zeta = Q_\zeta(x_{p1}(t_f; \zeta))$$

(D-153) makes the position and angular error weights in the  $x_p(\zeta)$  coordinate system compatible with those used in deriving  $U_\zeta$ . Note that  $U_x$ ,  $U_z$  and  $U_\psi$  measure position error as a scalar while  $U_\zeta$  senses a two dimensional position error. The weighting matrices given by (D-149) through (D-154) provide like weights to like errors and the influence on performance due to time scale distortion is avoided by the "velocity" factor in (D-153) and (D-154).

To relate the docility index given in (D-138) to actual vehicle performance, a simulation study was undertaken. The vehicle simulation equations provided a detailed description of the dynamic structure of an

actual re-entry vehicle. This comprehensive model actually provided an impediment to good performance for the regulators designed here because these regulators are based upon a dynamic hypothesis that is deficient in many respects. Of the simulation results obtained, those from three numerical experiments are presented here. In each case the nominal trajectory began with

$$X(t_0) = \text{order } 10^5 \text{ feet}$$

$$Z(t_0) = \text{order } 10^5 \text{ feet}$$

$$t_0 = 0; t_f = \text{order } 10 \text{ seconds}$$

$$\gamma(t_0) \in [0, \pi/4]; \gamma(t_f) \in (\pi/4, \pi/2]$$

The three tests are described as follows:

- 1)  $X_p(t_0) - X_n(t_0) = - \text{order of } 10^3 \text{ feet}, x_i(t_0) = 0 \text{ otherwise}$
- 2)  $Z_p(t_0) - Z_n(t_0) = - \text{order of } 10^3 \text{ feet}, x_i(t_0) = 0 \text{ otherwise}$
- 3) No initial error, 0.9 times nominal air density on  $[0, t_f/2]$ , 1.1 times nominal air density on  $(t_f/2, t_f]$ .

Figure D-6 shows the result of the first test. For an initial  $X$  perturbation the perpendicular path errors are plotted on a log scale. The error magnitudes have been normalized, and while the relative errors of the regulators are accurate, their absolute values have no significance. All three time independent controllers behave in the way one would expect. All begin with the same trajectory error and in each case the error builds up slightly because of autopilot effects. Because

$$|\gamma_n(t_0)| < |\gamma_n(t_0) - \gamma_n(t_f)| < |\gamma_n(t_0) - \pi/2| \quad (D-155)$$

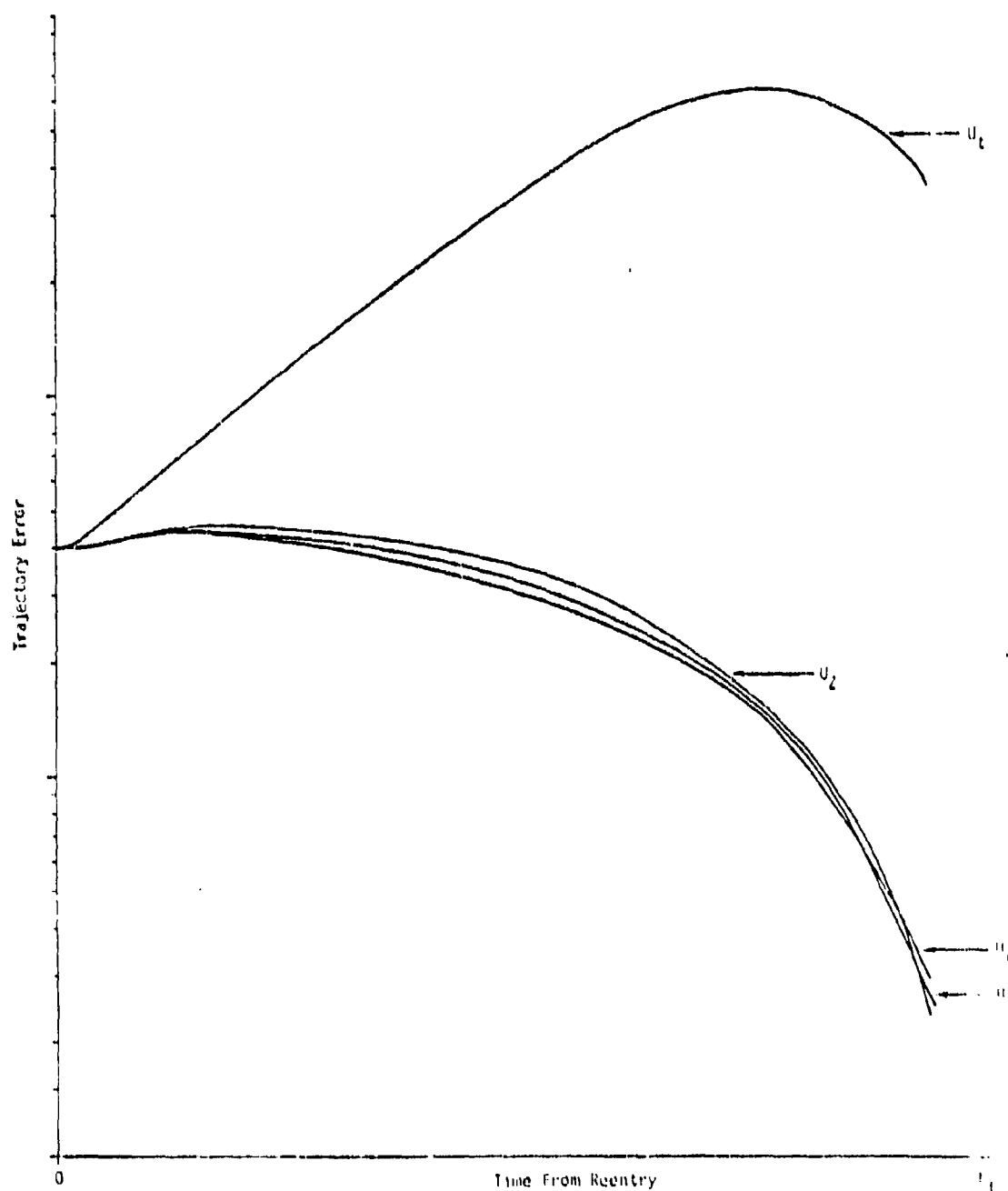


Figure D-6. Trajectory Errors for an Initial X Error

on the trajectory of interest, one would expect from (D-147) that the preference ordering of the regulators would initially be  $U_x$  first,  $U_*$  second and  $U_z$  third. This is indeed the case as shown in Figure D-6. For that part of the trajectory satisfying (D-155) the docility index provides an ordering in accord with the trajectory following fidelity of the associated regulator. Although the initial portion of the trajectory is subject to aberrant drag forces and acceleration limits, the slowly varying control gains tend to reduce sampler and autopilot effects. The dynamic equation given by (D-89) is a fully adequate regulator synthesis model for 90% of the trajectory. The comparison of the time independent controllers at termination is obscured by autopilot influences. Near the end of the trajectory, the regulator gains are rapidly varying, and the autopilot has difficulty in providing a faithful reproduction of the required actuating signal. Even here (see Table D-2) the comparison of  $U_z$  and  $U_*$  with  $U_x$  is that predicted on the basis of Equation (D-147). The former regulators have impact errors that are within the best accuracy to be expected while  $U_x$  has a somewhat larger error.

The performance of  $U_t$  as given in Figure D-6 and Table D-2 appears superficially to be incorrect. Far from causing a diminution of the initial error,  $U_t$  causes the trajectory following error to increase by an order of magnitude. The error of impact is inferior to that obtainable with no feedback regulator at all. Another way of comparing  $U_t$  with the set of  $U_r$  is in terms of the amount of control used on the trajectory. In a guidance system using a performance index like (D-11), the regulator seeks to use as little control force as possible while simultaneously maintaining good trajectory following qualities. The magnitude function  $|R^{-1}GKX|$  is a measure of the degree of apprehension with which the regulator views its instantaneous state. Thus,

$$\psi(\omega) = \int_{t_0}^{t_f} |R^{-1}G_r'K_rX_r|dt \quad (D-156)$$

Table D-2. Guidance Law Performance

Closed-loop Regulator	Perturbations	Performance Deviations		
		$\Delta DR$ Ft	Error in Flight Time % of Nominal	$\frac{\int  u_i  dt}{\int  u_t  dt}$
$u_t$	Initial Downrange	1572	.031	1
	Initial Altitude	3199	.34	1
	Density	325	-.87	1
$u_x$	Initial downrange	6.3	-.11	$1.45 \times 10^{-4}$
	Initial Altitude	16.2	-.69	$5.35 \times 10^{-3}$
	Density	9.8	-.76	$7.7 \times 10^{-2}$
$u_z$	Initial Downrange	0.3	-.17	$9.3 \times 10^{-3}$
	Initial Altitude	0.4	-.70	$6.9 \times 10^{-3}$
	Density	5.0	-.77	$5.7 \times 10^{-1}$
$u_w$	Initial Downrange	2.0	-.15	$1.07 \times 10^{-2}$
	Initial Altitude	2.9	-.64	$5.1 \times 10^{-3}$
	Density	4.8	-.77	$5.9 \times 10^{-1}$

is a measure of disapprobation for the closed-loop vehicle trajectory. Defining  $\Psi(\zeta)$  in the obvious way,  $\Psi$  provides an indication of how control intensive each of the regulators is. The actual value of the actuating signal was not used as the integrand in (D-156) because saturation in the actuators tends to desensitize this index. From table D-2 where the relative values of  $\Psi$  are given, the regulator  $U_t$  is seen to use a factor of  $10^2$  more control than is needed by the time independent controllers. The excessive use of acceleration on the part of  $U_t$  is coupled with trajectory following performance that is approximately  $10^2$  worse than that attained with the  $U_p$  regulators.

The reason for the conspicuous inferiority of  $U_t$  lies in the way the trajectory following problem is posed. The time based regulator tries not to minimize the true trajectory error, but rather moves to correct the error measured by  $x$  in (D-5). For the test shown in Figure D-6 the initial  $x$  error was such as to initiate re-entry at a point closer to the target than the nominal starting point. Because the controller has no way of slowing the vehicle directly,  $U_t$  reacts to that portion of the error that is inherently a time translation by increasing the path length of the perturbed trajectory. Increasing path length is control energy intensive and tends to cause large errors normal to the trajectory. This "time-equivalent" bubble is characteristic of time based regulators and is not present in the response of the modified LQ regulators. Table D-2 indicates that  $U_t$  is able to achieve much tighter control over time of flight than can any of the  $U_p$ . Unfortunately, this attribute is not of any particular advantage in this mission.

Figure D-7 shows the trajectory bubble for an initial  $z$  error. Only the nominal and the  $U_t$  trajectory are shown. The time independent controllers would be indistinguishable on the scale of this drawing. Figure D-7 is not shown to exact scale but is indicative of qualitative features shown by the actual vehicle trajectories. As before, a small initial error is caused to grow by  $U_t$  in order to slow the effective forward

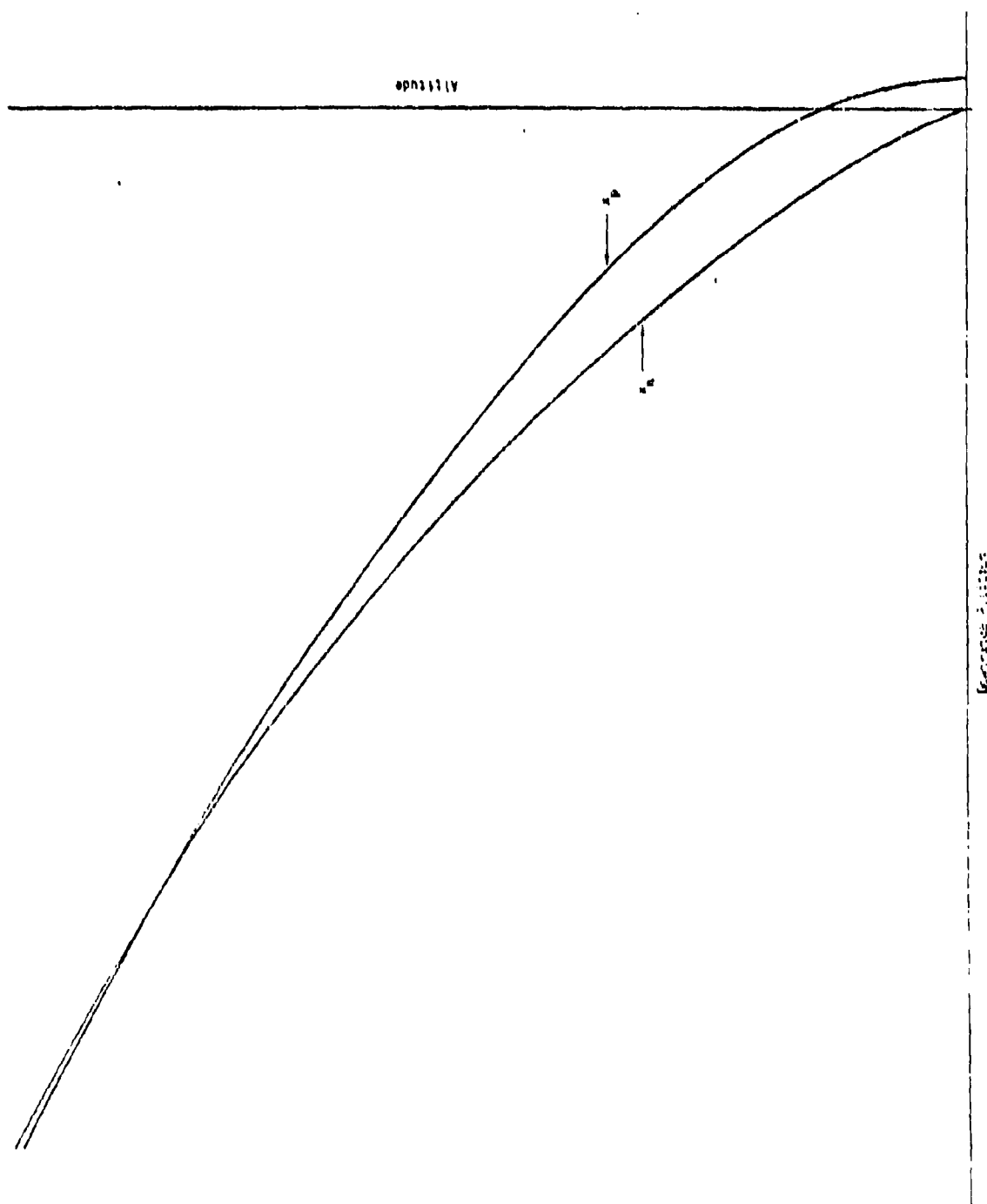


Figure D-7. Vehicle Trajectory for Initial Z Error and Time as the Independent Variable

velocity. As was the case with an initial  $X$  error,  $U_t$  overcompensates for the initial time translation and has a perturbed flight time greater than the nominal value. This timing error is presumably due to controller saturation near impact.

The improvement factors associated with the time independent controllers are repeated in this example. The impact error of  $U_t$  is orders of magnitude greater than that accruing to the alternative regulators. The improvement in control utilization is again on the order of 100. Although not shown in Figure D-7, the relative performance of  $U_x$ ,  $U_z$  and  $U_w$  was in accordance with the predicted on the basis of the docility index  $H$ . The previously encountered difficulty with  $U_x$  near impact manifests itself again. The excellent performance of  $U_z$  should be considered to be more a function of fortuitous circumstance than design.

The final example provides an interesting assessment of the robustness of the guidance laws studied here. In this simulation there was no initial error, but the dynamic equation of the vehicle was changed by decreasing air density by 10% on the first half of the re-entry trajectory and increasing it by 10% on the last half. Ideally, the regulator output should be nearly zero since there are only slight path following errors created by the open-loop portion of the guidance law. The three time independent guidance laws do follow the path quite closely, albeit at a different rate than does the nominal. The related errors are uniformly less than 10 feet. On the other hand, as shown in Figure D-8,  $U_t$  finds the density variation particularly bewildering. In the low density portion of the flight a large error builds up as  $U_t$  tries to slow the vehicle by increasing path length. When the sign of the density changes,  $U_t$  must now increase its speed along the nominal path starting with what is now a sizable state error. It does this in part by crossing over the nominal path and impacting the ground short of the target. Because of this terminal maneuver, the factor by which  $U_t$  deteriorates performance is less than that found in some of the earlier tests.

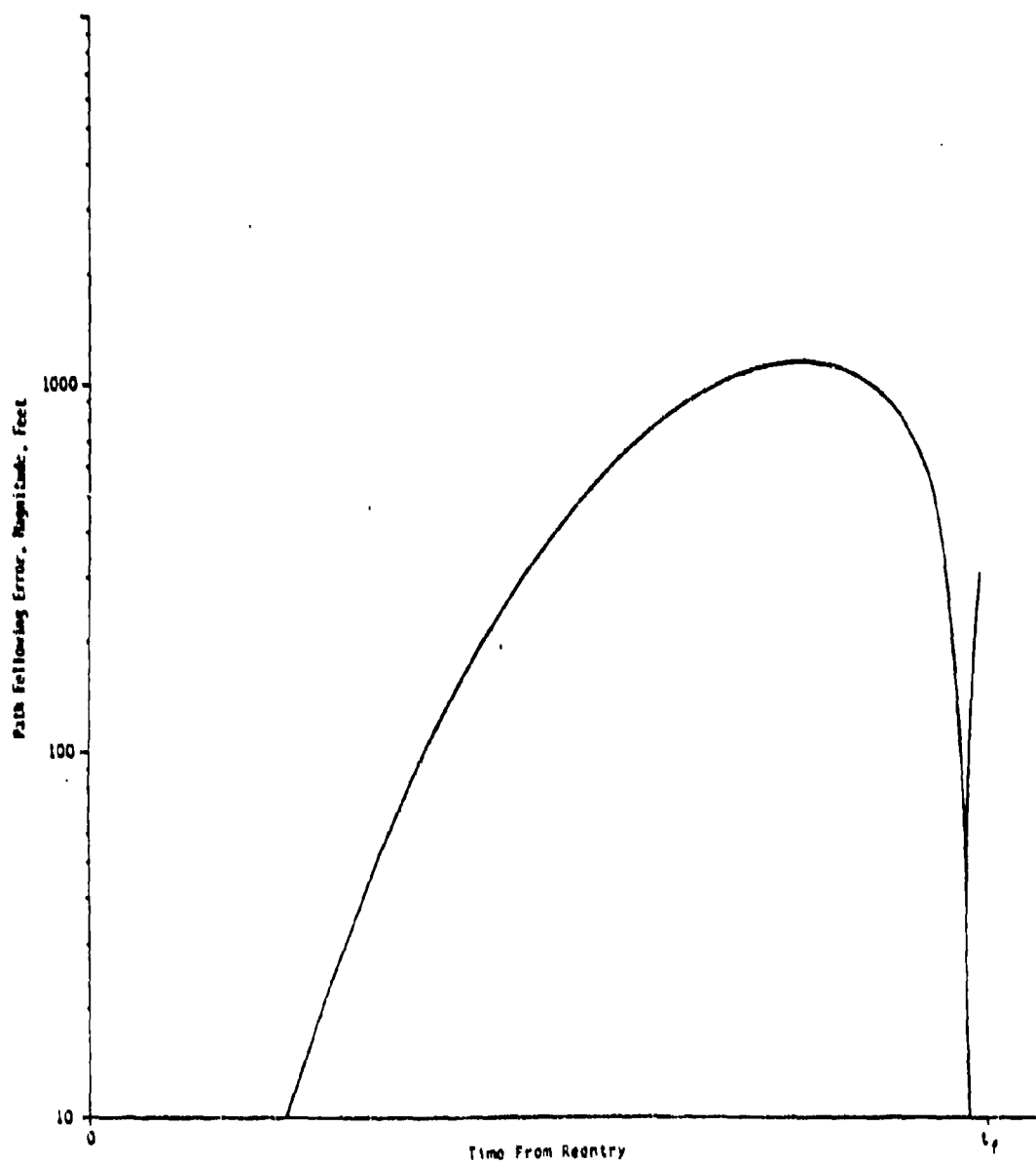


Figure D-8. Trajectory Errors for Density Variation and Time as the Independent Variable

One peculiarity of the path flown by  $U_t$  is the fact that the time of flight differs from nominal to a greater degree than do the other regulators. This may be due to the disadvantageous state into which  $U_t$  forces the vehicle midway in the flight. As Table D-2 shows,  $U_t$  uses excessive amounts of control force. As before  $U_z$  and  $U_*$  are clearly superior to  $U_x$ .

While not exhaustive, this simulation study illustrates some of the behavioral anomalies of  $U_t$ . The time independent regulators give performance that is several orders of magnitude superior to that attained by  $U_t$ . A comparison of  $U_x$ ,  $U_z$  and  $U_*$  on portions of the trajectory where the neglected vehicle dynamics had the least influence suggests that the docility index given by (D-147) is suitable in this application. Further study is necessary to resolve certain apparent aberrations in relative performance.

#### D-2.8 Conclusion

An aerodynamically controlled re-entry vehicle has dynamic peculiarities which tend to discourage the use of "linear-quadratic" feedback regulators in guidance. The disadvantageous features of the vehicle stem largely from its weak controllability. By the simple artifice of using a trajectory variable in place of time as the independent variable of evolution, important deficiencies of the LQ regulator are avoided and a robust guidance law produced.

The selection of this independent variable from the available alternatives is complicated by the often contradictory exigencies of guidance law simplicity and the dynamic response of the vehicle. Using a simplified analysis model, this report provides an index of quality for the closed-loop response characteristics of the vehicle. This index is phrased in terms of the local energy content associated with perturbations from the nominal trajectory. In terms of this index it is possible to rank dif-

ferent choices for an independent variable.

Although the index was selected with a view toward maintaining a reasonable level of analytical tractability, it is still true that the form of  $H$  precludes the development of a direct algorithm for finding the best  $x_{p1}$ . Some intuitively appealing choices for an independent variable are fairly easily compared, and it has been shown that the "natural" independent variable  $Z$  has desirable closed-loop properties. For the trajectory considered here either  $U_z$  or  $U_*$  would be adequate. The superiority of these regulators to the classical LQ regulator is readily apparent both in the fidelity of trajectory following and in the judicious use of available control resources. The performance of the time based regulator is so poor that it does not appear to be a rational candidate for this type of re-entry mission.

D-3. SELECTION OF THE INDEPENDENT GUIDANCE VARIABLE THROUGH A  
STATE DEPENDENT ROTATION

In the previous section the use of a state variable for the independent variable of the controller was examined. In the analysis it was found that the transformation from a time based system to a system based on any monotonic state variable avoids the undesirable performance of the time based system and a docility index was derived which provides a basis of comparison among the state variables in order that one might be selected over the others.

The docility index and simulation results indicated that the locally best choice for the angle of rotation which defines the independent variable is the instantaneous flight path angle. An important restriction on the previous appendix is that the coordinate system in which the regulator operated was time invariant. This leads to certain ambiguities in the interpretation of the docility index. Because local docility is being measured, the relative advantages of different independent variables tends to change along the realized trajectory.

In this appendix the constraint of a time invariant transformation used in defining the evolutionary variable is removed and independent variables depending on the instantaneous state of the vehicle are considered.

D-3.1 Problem Description

In this section attention is restricted to the class of systems characterized by (D-119). A rather subtle difficulty emanates from a study of the implications of (D-119). Corresponding to different choices for  $\zeta$  there are different vehicle descriptions given by (D-119) and as a consequence different regulators given by (D-68). To provide a guidance law which yields the best vehicle performance the analyst should select that coordinate system (value of  $\zeta$ ) in which the vehicle is most amenable to

control (most docile). To facilitate comparison of different choices of  $\zeta$  a scalar valued, local docility index was defined in Appendix D-2. If the perturbation model  $[F(\zeta), G(\zeta)]$  associated with (11) is controllable it is well known that a state error can be eliminated in the "time" interval  $[x_{p1}(t_1), x_{p1}(t_2)]$  with minimum expenditure of control power  $P$  given by

$$P(x_r(x_{p1}(t_1), t_1, t_2) = (x_{p1}(t_2) - x_{p1}(t_1))^{-1} \int_{x_{p1}(t_1)}^{x_{p1}(t_2)} U^2(x_{p1}) dx_{p1} \quad (D-157)$$

It was further shown in Section D-2 that if  $|t_2 - t_1|$  is small, there is a natural basis for the system state space of the perturbation equation associated with (D-119)  $\{n_i; i=1, \dots, n-1\}$  such that

$$P(n_i; t_1, t_2) = \alpha_i |t_2 - t_1|^{-2i} \quad i=1, \dots, n-1 \quad (D-158)$$

The sequence  $\{\alpha_i; i=1, \dots, n-1\}$  measures the energy content in trajectory errors in different directions in the state space. The most docile system would be one which took as little control energy to control as possible. It is usually impossible to uniformly minimize the  $\alpha_i$  both because of their complicated dependence on  $\zeta$ , and because of their dependence on  $x_r(x_{p1}(t_1))$ . Since this latter quantity is often best thought of as being random, the docility index found most expedient in Section D-2 is given by

$$H(S) = E \left\{ \prod_{i=1}^{n-1} \alpha_i(S) \right\} \quad (D-159)$$

The locally best choice of  $\zeta$  is that which minimizes  $H(\zeta)$

$$H(\zeta^*) = \inf_{\zeta} H(\zeta) \quad (D-160)$$

At this point in the development presented previously certain difficulties arose. The choice of  $\zeta$  rationalized by (D-160) yields that transformation which gives the locally most docile system equations. Unfortunately the locally optimal value of  $\zeta$  changes as the vehicle moves along its path. Since  $\zeta$  was initially constrained to be a constant, the values of  $\zeta$  studied were chosen with the value of  $\zeta^*$  in (D-160) used only as a loose indication of the most advantageous choices for  $\zeta$ . It is the intent of this appendix to present the results of a study in which the performance of regulator derived on the basis of continuously using the "locally optimal" coordinate system is explored. This involves some substantial changes in the evaluation of  $H$  since the "locally optimal" coordinate system is both time variable and trajectory dependent.

### D-3.2 A Locally Best Coordinate System

To illustrate the notions described above, consider the simple dynamic model of (D-89). As is the case in appendix D-2 the class of transformations of interest in this study are rotations in the X-Z plane given by (D-90). In contrast, however, in this appendix  $\zeta$  will be permitted to be a differentiable function of time. Direct calculation yields the dynamic equation of the vehicle in the transformed coordinate system

$$\dot{x}_p(\zeta) = \begin{pmatrix} \dot{\zeta} x_{n2} + V \cos(\zeta - \gamma) \\ -\dot{\zeta} x_{n1} - V \sec(\zeta - \gamma) \\ AV^{-1} \end{pmatrix} \quad (D-161)$$

where  $\zeta$  must be such that  $x_{p1}(\zeta)$  is monotonic.

Previously a similar class of transformations were considered with the important restriction that  $\zeta$  be constant. To facilitate comparisons among various possible selections for  $\zeta$ , suppose that the trajectory error at time  $t_1$  is given by

$$x(t_1) = \epsilon \begin{pmatrix} \cos \lambda \\ \sin \lambda \\ \xi \end{pmatrix} \quad (D-162)$$

where  $\lambda$  is a random variable uniformly distributed on  $[0, 2\pi]$ , and  $\xi$  is uncorrelated with  $\lambda$  and satisfies

$$E(\xi) = 0; \quad E(\xi^2) = \Sigma_Y \quad (D-163)$$

The form of  $x(t_1)$  is easily rationalized. A position error of amplitude  $\epsilon$  exists in the (X-Z) plane in a direction characterized by  $\lambda$ . An error in flight path angle also exists at time  $t_1$ . The relative amplitudes of the position and angular error are quantified by  $\Sigma_Y$ .

It is important to note that a given error in a time based model at the vehicle will appear as a different error in the coordinate system  $x_p$ . The most obvious reason for this is the fact that no perturbation can be perceived in the direction of independent variable  $x_{p1}$ . Hence, there is an aliasing of errors when different coordinant systems are compared. In order that H provide a comparison of docility for different vehicle descriptions, a common initial perturbation is a requisite.

The choice of  $x(t_1)$  given by (D-162) generalizes that used previously slightly. Direct calculation as suggested in this reference yields

$$H(\zeta = \zeta_0) = \epsilon^2 \frac{V^2}{6} \left[ \Sigma_\lambda + \frac{R^{-2}}{4} \sec(\gamma - \zeta_0)(1 + \sec^2(\gamma - \zeta_0)) \right] \quad (D-164)$$

where  $R = A^{-1}V$ .

The contribution of  $\Sigma_Y$  to docility is independent of  $\zeta_0$  as would be expected since  $\gamma$  is left invariant by the transformation  $T_R$ . The position component can be minimized by selecting  $\zeta_0 = \gamma$ . Then

$$H(\zeta=Y) = \frac{\epsilon^2 V^2}{6} \left[ \Sigma_Y + \frac{A^2 V^{-4}}{4} \right] \quad (D-165)$$

While the substitution of  $\zeta_0=Y$  in (D-164) is appealing, it violates the constraint that  $\zeta$  be constant. Hence (D-165) could be satisfied at a single point on the trajectory, but it could not hold uniformly. Since terminal miss is an important performance contributor, an attractive candidate guidance law could be one which was locally most docile near impact; i.e.  $\zeta_0=Y_n(t_f)$ . Such a guidance law would tend to be less favorable in the early stages of re-entry.

Because of the allure of the trajectory dependent rotation  $\zeta = Y_p$ , the appendix outlines the calculation of  $H(\zeta = Y_p)$ . This calculation is made difficult because of both the time variable and stochastic nature of the sample of paths of  $\zeta$ . To compute the docility index for  $\zeta = Y_p$ , observe that from (D-161)

$$\dot{x}_p = \begin{pmatrix} AV^{-1}x_{n2} + V \\ -AV^{-1}x_{n1} \\ AV^{-1} \end{pmatrix} \quad (D-166)$$

In (D-166) and the equations which follow, the dependence of the variable on  $\zeta$  will be suppressed since only the single transformation  $T_R(\zeta = Y_p)$  is being considered. Under the usual monotonicity assumptions, it follows that

$$\frac{dx_p}{dx_{p1}} = \begin{pmatrix} 1 \\ -\Delta^{-1}x_{n1} \\ \Delta^{-1} \end{pmatrix} = f_r \quad (D-167)$$

## LOGICON

where  $\Delta = x_{n2} + A^{-1}V^2$ . To compute the performance of the regulator associated with (D-166), the dynamic equation of the perturbation variables must be computed (See D-66)

$$\frac{dx_r}{dx_{pl}} = F_r x_r + G_r u_r$$

where

$$F_r = \left. \frac{\partial f_r}{\partial x} \right|_{(x_n, u_n)} ; G_r = \left. \frac{\partial f_r}{\partial u} \right|_{(x_n, u_n)}$$

Returning to (D-167) and noting that A is the scalar actuating signal

$$F_r = \begin{pmatrix} 0 & 0 & 0 \\ -\Delta^{-1} & x_{n1}\Delta^{-2} & 0 \\ 0 & \Delta^{-2} & 0 \end{pmatrix} ; G_r = \begin{pmatrix} 0 \\ -x_{n1} A^{-2} V^2 \Delta^{-2} \\ A^{-2} V^2 \Delta^{-2} \end{pmatrix} \quad (D-168)$$

To compute the docility index H, the controllability matrix of  $(F_r, G_r)$  must first be evaluated. As is well known, the controllability matrix  $C_n$  is given by

$$C_2 = [M_0, M_1 \quad \dots]$$

$$M_0 = G_r \quad (D-169)$$

$$M_{k+1} = -F_r M_k + \dot{M}_k$$

Clearly the system described by (D-167) cannot be controllable in the usual sense since its first coordinate is degenerate. For the purpose of this study, the system (D-167) will be said to be controllable if the

space orthogonal to (1,0,0) is in the controllability subspace.

It was shown in previously that if  $x_{p1}(t_2) - x_{p1}(t_1) = dx_{p1}$  is small

$$P(x(t_1); dt) = dx_{p1}^{-1} x'(t_1) W^{-1}(t_1, t_2) x(f_1)$$

where

$$W(t_1, t_2) = \sum_{j=0}^{\infty} \frac{dx_{p1}^{(1+j+2)}}{1!j!(1+j+1)} M_1(t_0) M_j(t_0)$$

For small  $dx_{p1}$  it was further shown that there is a natural decomposition of the controllability subspace into directions which differ in their power content. Specifically if

$$\eta_1 = M_0 ||M_0||^{-1}$$

then

$$P(\eta_1; dx_{p1}) \approx ||M_0||^{-2} dx_{p1}^{-2} \quad (D-170)$$

Or if C is such as to make  $||\eta_2|| = 1$  and

$$\eta_2 = C(M_1 - M_1' M_0 (M_0' M_0)^{-1} M_0)$$

then

$$P(\eta_2; dx_{p1}) \approx \frac{1}{3} (\eta_2' M_1 M_1' \eta_2)^{-1} dx_{p1}^{-4} \quad (D-171)$$

Since the derivation of (D-170) and (D-171) is contained in Appendix D-2, it will not be repeated. It might, however, be useful to review the intuitive meaning of these relations. Comparing (D-170) and (D-171), it is clear that errors in the  $\eta_1$  direction require far less control energy

## LOGICON

for their eradication than do errors in the  $n_2$  direction. The reason for this is quickly discernible. The "easy" direction  $n_1$  is seen to be along  $G_r$ , the direction of direct influence of the actuating signal  $u_r$  in (D-67). The "hard" direction  $n_2$  is orthogonal to  $G_r$ . For the controller to reach an error in the  $n_2$  direction, it must work through the system dynamics (See the  $F_r$  and  $G_r$  terms in (D-169). Since the  $n_2$  direction can only be influenced through the "low pass" intermediary of the system equation (D-166), the power required to eliminate the  $n_2$  error in a short time interval becomes quite large.

From (D-170) and (D-171) it follows directly that

$$n_1 = (1+x_{n1}^{-2})^{1/2} \begin{pmatrix} 0 \\ -1 \\ x_{n1}^{-1} \end{pmatrix}; n_2 = (1+x_{n1}^{-2})^{1/2} \begin{pmatrix} 0 \\ x_{n1}^{-1} \\ 1 \end{pmatrix} \quad (D-172)$$

Equation (D-172) has a rather interesting but subtle interpretation. From (D-93) it follows that  $x_{p2}$  is a position variable and  $x_{p3}$  is flight path angle. Because  $x_{n1}$  is large over most of the trajectory, (D-172) indicates that a position error is "easy" to correct while an error in flight path angle is "hard". This is counter-intuitive because (D-89) shows that an acceleration acts directly on flight path angle, and indeed if  $\zeta$  were constant, the regulator always finds  $Y$  to be the easy variable to control. The reason for this anomalous behavioral characteristic lies in the fact that the coordinate system defined by  $T_R$  is now influenced by the controller. The punctilious response induced by  $J$  results in the curious relationship of  $n_1$  and  $n_2$ .

To compute the power figures given in (D-170) and (D-171), note that

$$M_0 = \begin{pmatrix} 0 \\ -x_{n1} A^{-2} V^2 \Delta^{-2} \\ A^{-2} V^2 \Delta^{-2} \end{pmatrix} \quad (D-173)$$

If we assume that A and V are slowly varying and  $x_{n1}$  is large

$$M_1 = \begin{pmatrix} 0 \\ -A^{-1} V (\Delta^{-1} + 2\Delta^{-3} x_{n1}^2) \\ 2 A^{-1} V \Delta^{-3} x_{n1} \end{pmatrix} \quad (D-174)$$

Substituting (D-172) - (D-174) into (D-170) and (D-171) yields

$$\begin{aligned} P(\eta_1; dx_{p1}) &= x_{n1}^{-2} A^2 V^{-2} \Delta^2 (dt)^{-2} \\ P(\eta_2; dx_{p1}) &= \frac{1}{3} A^{-2} V^2 x_{n1}^2 \Delta^{-2} (dt)^{-3} \end{aligned} \quad (D-175)$$

where it has been noted that  $dx_{p1} = AV^{-1} \Delta dt$ .

(D-175) gives the power content of unit errors in the  $\eta_1$  and  $\eta_2$  directions. Because a given initial error will be transformed by  $T(\zeta)$  into a different error in the  $x_r$  - coordinate system, an amplitude normalization is required. It can be shown directly that if  $\zeta = \zeta_0$ , a constant, then

$$x_r(\zeta_0) = \begin{pmatrix} 0 & 0 & 0 \\ -\sin \gamma \sec(\gamma - \zeta_0) & \cos \gamma \sec(\gamma - \zeta_0) & 0 \\ -AV^{-2} \cos \zeta_0 \sec(\gamma - \zeta_0) & -AV^{-2} \sin \zeta_0 \sec(\gamma - \zeta_0) & 1 \end{pmatrix} x \quad (D-176)$$

## LOGICON

When  $\zeta = \gamma_p$  things are more complex. Note first that if  $\gamma_p \approx \gamma_n$

$$dx_p = dT_R(\zeta) x_n + T_R(\zeta) dx_n \quad (D-177)$$

Suppose the error at time  $t_1$  is given by

$$x = e \begin{pmatrix} \cos \lambda \\ \sec \lambda \end{pmatrix} \quad (D-178)$$

where  $E \ll 1$ . From (D-177) and (D-178), the error in the rotated coordinate system  $x(\zeta)$  becomes

$$x(\zeta) = e \begin{pmatrix} \xi x_{n2} + \cos(\lambda - \gamma) \\ -\xi x_{n1} + \sin(\lambda - \gamma) \end{pmatrix}$$

To reflect this error into the  $x_r$  coordinate system note that

$$x_r = T_r x(\zeta)$$

where

$$T_r = \begin{pmatrix} 0 & 0 & 0 \\ -f_{r2} & 1 & 0 \\ -f_{r3} & 0 & 1 \end{pmatrix}$$

Hence

$$x_r = \epsilon \begin{pmatrix} 0 \\ -x_{n1} \Delta^{-1} (\xi x_{n2} + \cos(\lambda - \gamma)) - \xi x_{n1} + \sec(\lambda - \gamma) \\ \Delta^{-1} (\xi x_{n2} + \cos(\lambda - \gamma)) + \xi \end{pmatrix} \quad (D-179)$$

By way of comparison, if  $\zeta = \zeta_0$ ,

$$x_r(\zeta_0) = \begin{pmatrix} 0 \\ \sec(\gamma - \zeta_0) \sin(\lambda - \gamma) \\ -AV^{-2} \sec(\gamma - \zeta_0) \cos(\lambda - \zeta_0) + \xi \end{pmatrix}$$

To determine the components of  $x_r$  in the  $\eta_1$  and  $\eta_2$  directions, note that if  $x_{n1} \gg 1$

$$\eta_1' x_r = \epsilon x_{r2} \quad (D-180)$$

$$\eta_2' x_r = \epsilon x_{n1}^{-1} \sin(\lambda - \gamma) \quad (D-181)$$

Let (D-180) and (D-181) be the amplitudes of the errors in the  $\eta_1$  and  $\eta_2$  directions respectively. Suppose further that  $\lambda$  is uniformly distributed on  $[0, 2\pi]$ , that  $\lambda$  is uncorrelated with  $\xi$  and that

$$E\xi = 0, E\xi^2 = \Sigma_\gamma$$

Then substituting these relations into (D-159)

$$H(\zeta = \gamma_p) = \frac{\epsilon^2}{6} \left[ \Sigma_\gamma (1 + \Delta^{-1} x_{n2})^2 + \frac{3}{4} x_{n1}^{-2} + \frac{\Delta^{-2}}{4} - \frac{2x_{n1}^{-1} \Delta^{-1}}{\pi} \right] \quad (D-182)$$

## LOGICON

Direct calculation from (D-159) yields

$$H(\zeta = \zeta_0) = \frac{\varepsilon^2 v^2}{6} \left[ \sum_Y + \frac{A^2 v^{-4}}{4} \sec^2 (\gamma - \zeta_0) (1 + \sin^2 (\gamma - \zeta_0)) \right] \quad (D-183)$$

If  $A$  and  $V$  are nearly constant, a comparison of system performance using constant and variable  $\zeta$  is made easier if the docility index is parameterized in terms of  $R$  and  $\theta$  (See Figure D-10) Direct calculation yields

$$H(\zeta = \gamma_p) = \frac{\varepsilon^2}{6} \left[ \sum_Y (2 - \sec \theta)^2 + \frac{R^{-2}}{4} (3 \csc^2 \theta + \sec^2 \theta - \frac{8}{\pi} \sec \theta \csc \theta) \right]$$

$$H(\zeta = \zeta_0) = \frac{\varepsilon^2 v^2}{6} \left[ \sum_Y + \frac{R^{-2}}{4} \sec (\gamma - \zeta_0) (1 + \sec^2 (\gamma - \zeta_0)) \right] \quad (D-184)$$

Comparing (D-164) and (D-184), it is clear that  $\zeta = \gamma_p$  shows an improvement over  $\zeta = \zeta_0$  on the order of  $v^2$ .

The result given in (D-184) is initially rather surprising. As expected  $\zeta = \gamma_p$  is superior to any constant value for  $\zeta$  when  $H$  is considered over the whole trajectory. Still the improvement factor is quite large on the trajectories considered. The reason for the pronounced enhancement of regulator performance lies in the way errors are measured when  $\zeta$  is trajectory dependent. For now suffice it to say that letting  $\zeta = \zeta_p$  adds a new degree of flexibility to the regulator given by (D-68). To see this observe that the analyst studying the performance of the regulator associated with  $\zeta = \zeta_0$  may select  $\zeta_0$  to provide good performance on one segment of the trajectory. Still, once  $\zeta_0$  is chosen, system behavior is circumscribed by the restrictions inherent in the fixed coordinate system. In contrast,  $\zeta = \gamma_p$  is not fixed initially and in fact

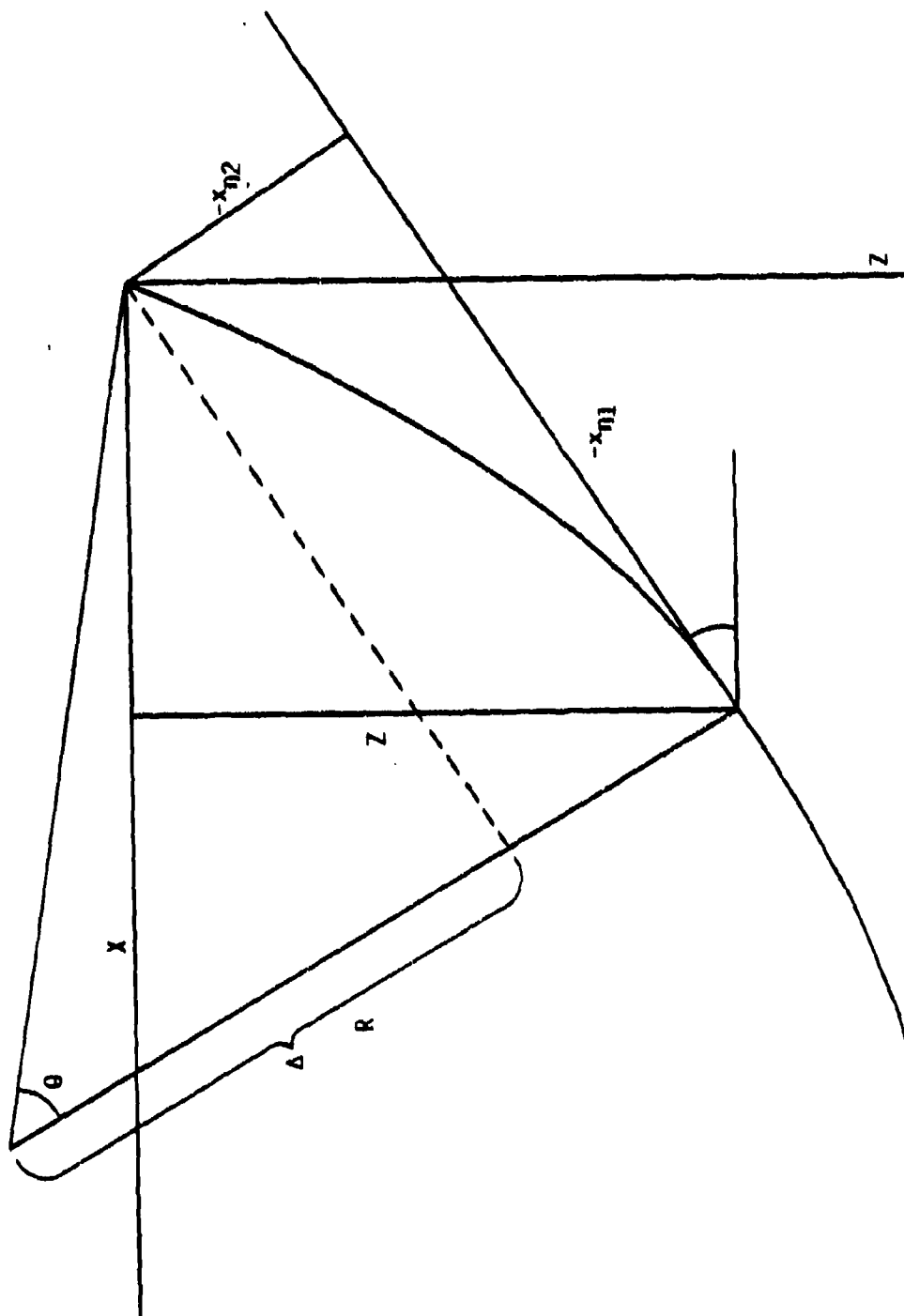


Figure D-9. Parameterization of  $R$  and  $\theta$

## LOGICON

---

will change as a function of trajectory errors. More fundamentally,  $\gamma_p$  is a controllable quantity. Therefore, when  $\zeta = \gamma_p$ , the regulator can actually control the coordinate system in which errors are measured. The way in which the regulator utilizes the pliancy of the coordinate system is rather cunning.

## REFERENCES

- D-1. G.R. Wells, "Advanced Guidance Time Varying 'R' Matrix," Logicon IOC No. SA-75084-R2870-042, dated October 1975
- D-2. D.D. Swarder, "Preliminary Study of Guidance Laws in Time Variable Coordinate Systems, Part 2," Logicon IOC No. SA-75067-R2870-029, dated August 1975
- D-3. G.R. Wells, "Commentary on Swarder's Guidance Law Recommendations," Logicon IOC No. SA-75075-R2870-036, dated September 1975
- D-4. G.B. Skelton, "Launch Booster Gust Alleviation," AIAA Paper 66-969, Boston, Mass. 1968
- D-5. D.D. Swarder, "Preliminary Study of Guidance Laws in Time Variable Coordinate Systems," Logicon IOC No. SA-75050-R2870-028, dated July 1975
- D-6. Willems, J. E. and Mitter, S. K., "Controllability, Observability, Pole Allocation, and State Reconstruction", IEEE Trans. on Automatic Control, Vol. AC-16, dec. 1971, pp. 582-595
- D-7. Swarder, D. D. and Wells, G. R., "Guidance Laws for Aerodynamically Controlled Re-Entry Vehicles, J. of Spacecraft and Rockets", Vol. 14, No. 2, Feb. 1977, pp. 111-117
- D-8. Swarder, D. E. and Archer, S. M., "A Passively Adaptive Regulator for Following a Reference Trajectory", Proceedings of the 1976 Conference on Decision and Control, IEEE, Dec. 1976, pp. 1069-1074
- D-9. Muller, P. C. and Weber, H. I., "Analysis and Optimization of Certain Qualities of Controllability and Observability for Linear Dynamical Systems", Automatica, Vol. 8, 1972, pp. 237-246
- D-10. Johnson, C. D., "Optimization of Certain Quality of Complete Controllability and Observability for Linear Dynamical Systems," Trans. of the ASME, Journal of Basic Engineering, June 1969, pp. 228-238

APPENDIX E  
ADDITIONAL STEERING LAW TOPICS

In this appendix, two topics related to the general problem of development of steering laws for an aerodynamically-controlled reentry vehicle are considered.

In Section E-1, the influence of autopilot states in the calculation of controller gains calculated using the LQ regulator formulation is examined. This analysis is motivated by the potential reduction in model size achievable if the influence of the autopilot states is weak.

In Section E-2, certain aspects of imperfect state estimates and their relationship to the LQ regulator used for the steering law (or controller) are examined. This analysis is motivated by the realization that the on-board sensors are imperfect and indeed can also experience failures.

E-1. INFLUENCE OF AUTOPILOT STATES ON SYSTEM PERFORMANCE

E-1.1 Introduction

Simulation of the nonlinear model of an aerodynamically-controlled reentry vehicle has indicated a potential source of instability associated with the autopilot loops. The LQ regulator portion of the guidance law is derived on the premise that the vehicle states are continuously observable and the actuating signals vary in response to changes in state. Actually, guidance is accomplished from sampled observations of state errors, and if the guidance loop gains are too high, unpredicted instability can occur. This problem has proved to be particularly troublesome in the autopilot loops when autopilot states are included in the guidance law.

Stability margins in the nonlinear model can be significantly improved by the simple artifact of reducing or eliminating the penalties associated

## LOGICON

---

with the autopilot errors in the performance index. Small weighting on autopilot errors tends to yield small feedback gains and this in turn minimizes the stability problems created by sampling. Indeed, satisfactory system performance has been attained by simply setting the autopilot gains equal to zero.

This latter observation suggests that the dynamic properties of the autopilot may not be essential in the gain calculation for the LQ regulator guidance law. If the autopilot could be eliminated from the linear vehicle model, this would simplify considerably the solution of the Riccati equation which is an intermediate step in the gain calculation. There would be fewer weightings to be selected in the performance index and the overall design problem would be made easier.

This appendix gives the results of a study of the influence of model simplification on closed-loop performance. The results are preliminary in that only the properties of the linear perturbation model are explored. A more complete analysis will require simulation of the nonlinear vehicle model to validate the results derived here.

### E-1.2 Model Reduction

Suppose the dynamical equations of the perturbation variables  $(x,u)$  satisfy the linear differential equation

$$\dot{x} = F(t)x + G(t)u \quad (E-1)$$

$$x(t_0) = x_0$$

The advanced guidance law is that feedback regulator which minimizes

$$J = x(t_f)' P_f x(t_f) + \int_{t_0}^{t_f} (x' Q x + u' R u) dt \quad (E-2)$$

## LOGICON

The structure of the advanced guidance law has been explored in many references (see for example, Reference E-1) and the form of the guidance law can be given explicitly

$$u = -R^{-1}G'Px \quad (E-3)$$

subject to

$$\dot{P} = -F'P - PF + PGR^{-1}G'P - Q; \quad t_0 \leq t \leq t_f \quad (E-4)$$

$$P(t_f) = P_f$$

Although not usually of great significance, the cost  $J$  can be evaluated for a variety of linear control laws. Denote by  $u_M$  the guidance law given by

$$u_M = -R^{-1}G'Mx \quad (E-5)$$

where  $M$  is a nonnegative symmetric matrix. From (E-3) the advanced guidance law is given by  $u_p$ .

Let  $J_M$  be the performance associated through (E-2) to the control  $u_M$ . Suppose that it is possible to write  $J_M$  in the form

$$J_M(t_0) = x(t_0)' P_M(t_0) x(t_0) \quad (E-6)$$

for all  $t_0 \leq t_f$ . Then

$$\frac{\partial J_M(t_0)}{\partial t_0} = \dot{x}(t_0)' P_M(t_0) x(t_0) + x' \dot{P}_M x + x' P_M \dot{x} \quad (E-7)$$

From (E-1) and (E-5)

$$\dot{x} = (F - GR^{-1}G'M)x \quad (E-8)$$

## LOGICON

---

Differentiating the right side of (E-2) with respect to  $t_0$ , it follows that

$$\frac{\partial J_M(t_0)}{\partial t_0} = -x(t_0)' Q(t_0) x(t_0) - u'(t_0) R(t_0) u(t_0) \quad (E-9)$$

Combining (E-7) and (E-9)

$$\dot{P}_M = -(F - GR^{-1}G'M)' P_M - P_M (F - GR^{-1}G'M) - Q - MGR^{-1}G'M \quad (E-10)$$

$$P_M(t_f) = P_f.$$

If we substitute  $M = P$  in (E-10)

$$\dot{P}_P = -(F - GR^{-1}G'P)' P_P - P_P (F - GR^{-1}G'P) - Q - P_P GR^{-1}G'P_P \quad (E-11)$$

$$P_P(t_f) = P_f$$

Comparing (E-4) and (E-11), it is clear that

$$P_P = P$$

and as a consequence the performance of the regulator  $u_p$  is given by

$$J = x(t_0)' P x(t_0). \quad (E-12)$$

Thus, in addition to its role in the gain calculation,  $P$  is actually the "cost" matrix as well.

Suppose that  $M$  is nearly equal to  $P$ ; i.e.

$$M = P + \delta P; \quad ||\delta P|| \ll ||P||$$

# LOGICON

Denote by  $\delta P_M$  the corresponding variation in  $P_M$ :

$$P_M = P + \delta P_M \quad (E-13)$$

From (E-10)

$$\begin{aligned} \dot{P}_M &= \dot{P} + \delta \dot{P}_M \\ &= -\left(F - GR^{-1}G'(P + \delta P)\right)'(P + \delta P_M) - (P + \delta P_M)\left(F - GR^{-1}G'(P + \delta P)\right) \\ &\quad - Q - (P + \delta P)GR^{-1}G'(P + \delta P) \end{aligned}$$

Using (E-11)

$$\begin{aligned} \delta \dot{P}_M &= -\left(F - GR^{-1}G'(P + \delta P)\right)' \delta P_M - \delta P_M \left(F - GR^{-1}G'(P + \delta P)\right) \\ &\quad - \delta P GR^{-1}G' \delta P \end{aligned} \quad (E-14)$$

$$\delta P_M(t_f) = 0.$$

To gain insight into the structure of (E-14) consider the following identity. Let  $\Lambda(t)$  be defined by

$$\Lambda(t) = \int_t^{t_f} (e^{A'(t-\tau)} B e^{A(t-\tau)}) d\tau \quad (E-15)$$

Then

$$\frac{d\Lambda(t)}{dt} = -B + \int_t^{t_f} \frac{\partial}{\partial t} (e^{A'(t-\tau)} B e^{A(t-\tau)}) d\tau$$

$$\frac{d\Lambda}{dt} = -B + A'\Lambda + \Lambda A \quad (E-16)$$

$$\Lambda(t_f) = 0$$

Comparing (E-14) and (E-16), assuming the coefficient matrices in (E-14) are nearly constant and using the fact that  $P + \delta P \approx P$

$$\delta P_M(t_0) = \int_{t_0}^{t_f} e^{-(F - GR^{-1}G'P)'(t_0 - \tau)} \delta P GR^{-1}G' \delta P e^{-(F - GR^{-1}G'P)'(t_0 - \tau)} d\tau \quad (E-17)$$

If  $(F, G)$  is controllable, the maximum eigenvalue  $e^{-(F - GR^{-1}G'P)}$  can be used as a norm of the matrix exponential. Clearly

$$||\delta P_M(t_0)|| \leq (t_f - t_0) ||GR^{-1}G'|| ||\delta P||^2 \quad (E-18)$$

Consequently, a variation in  $P$  gives no first order change in  $P_M$ ; i.e.

$$\left. \frac{\partial P_M}{\partial M} \right|_{M=P} = 0 \quad (E-19)$$

The sensitivity of system performance to changes in gain is zero near  $-R^{-1}G'P$ . Any changes in the system model which create small changes in gain will cause essentially no change in system performance.

## LOGICON

The small sensitivity to gain changes is important in this application only if we can show that the desired changes in system structure give rise to small changes in gain. Elimination of the autopilot states changes the order of the system equations and is not a small variation in the usual sense. Suppose  $F$  and  $G$  experience perturbations  $\delta F$  and  $\delta G$ , respectively. The corresponding value of the cost matrix becomes

$$\dot{P} + \delta \dot{P} = -(F + \delta F)'(P + \delta P) - (P + \delta P)(F + \delta F) + (P + \delta F)(G + \delta G)R^{-1}(G + \delta G)'(P + \delta P) - Q$$

Consequently

$$\delta \dot{P} = -(\bar{F} - \bar{G}R^{-1}\bar{G}'\bar{P})'\delta P - \delta P(\bar{F} - \bar{G}R^{-1}\bar{G}'\bar{P}) \quad (E-20)$$

$$-P(\delta F - \delta GR^{-1}\bar{G}'\bar{P}) - (\delta F - \delta GR^{-1}\bar{G}'\bar{P})'P$$

$$\delta P(t_f) = 0$$

where

$$\bar{F} = F + \delta F, \quad \bar{G} = G + \delta G, \quad \bar{P} = P + \delta P$$

The equation for  $P$  has the same stability properties as does that for the  $P$  matrix associated with the perturbed system. It follows from (E-20) that  $||\delta P||$  will be small if  $||P(\delta F - \delta GR^{-1}\bar{G}'\bar{P})||$  is small. One of the factors is fairly obvious. If  $\delta F$  and  $\delta G$  are small, then  $G \approx \bar{G}$ . Consequently,  $\delta F - \delta GR^{-1}\bar{G}'\bar{P}$  is small if the first variation in the closed-loop dynamic matrix is small. A small change in the closed-loop system dynamics will produce a small change in  $P$ , but the converse is not as strong. To gain more insight into the effect of the autopilot states, a simple example is useful.

AN EXAMPLE

Suppose we consider a simple trajectory in the plane described by

$$\begin{aligned}\dot{X} &= \cos Y \\ \dot{Z} &= \sin Y \\ \dot{Y} &= A \\ \dot{A} &= a_n(A - A_c)\end{aligned}\tag{E-21}$$

The variables have the obvious interpretation and  $a_n$  is the nominal corner frequency of the acceleration command autopilot. The perturbation equations associated (E-21) are easily derived and have the form given in (E-1) with

$$F = \begin{bmatrix} 0 & 0 & -\sin Y & 0 \\ 0 & 0 & \cos Y & 0 \\ 0 & 0 & 0 & 1 \\ 0 & 0 & 0 & a_n \end{bmatrix}, \quad G = \begin{bmatrix} 0 \\ 0 \\ 0 \\ -a_n \end{bmatrix}\tag{E-22}$$

Suppose we wish to investigate the influence of the autopilot state. One way in which the autopilot can be effectively eliminated is to set the autopilot corner frequency equal to  $a_M$  where  $a_M \gg 1$ .

$$\delta F = \begin{bmatrix} 0 & 0 & 0 & 0 \\ 0 & 0 & 0 & 0 \\ 0 & 0 & 0 & 0 \\ 0 & 0 & 0 & a_M - a_n \end{bmatrix}; \quad \delta G = \begin{bmatrix} 0 \\ 0 \\ 0 \\ a_n - a_M \end{bmatrix}\tag{E-23}$$

# LOGICON

Clearly, neither  $\delta F$  nor  $\delta G$  is small.

Let us partition  $P$ ,  $F$ ,  $G$ , and  $Q$  as follows:

$$P = \begin{bmatrix} P_{11} & P_{12} \\ P_{21} & P_{22} \end{bmatrix}, \quad F = \begin{bmatrix} F_{11} & F_{12} \\ F_{21} & F_{22} \end{bmatrix}, \quad G = \begin{bmatrix} 0 \\ G_2 \end{bmatrix}, \quad Q = \begin{bmatrix} Q_{11} & 0 \\ 0 & 0 \end{bmatrix} \quad (E-24)$$

where  $P_{22}$ ,  $F_{22}$ ,  $G_2$ , etc. are scalars and the other elements are of compatible dimension. We will assume that weighting  $Q$  on state errors provides no penalty for deviations in autopilot state from nominal. Since the actuating signal is one dimensional,  $R$  is scalar and will be denoted by  $r$ .

Expanding (E-4) and noting that  $P$  is symmetric

$$\dot{P}_{11} = -F_{11}'P_{11} - P_{11}F_{11} - P_{12}F_{21} - F_{21}'P_{12} - Q_{11} + \frac{G_2^2}{r} P_{12}P_{12}' \quad (E-25)$$

$$\dot{P}_{22} = -2F_{22}P_{22} - P_{21}P_{12} - F_{21}'P_{21}' + \frac{G_2^2}{r} P_{22}^2$$

$$\dot{P}_{12} = -P_{11}F_{12} - P_{12}F_{22} - F_{11}'P_{12} - F_{21}'P_{22} + \frac{G_2^2}{r} P_{12}P_{22}$$

$$P_{12}(t_f) = 0, \quad P_{22}(t_f) = 0$$

Let us assume that  $a_n$  and therefore  $F_{22}$  is large compared to one and that  $P_{12}$  and  $P_{22}$  are of comparable norm. Then

$$\dot{P}_{22} \approx -2F_{22}P_{22} + \frac{G_2^2}{r} P_{22}^2 \quad (E-26)$$

## LOGICON

The nontrivial stationary value of  $P_{22}$  is given by

$$P_{22} = \frac{2rF_{22}}{G_2^2} = \frac{2r}{a_n} \quad (E-27)$$

Suppose  $P_{22}$  differs from the solution given in (E-27) by a small amount  $\epsilon$ . Then

$$\begin{aligned} -2F_{22}(P_{22} + \epsilon) + \frac{G_2^2}{r} (P_{22} + \epsilon)^2 &\approx (-2F_{22} + \frac{2G_2^2}{r} P_{22})\epsilon \\ &= 2F_{22}\epsilon \end{aligned}$$

From (E-26) then

$$\dot{\epsilon} = 2F_{22}\epsilon \quad (E-28)$$

In (E-28),  $F_{22} = a_n$  and  $a_n > 0$ . The stability properties of (E-28) are more easily seen if we use the change of variable  $\tau = t_f - t$ . Equation (E-28) becomes

$$\frac{d\epsilon}{d\tau} = -2a_n\epsilon \quad (E-29)$$

Equation (E-29) is stable thus suggesting that  $P_{22}$  is very close to the value given in (E-27) for all  $t$  outside of a small interval containing  $t_f$ .

Next, let us look at  $P_{12}$  in more detail. From (E-25)

$$\dot{P}_{12} = -\left(F'_{11} + \left(F_{22} - \frac{G_2^2}{r} P_{22}\right) I\right) P_{12} - P_{11}F_{12} \quad (E-30)$$

# LOGICON

But

$$F_{22} - \frac{G_2^2}{r} P_{22} = -a_n$$

or

$$\dot{P}_{12} = -(F'_{11} - a_n I) P_{12} - P_{11} F_{12}$$

By assumption  $a_n I \gg F'_{11}$  and thus

$$\dot{P}_{12} = a_n P_{12} - P_{11} F_{12} \quad (E-31)$$

The stability properties of the equation for  $P_{12}$  in (E-31) are those exhibited by  $c$  in (E-29). Consequently,

$$P_{12} \approx \frac{P_{11} F_{12}}{a_n} \quad (E-32)$$

We are now in a position to complete the analysis of the  $P$  equation by looking at  $P_{11}$ . Since  $F_{21} = 0$ ,

$$\dot{P}_{11} = -F'_{11} P_{11} - P_{11} F_{11} - Q_{11} + \frac{G_2^2}{r} P_{12} P'_{12} \quad (E-33)$$

But

$$\frac{G_2^2}{r} P_{12} P'_{12} = \frac{a_n^2}{p} \frac{P_{11} F_{12} F'_{12} P_{11}}{a_n^2}$$

$$= P_{11} F_{12} r^{-1} F'_{12} P_{11}$$

## LOGICON

Consequently

$$P'_{11} = -F_{11}P_{11} - P_{11}F_{11} - Q_{11} + P_{11}F_{12}r^{-1}F_{12}P_{11} \quad (E-34)$$

Equation (E-34) is precisely the equation that would result if

$$F = \begin{bmatrix} F_{11} & 0 \\ 0 & 0 \end{bmatrix}, \quad G = \begin{bmatrix} F_{12} \\ 0 \end{bmatrix} \quad (E-35)$$

From the preceding equations it becomes clear that if the autopilot corner frequency  $a_n$  is large,

$$||P_{22}|| = O\left(\frac{1}{a_n}\right) \quad (E-36)$$

$$||P_{12}|| = O\left(\frac{1}{a_n}\right)$$

The limiting value of  $P_{11}$  is that which would be associated with a reduced order model containing no autopilot dynamics. If we assume that  $a_M \gg a_n$ ,

$$P_M(t_0) \approx \begin{bmatrix} (P_p)_{11} & 0 \\ 0 & 0 \end{bmatrix}$$

or

$$||\delta P|| = O\left(\frac{1}{a_n}\right) \quad (D.(E-37))$$

From (E-37) it is evident that the large magnitude variation in  $F$  and  $G$  gives rise to a small variation in  $P$ . Because of the small closed-loop sensitivity to variations in gain (see E-19), the system performance will be unaffected by the elimination of the autopilot state in (E-21) if the nominal corner frequency  $a_n$  is high.

## E-1.3 Conclusions

This section has provided a preliminary analysis of the influence of elimination of autopilot states on closed-loop system performance. If the autopilot dynamics are neglected, certain stability problems are reduced and the calculation of the guidance gains is made simpler. Because the effective order of the system dynamic equation is reduced, the removal of the autopilot does not correspond to a small variation in the  $[F, G]$  matrix. Consequently, the usual perturbation arguments can not be used to study performance sensitivity.

The proof that autopilot states are of little importance proceeds in two parts. First, it was shown that linear regulators with gains close to those appropriate for the advanced guidance law have performance that is indistinguishable from that attained with the correct gain. This is a general property of the advanced guidance law. Small gain errors from whatever source have negligible influence on performance.

The next step is to show that a change in system order yields a small change in gain. In contrast to the preceding sensitivity property, the influence of order reduction makes essential use of the structure of  $[F, G]$ . Order reduction causes a big change in the nominal dynamical matrices of the linear perturbation model. To show that the ensuing gain change is small, requires more than a sensitivity argument because second and higher order perturbation terms must be retained. One may either show that the solutions to (E-20) are small or show directly that the value of  $P$  corresponding to  $[F, G]$  is close to that associated with  $[F, G]$ . It was shown by example that for motion in the  $x$ - $z$  plane, the acceleration command autopilot has little influence on system performance if the nominal autopilot corner frequency is high. It is expected that a similar conclusion would follow from analysis of the seven dimensional models for motion in  $R^3$ .

## LOGICON

---

Since only the dominant terms in the Riccati equation were retained in this analysis, it is impossible to state quantitatively how large  $a_n$  must be to permit its benign neglect. A more detailed analysis would be necessary to provide this type of information.

**E-2. INFLUENCE OF SENSOR FAILURES ON LQG REGULATORS****E-2.1 Introduction**

The solution to the linear-quadratic Gaussian (LQG) regulator problem has a number of attractive features which suggest its use in applications (see Reference E-2). The synthesis algorithm leads to a linear feedback regulator with gain given by the solution to a matrix ordinary differential equation. The controller is, thus, relatively easy to implement. Of primary interest in this paper is another idiosyncrasy of the LQG regulator; certainty equivalence. As pointed out by many investigators, the LQG regulator has a natural decomposition into a filter which generates the best mean-square estimate of the system state and a fixed gain controller independent of the observation mechanism. This latter property is desirable in on-line applications because to make the controller parameters contingent on the realization of the exogenous influences, would yield a system of unacceptable complexity.

This appendix considers a situation of a somewhat more general sort. Specifically, concern is centered on the influence of changes in the observation equation. The motivation for this work was a study of the operational characteristics of reentry vehicles. Such systems have continuous sensors; e.g., an inertial measurement package; and may, at discrete time points, make additional position measurements using a separate group of sensors. Particularly these latter measurements are subject to untoward influences due to both environmental effects and internal failures. It is, therefore, of interest to determine how the regulator should be modified in response to these events of uncertain occurrence.

There are many excellent papers extolling the virtues and explaining the limitations of LQG regulators. This appendix will use the notation conventions of Tse and Reference E-5 whenever possible. Of particular interest is the exploration of the nuances of a supposition of Tse to the effect

that an optimal regulator will have the certainty equivalence property if (Reference E-3, pg. 780):

- 1) The conditional mean of the state characterizes the observation  $\sigma$ -field
- 2) The conditional mean of the state has the same dynamical equation as does the state.
- 3) The cost is quadratic.

#### E-2.2 Problem Description

The system to be controlled and the feedback link will be described by linear equations (see Reference E-2):

$$\dot{x} = Ax + Bu + \xi \quad 0 \leq t \leq T \quad (E-38)$$

$$y = Cx + \theta \quad (E-39)$$

where  $x$  is the system state,  $u$  the actuating signal, and  $y$  the observation signal. The signals  $\xi$  and  $\theta$  are white noise processes independent of each other and independent of  $x(0)$  where  $x(0)$  is Nor  $(\hat{x}_0, \Sigma(0))$ . For reasons that were explained in the introduction, it is advantageous to generalize the observation equation (E-39) slightly. Let  $I$  be a discrete set with elements  $\{t_1, \dots, t_n\}$  and assume

$$\begin{aligned} E \xi(t) &= 0 ; E \xi(t) \xi(\tau) = \Xi(t) \delta(t - \tau) \\ E \theta(t) &= 0 ; E \theta(t) \theta(\tau) = \begin{cases} \theta(t) \delta(t - \tau) & t \notin I \\ \theta(t) & t = \tau \in I \\ 0 & \text{Otherwise} \end{cases} \end{aligned} \quad (E-40)$$

The feedback link transmits continuous aggregated observations of the system state with white additive noise except for a discrete set of times of which a higher quality set of observations is transmitted. These latter

## LOGICON

observations may differ in type from the former, and  $C$  may be discontinuous on  $I$ . The performance index is quadratic

$$J = E [x'(t) Sx(t)] + \int_0^T (x'Qx + u'Ru)dt \quad (E-41)$$

where  $S$ ,  $Q$ , and  $R$  satisfy the usual hypotheses.

The basic element which distinguishes this problem from that of Tse is the possibility of sensor failure. Let the random process  $r(t)$  represent the mode of operation of the feedback measurement link and suppose  $C$  and  $\Theta$  depend upon  $r$ ; i.e.,

$$(C(t), \Theta(t)) = (C_i(t), \Theta_i(t)) \text{ if } r(t) = i \quad (E-42)$$

Thus, the feedback measurement gain  $C$  or the observation noise level  $\Theta$  may change in some random fashion. The indicator variable  $r$  is a finite state Markov process characterized for small  $\Delta$  by:

$$\text{Prob } (r(t + \Delta) = j | r(t) = i) = \begin{cases} 1 - \rho_{ij}(t)\Delta + O(\Delta) & i = j, t \notin I \\ \rho_{ij}(t)\Delta + O(\Delta) & i \neq j, t \notin I \\ \rho_{ij}(t)\Delta + O(\Delta) & t \in I \end{cases} \quad (E-43)$$

Let  $N = [\rho_{ij}]$ . To see the implication of (E-42) and (E-43) suppose that  $r = 1$  corresponds to normal operation and  $r = 2$  represents a degraded observation; e.g.,  $\Theta_2(t) > \Theta_1(t)$  or  $C_2(t) C_2'(t) < C_1(t) C_1'(t)$ . Equation (E-43) gives a failure "rate" of  $\rho_{12}(t)$  for  $t \notin I$ . If  $N(t) = I$  for  $t \in I$ , (E-43) admits the possibility of failure coincident with discrete update. This could be due to a component overload, or to the fact that a prior failure only becomes apparent when the updating sensors are interrogated.

If the realization of  $r$  were known a priori, (E-38) - (E-40) would delineate the LQG regulator problem. The optimal causal control policy is linear and Equation (E-38) (formally) generates a Gaussian random process. Under (E-42) and (E-43), this will no longer be true. Let  $\{\mathcal{F}_t; t \in [0, T]\}$  be the observation  $\sigma$ -fields at the controller;

$$\mathcal{F}_t = \sigma\{y(\tau), r(\tau); \tau \in [0, t]\} \quad (E-44)$$

Note that perfect measurement of  $r$  is permitted in the feedback link. This is an idealization, of course, but this assumption leads to a far more analytically tractable problem. The basic problem is to find a function  $u(t)$  adapted to  $\mathcal{F}_t$  such that (E-41) is minimized.

### E-2.3 Solution Algorithm

Before considering the control problem, consider first the problem of estimating  $x$ . At first glance this might appear to be a formidable obstacle because of the random coefficients in the observation equation. Actually this is not the case. Because  $r(t)$  is  $\mathcal{F}_t$  measurable and a Markov process, the equations of evolution of the conditional mean take on the form one would intuitively expect. A certain amount of tedious calculation yields the following results: Let

$$\hat{x}(t) = E \{x(t) \mid \mathcal{F}_t\} \quad (E-45)$$

Then

$$\begin{aligned} \dot{\hat{x}} &= A\hat{x} + Bu + W_1 v; \quad r(t) = 1, \quad t \notin I \\ \hat{x}(t) &= \hat{x}(t^-) + W_1(t)v(t); \quad r(t) = 1, \quad t \in I \\ \hat{x}(0) &= \hat{x}_0 \end{aligned} \quad (E-46)$$

where

$$E v = 0; E v(t) v'(\tau) = \begin{cases} \phi_i(t) \delta(t - \tau); & t \notin I, r(t) = i \\ \phi_i(t) + C_i(t) \Sigma(t^-) C_i'(t); & t \in I, r(t) = i \\ 0 & \text{Otherwise} \end{cases} \quad (E-47)$$

$$W_i(t) = \begin{cases} \Sigma(t) C_i'(t) \phi_i^{-1}(t) & ; t \notin I, r(t) = i \\ \Sigma(t^-) C_i'(t) [C_i(t) \Sigma(t^-) C_i'(t) + \phi_i(t)]^{-1} & ; t \in I, r(t) = i \end{cases} \quad (E-48)$$

$$\begin{aligned} \dot{\Sigma}(t) &= A \Sigma + \Sigma A' - \Sigma C_i' \phi_i^{-1} C_i \Sigma + \Sigma & ; t \notin I, r(t) = i \\ \Sigma(t) &= [I - K_i(t) C_i(t)] \Sigma(t^-) & ; t \in I, r(t) = i \\ \Sigma(0) &= \Sigma_0 \end{aligned} \quad (E-49)$$

Observe that if  $t \notin I$  the equation for  $\dot{x}$  "has the same dynamic(s) as the original process except with different driving disturbance" (Reference E-3 py. 780). For  $t \in I$ ,  $\dot{x}$  may have discontinuities, a property not shared by  $x$ . Note that the noise intensity is random in (E-46) both through  $W$  and the covariance of  $v$ . Particularly the former depends upon the past history of  $r$  through its dependence on  $\Sigma$ . Further,  $W$  is not deterministic as was the case in (E-2), but it is adapted to  $\mathcal{F}_t$ .

Using the argument of Tse in toto it can be shown that

$$J = E \left\{ \dot{x}'(t) S x(t) + \int_0^T (\dot{x}' Q \dot{x} + u' R u) dt + \text{Tr}(S \Sigma(T)) + \int_0^T Q A d\tau \right\} \quad (E-50)$$

In contrast to the LQG problem, the last two terms in (E-50) are random. Because the last two terms are also unaffected by the control policy, a control problem of a fairly standard sort results. It is shown in Section E-2.6 that the optimal quadratic regulator is given by

$$u = -R^{-1}B' K \dot{x} \quad (E-51)$$

with

$$J = \hat{x}_0' K(0) \hat{x}(0) + P_{r(0)}(0) + E \left\{ \text{Tr}(S \Sigma(T)) + \int_0^T Q \Sigma d\tau \right\} \quad (E-52)$$

where

$$\dot{K} = -A'K - KA - KBR^{-1}B'K + Q \quad (E-53)$$

$$K(T) = S$$

$$\dot{p} = -Np - r \quad t \in I \quad (E-54)$$

$$p(t^-) = Np(t) = r \quad t \in I$$

$$p(T) = 0$$

where  $p$  and  $r$  are vectors with elements

$$p = [p_i] ; \quad r = [\text{Tr } KW_i < v \quad v > W_i'] \quad (E-55)$$

#### E-2.4 Properties of the Optimal Regulator

The most interesting attribute of the optimal regulator given by (E-51) is the fact that the certainty equivalence property is preserved in the presence of sensor failure. The evolutionary equations of  $\hat{x}$  satisfy the dynamical equations of the controlled system almost everywhere, and this produces the desired result. The resulting closed-loop system does not have Gaussian solutions because of the multiplicative influence of the random process  $r$ .

It is interesting to compare the result derived here with that derived in a closely related problem. In Reference E-4, full state feedback was permitted and consequently  $x = \hat{x}$ . In this reference the times of discontinuity were not predictable as they are here. Even after factoring out some other dissimilarities in the statements of the two problems, a fundamental difference in the solutions remains. The primary reason for this is the fact that the change in state at points of discontinuity in Reference E-4 was "multiplicative"; i.e.,

## LOGICON

---

$$x(t) = r_{ij}x(t^-) \text{ if } r(t) = j, r(t^-) = i,$$

while that of (E-46) is additive. Although the system of Reference E-4 satisfies all of the desiderata of Tse, separation in its strongest form, (E-51) fails. In the referenced problem, the control component of the optimal regulation policy is independent of the additive noise terms but depends explicitly on  $r$ , and consequently can be seen to possess a weaker form of separation. In both cases the "filter" portion of the regulator depends upon the exogenous variables.

Though (E-51) is unrelated to sensor reliability, the same is not true of the performance. Equation (E-52) has a natural decomposition into a state independent term related to filter performance. The components of this latter term proportional to  $E(\Sigma)$  clearly increase as the likelihood of failure increases. The driving term in the  $p$  equation,  $r$ , is proportional to  $C'C$  and inversely proportional to  $\phi$ . The  $P_{r(0)}(0)$  component of cost tends to decrease with improved filter performance. While these terms can not be expected to cancel, they do provide some measure of compensation.

The structural result given by (E-51) and (E-53) can be generalized weakly to the case where the parameters of the open-loop system (E-38) vary with  $r$ . Using classical techniques, it can be shown that if  $\Sigma$  depends upon  $r$ , (E-51) and (E-53) still give the control portion of the optimal regulator. If, however,  $(A, B)$  varies with  $r$ , the gain in (E-51) must be made contingent on  $r$ . This effect was observed in the noise-free problem with random jump parameters.

### E-2.5 Conclusion

This appendix has considered the influence of changes in the parameters of the observation equation on the feedback regulator optimal with respect to a quadratic performance index. The feedback gains were seen to be unaffected by sensor variability of a specified type. This characteristic

has important practical implications because the controller gains are often stored on a special purpose computer for on-line implementation of the regulator.

The underlying explanation for the strong separation displayed by the controller lies in the passive nature of the learning task as perceived by the controller. This avoids the dual control problem which would arise if  $r$  were not perfectly sensed. As pointed out by Tse in Reference E-3, the dual control problem will admit no such easy solution as obtained here.

#### E-2.6 Proof of Equation E-51

The proof of (E-51) follows the standard formalism of dynamic programming. Let  $J^*(t, \hat{x}(t), r(t))$  be the minimum cost to go;

$$J^*(t, \hat{x}(t), r(t)) = E \left\{ x'(T) S x'(T) + \int_t^T (x' Q x + u' R u) d\tau \mid \mathcal{F}_t \right\} \quad (E-56)$$

It is well known that  $J^*$  satisfies an equation of the Bellman type

$$0 = \min_{u(t)} ((\hat{x}'(t) Q \hat{x}(t) + u(t) R u(t)) dt + E \{ dJ^* \mid \mathcal{F}_t \}) \quad (E-57)$$

Generalizing Reference E-5 to the vector case

$$\begin{aligned} dJ^*(t, \hat{x}(t); r(t)) &= J_t^* dt + J_x^* d\hat{x}(t) + \frac{1}{2} \text{Tr}(J_{xx}^* d \langle x_c, x_c \rangle) \\ &+ J^*(t), \hat{x}(t), r(t)) - J^*(t, \hat{x}(t^-)) - J_x^* \Delta x(t) \end{aligned} \quad (E-58)$$

where  $\hat{x}_c$  and  $\Delta \hat{x}$  are the continuous and discontinuous parts of  $x$ , respectively. From (E-46)

$$\langle \hat{x}_c, \hat{x}_c \rangle = W_1 \Theta_1 W_1' dt \quad (E-59)$$

# LOGICON

Substituting (E-58) and (E-59) into (E-57)

$$0 = \begin{cases} \min_u \hat{x}'R\hat{x} + u'Ru + J_x^*(t, \hat{x}, i)(Ax + Bu) + \frac{1}{2} \text{Tr}(J_{xx}^*(t, \hat{x}, i)W_i \otimes_i W_i) \\ + \sum_j \rho_{ij} J^*(t, \hat{x}(t), j) & \text{if } t \notin I, r(t) = i \\ \min_{u,j} \rho_{ij} J^*(t, \hat{x}(t), j) - J(t, \hat{x}(t^-), i) & \text{if } t \in I, r(t) = i \end{cases} \quad \begin{matrix} (E-60) \\ (E-61) \end{matrix}$$

Note (E-61) is control independent.

If we assume that  $J^*$  has the form

$$J^*(t, \hat{x}, r) = \hat{x}'K_r\hat{x} + p_r \quad (E-62)$$

then

$$u = -R^{-1}B'K_i\hat{x} \quad \text{if } R(t) = i \quad (E-63)$$

Note that  $u$  in (E-63) is used for all  $t$  since  $I$  is discrete. Direct substitution of (E-62) and (E-63) into (E-60) yields (note  $\sum_j \rho_{ij}(t) = 0$  if  $t \notin I$ )

$$K_i = -A'K_i - K_iA - K_iBR^{-1}BK_i + Q; \quad i = 1, \dots, N; \quad t \notin I$$

$$K(T) = S \quad (E-64)$$

$$p = -Np - r$$

$$p(T) = 0 \quad (E-65)$$

where  $p$  is a vector with elements  $p_i$  and the  $i$ th element of  $r$  is

$$r_i = \text{Tr}(KW_i \langle v, v \rangle W_i) \quad (E-66)$$

Equation (E-61) has somewhat different properties.

# LOGICON

$$E \left\{ \sum_j \rho_{ij} (\hat{x}(t^-) + \Delta \hat{x})' K_j(t) (\hat{x}(t^-) + \Delta \hat{x}) + \rho_{ij} p_j(t) \right\}$$

$$= \sum_j \rho_{ij} (\hat{x}'(t^-) K_j(t) \hat{x}(t^-) + \text{Tr} K_j(t) W_j) < v, v > \dot{W}_j + P_j(t)$$

Since  $\sum_j \rho_{ij}(t) = 1$ , if  $t \in I$ ,

$$K_j(t) = K_j(t^-) \quad (E-67)$$

$$N(t)p(t) = p(t^-) - \Gamma \quad (E-68)$$

Combining (E-64) - (E-68),

$$\dot{K} = -A'K - KA - KBR^{-1} B'K + Q; t \in 0, T \quad (E-69)$$

$$K(T) = S$$

$$\begin{cases} p = -Np - \Gamma; t \notin I \\ p(t^-) = N(t)p(t) + \Gamma; t \in I \end{cases} \quad (E-70)$$

$$p(T) = 0$$

$$u = -R^{-1}B'Kx$$

APPENDIX E  
REFERENCES

- E-1. D. D. Swarder, "Preliminary Study of Guidance Laws in Time Variable Coordinate Systems," Logicon IOC No. SA-75050-R2870-028, dated July 1975
- E-2. M. Athans, "The Role and Use of the Stochastic Linear-Quadratic Gaussian Problem in Control System Design," IEEE Trans. on Automatic Control, Vol. AC-16, No. 6, pp. 529-551, Dec. 1971
- E-3. E. Tse, "On the Optimal Control of Stochastic Systems," IEEE Trans. on Automatic Control, Vol. AC-16, No. 6, pp. 776-784, Dec. 1971
- E-4. D. D. Swarder, "Control of Jump Parameter Systems with Discontinuous State Trajectories," IEEE Trans. on Automatic Control, Vol. AC-18, No. 5, pp. 740-741, Oct. 1972
- E-5. A. Segall, "Stochastic Processes in Estimation Theory," IEEE Trans. on Information Theory, Vol. IT-22, No. 3, pp. 275-286, May 1976

APPENDIX F  
FLIGHT TEST TRAJECTORY DESIGN BY SIMPLICIAL PIVOTING

F-1. INTRODUCTION

This appendix describes the problem of weapon system flight test trajectory design for the purpose of improving operational system performance evaluation. It is shown that the observability of the principal reentry guidance system errors can be substantially enhanced by trajectories designed for this purpose. These errors are evaluated using a simulated post flight analysis of the measurements made by the reentry vehicle inertial measurement unit (RIMU) and by radar/camera ground sensors. The result of this evaluation for a flight test trajectory is the covariance matrix of the error in estimating the RIMU error sources. The measure of improvement provided by a designed trajectory is a weighted functional of this covariance matrix, where the weight assigned to each error source is its contribution to the CEP of a candidate operational trajectory. The search for a reentry trajectory which minimizes this functional and satisfies energy, vehicle, and instrumentation constraints is performed with a simplicial pivoting algorithm. The problem is solved for each of two RIMUs. First, the Small Hardened Inertial (gimballed) Platform (SHIP) is considered, and second, the Dormant (strapdown) Inertial Navigation System (DINS), with laser gyros is considered. The extent of SHIP and DINS error parameter estimation capability during a flight test is derived. The results show that significant improvement in the observability of SHIP principal error parameters can be attained.

The operational weapon system and its RIMU principal performance contributors are described in Sections 2 and 3 respectively. The flight test trajectory design problem to improve error source estimation is defined in Section 4. An approximate solution to this problem is sought by reducing the number of variables and applying a mechanized algorithm. Section 5 discusses the selection of the simplicial pivoting algorithm to solve this

## **LOGICON**

---

reduced problem. Section 6 gives results of the trajectory design study by comparing the parameter estimation realizable with the designed trajectories with that from two candidate flight test trajectories. A brief summary is given in Section 7.

F-2. OPERATIONAL SYSTEM DESCRIPTION

The operational system considered consists of an aerodynamically controlled reentry vehicle and a reentry inertial measurement unit (RIMU) deployed from a Minuteman III booster with a NS-20 guidance system. The NS-20 is modeled with the error sources and error source uncertainties corresponding to current accuracy estimates. The RIMUs considered here are the SHIP and the DINS platforms.

At launch, the RIMU is assumed coarsely aligned in azimuth and is aligned about the level axes using its accelerometers. The RIMU navigates from launch and is updated by comparisons with the more accurate NS-20.

The reentry navigation system is initialized at reentry with a state vector mapped from the estimated state at deployment and navigates through the reentry phase of the mission.

F-2.1 SHIP Error Model

The SHIP is modeled with a total of 93 accelerometer, gyro, gimbal mass unbalances, and platform compliance errors. The SHIP platform axes are aligned to a downrange, crossrange, and up orientation at launch and the accelerometer and gyro input axes are as shown in Figure F-1.

Accelerometer Error Model

The acceleration error for each accelerometer is modeled by:

$$\begin{aligned} \Delta A_i = & K_0 + K_1 A_i + K_s |A_i + K_0| + K_d \text{sign}(A_i + K_0) \\ & + K_2 A_i^2 + K_3 A_i^3 + K_{1p} A_i A_p + K_{1o} A_i A_o + K_{2o} A_o^2 \\ & + K_{21} A_i |A_i| + K_p A_p + K_o A_o + \beta A_p + \gamma A_o \end{aligned}$$

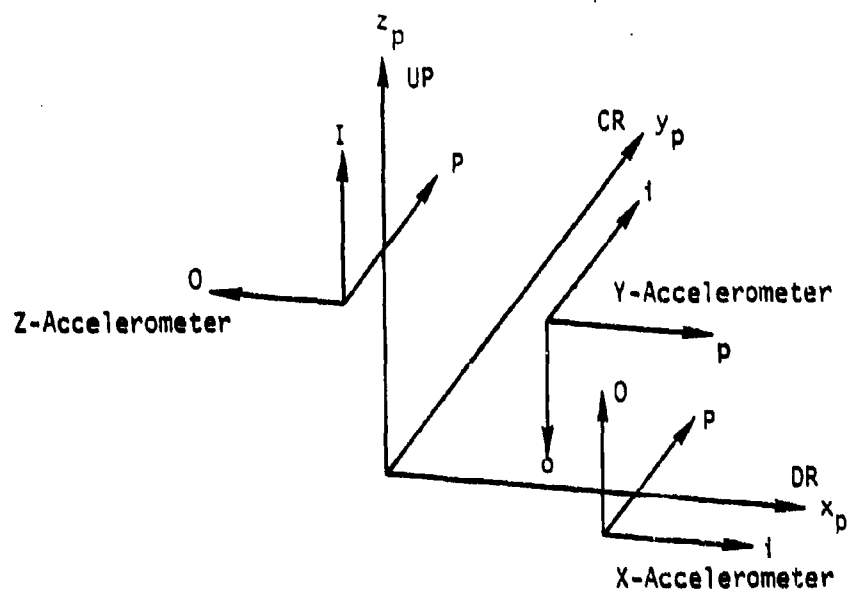


Figure F-1a. SHIP Accelerometer Orientations

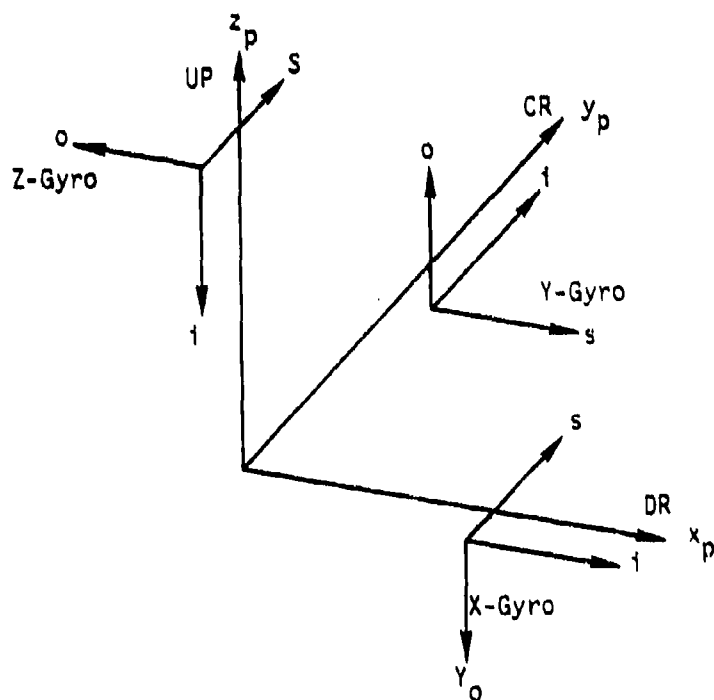


Figure F-1b. SHIP Gyro Orientations

## LOGICON

The coefficients for the error model and their description are:

- $K_0$  - bias
- $K_1$  - scale factor
- $K_s$  - absolute scale factor
- $K_d$  - hysteresis bias shift
- $K_2$  - input axis quadratic nonlinearity
- $K_3$  - cubic nonlinearity
- $K_{1p}$  - pendulous cross axis scale factor
- $K_{1o}$  - output cross axis scale factor
- $K_{2o}$  - output axis quadratic nonlinearity
- $K_{21}$  - input axis quadratic difference
- $K_o$  - output cross axis bias
- $\beta$  - input axis toward pendulous axis misalignment
- $\gamma$  - input axis toward output axis misalignment

and the subscripts (i, p, o) denote the input, pendulous, and output axes of the accelerometer.

### Gyro Error Model

The drift rate error about the gyro input axis is modeled by:

$$\begin{aligned}\dot{\phi}_i = & D_f + D_i A_i + D_o A_o + D_s A_s + D_{ii} A_i^2 + D_{io} A_i A_o \\ & + D_{is} A_i A_s + D_{oo} A_o^2 + D_{ss} A_s^2 + D_{os} A_o A_s\end{aligned}$$

The coefficients of the gyro error model are:

- $D_f$  - fixed drift
- $D_i$  - input axis mass unbalance
- $D_o$  - output axis mass unbalance
- $D_s$  - spin axis mass unbalance
- $D_{ii}$  - compliance

## LOGICON

---

$D_{io}$  - compliance  
 $D_{is}$  - compliance  
 $D_{oo}$  - compliance  
 $D_{ss}$  - compliance  
 $D_{os}$  - compliance

where the subscripts (i, o, s) denote the input, output, and spin axes of the gyro.

### Gimbal Mass Unbalance Model

The gimbal mass unbalances give rise to misalignments about the platform x, y, and z axes of the forms:

$$\begin{array}{l} \text{Misalignment} \\ \text{about x axis} \end{array} \quad \left\{ \begin{array}{l} \theta_{xy} = -K_{xy} A_y \\ \theta_{xz} = K_{xz} A_z \end{array} \right.$$

$$\begin{array}{l} \text{Misalignment} \\ \text{about y axis} \end{array} \quad \left\{ \begin{array}{l} \theta_{yx} = K_{yx} A_x \\ \theta_{yz} = -K_{yz} A_z \end{array} \right.$$

$$\begin{array}{l} \text{Misalignment} \\ \text{about z axis} \end{array} \quad \left\{ \begin{array}{l} \theta_{zx} = -K_{zx} A_x \\ \theta_{zy} = K_{zy} A_y \end{array} \right.$$

Where the  $A_x$ ,  $A_y$ ,  $A_z$  are in platform coordinates.

### Platform Compliance Model

Deformation of the platform caused by g-loading causes the accelerometers to be misaligned with respect to their theoretical input axes. The errors in acceleration caused by this deformation are modeled as:

$$\Delta A_i = K_{ijk} A_j A_k$$

## LOGICON

$\Delta A_i$  is the acceleration error along the  $i$ th axis caused by the  $A_j$  and  $A_k$  accelerations.

### Platform Alignment

The platform is misaligned at launch by the angles  $\phi_x$ ,  $\phi_y$ ,  $\phi_z$  about the platform axes. The acceleration error due to the platform misalignment is given by

$$\Delta \bar{A}(t) = \begin{pmatrix} \phi_x \\ \phi_y \\ \phi_z \end{pmatrix} \times \bar{A}(t)$$

where  $\bar{A}$  and  $\Delta \bar{A}$  are in platform coordinates.

### F-2.2 DINS Error Model

#### Coordinate Systems

The orientation of the plate axes on the RV is given by

x = roll  
y = pitch  
z = yaw

The orientation of the DINS accelerometers and gyros is described in Volume II.

#### Accelerometer Error Model

The DINS accelerometer error model is given in accelerometer coordinates and is applied to all three accelerometers. The acceleration in accelerometer coordinates is denoted by

$$\bar{A} = \begin{bmatrix} A_I \\ A_P \\ A_O \end{bmatrix}$$

## LOGICON

where the subscripts I, P, O refer to the input, pendulous, and output axes which comprise the right-handed accelerometer coordinate system. The angular rate about the accelerometer input, pendulous, and output axes is denoted by

$$\vec{W} = \begin{bmatrix} W_I \\ W_P \\ W_O \end{bmatrix}$$

The acceleration error along the input axis is given by

$$\begin{aligned} \delta A_I = & K_B + K_{I1}A_I + K_P A_P + K_O A_O + K_{I2}A_I^2 + K_{P2}A_P^2 + K_{O2}A_O^2 \\ & + K_{IP}A_I A_P + K_{IO}A_I A_O + K_{OP}A_O A_P + K_{I3}A_I^3 + K_{P3}A_P^3 \\ & + K_W W_I W_P \end{aligned}$$

The descriptions of the coefficients for the error model are:

- $K_B$  - bias
- $K_{I1}$  - scale factor
- $K_P$  - pendulous g sensitivity
- $K_O$  - output g sensitivity
- $K_{I2}$  - input quadratic nonlinearity
- $K_{P2}$  - pendulous quadratic nonlinearity
- $K_{O2}$  - output quadratic nonlinearity
- $K_{IP}$  - input-pendulous nonlinearity
- $K_{IO}$  - input-output nonlinearity
- $K_{OP}$  - output-pendulous nonlinearity
- $K_{I3}$  - input cubic nonlinearity
- $K_{P3}$  - pendulous cubic nonlinearity
- $K_{O3}$  - output cubic nonlinearity
- $K_W$  - anisoinertia

## LOGICON

Since DINS is a strapdown system, the accelerometers measure acceleration in a coordinate frame which changes as the RV attitude changes. In order to obtain the inertial velocity increments, the sensed body velocity increments must be transformed into the inertial coordinate system. One method of doing this would be to first transform the velocity increment from the sensor (accelerometer) frame S to the body frame B by

$$\Delta \vec{V}_B = [S \rightarrow B] \Delta \vec{V}_S$$

where the sensor-to-body matrix  $[S \rightarrow B]$  is constant in time. The incremental velocity in body coordinates could then be transformed into the inertial system I by

$$\Delta \vec{V}_I = [B \rightarrow I] \Delta \vec{V}_B$$

where the body-to-inertial matrix  $[B \rightarrow I]$  is determined by the body orientation, which in turn is obtained from the gyro measurements.

### Gyro Error Model

The DINS gyro error model is given in gyro coordinates and is applied to all three gyros. The acceleration in gyro coordinates is denoted by

$$\vec{A} = \begin{bmatrix} A_I \\ A_J \\ A_K \end{bmatrix}$$

where the I, J, and K axes form a right-handed coordinate system. The angular rate about the gyro I, J, and K axes is denoted by

$$\vec{W} = \begin{bmatrix} W_I \\ W_J \\ W_K \end{bmatrix}$$

Each gyro is designed to measure the rate about its I axis ( $W_I$ ).

## LOGICON

The error in the measurement of rate is given by

$$\begin{aligned}\delta W = & K_B + K_{RW} t^{-1/2} + K_I W_I + K_{IAI} W_I A_I + K_{IAJ} W_I A_J \\ & + K_{IAK} W_I A_K + K_J W_J + K_K W_K + K_{JAJ} W_J A_J + K_{KAK} W_K A_K\end{aligned}$$

The descriptions of the coefficients for the error model are:

- $K_B$  - fixed drift
- $K_{RW}$  - random walk drift
- $K_I$  - scale factor
- $\left. \begin{matrix} K_{IAI} \\ K_{IAJ} \\ K_{IAK} \end{matrix} \right\}$  acceleration sensitive scale factor
- $K_J$  - misalignment to J
- $K_K$  - misalignment to K
- $K_{JAJ}$  - acceleration sensitive misalignment to J
- $K_{KAK}$  - acceleration sensitive misalignment to K

### Plate Error Model

Deformation of the plate by g-loading causes the accelerometers to be misaligned. Due to a lack of physical test data, a simple bending model relating the structural compliance of the accelerometer cluster to the g-loading was chosen. This model is the same as the SHIP platform compliance model.

### F-2.3 Candidate Operational Trajectory

The operational trajectory assumed for this analysis is the standard MMIII -27.5 degree reentry angle accuracy studies trajectory terminated by a mixture of yaw maneuvers and coasts. The reentry trajectory is depicted in Figure F-2.

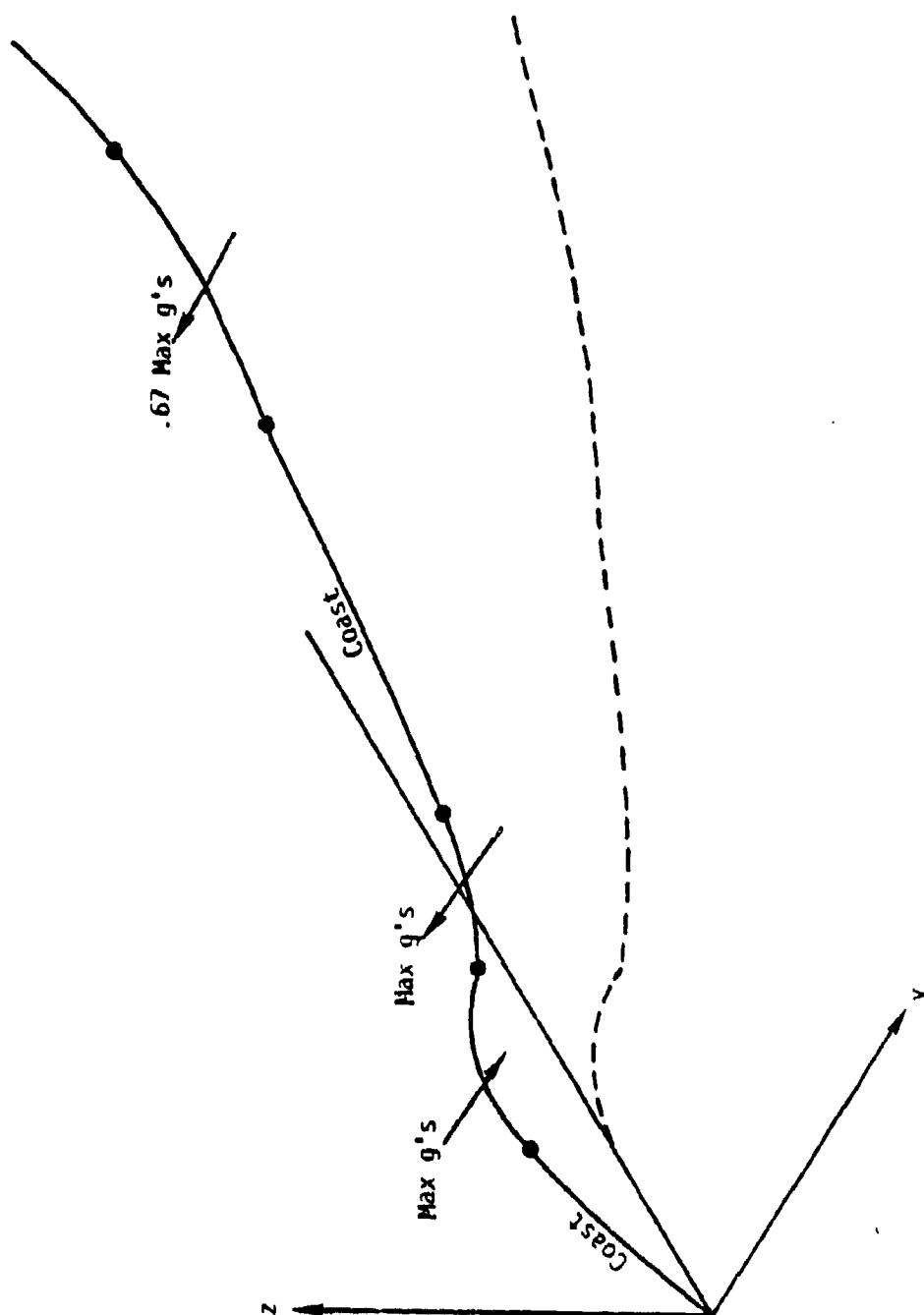


Figure F-2. Operational Yaw-Maneuvering Trajectory

**F.3 IDENTIFICATION OF PRINCIPAL PERFORMANCE CONTRIBUTORS**

The operational accuracy of a strategic missile system is calculated from an error source budget since the system accuracy cannot be measured directly in an operational environment with operational trajectories. Thus, an error source budget is estimated in testing activities and the system performance is calculated with error analysis techniques for the operational case.

Therefore, the accuracy of the operational performance estimate depends on the fidelity of the error source budget determined from testing activities and the sensitivity of the calculated operational performance to variations in the error source magnitudes. This sensitivity depends both on the magnitude of the particular error source value in comparison to the remainder of the error sources and on the error sensitivity of the particular source. For example, in a system where the budget accuracy is dominated by a single error source, a small change in the magnitude of that source will cause significant change in the calculated accuracy. At the same time for one of the smaller contributions, even though it might have a large individual error uncertainty, the same percent change will have a much smaller effect on calculated accuracy.

The criterion for selecting the principal performance contributors in this analysis is the sensitivity of system CEP to variations in the error source magnitudes about a priori budget values.

The system sensitivities were evaluated using the Logicon System Error Analysis Program (SEAP) which uses an extended Kalman filter to propagate system errors and to simulate the system measurement updates of an aided system. SEAP operates as shown in Figure F-3 to evaluate the performance of an optimal system mechanization.

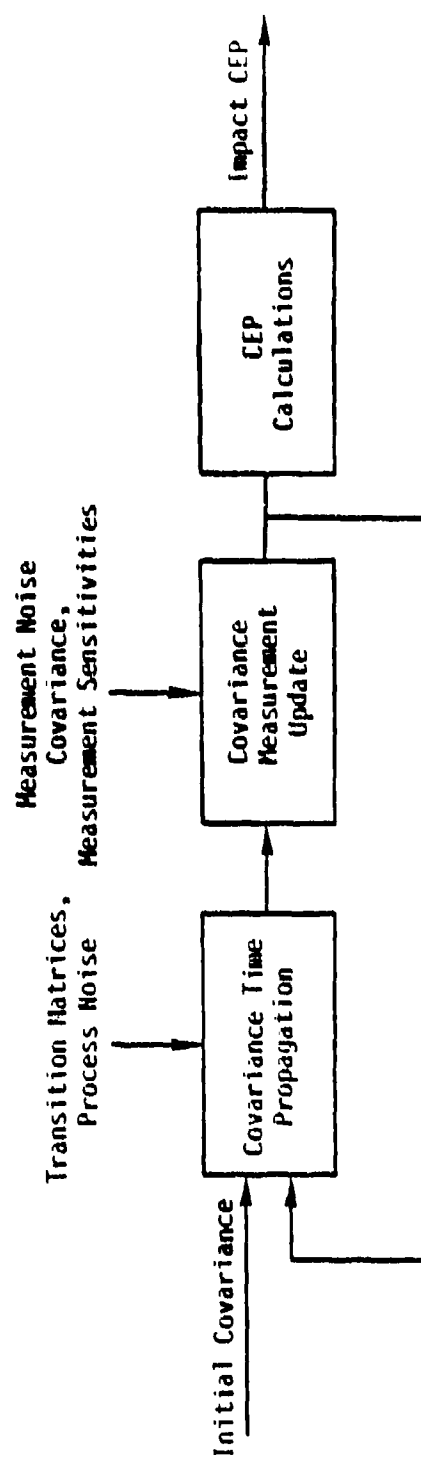


Figure F-3. System Error Analysis Program

**F-3.1     SHIP Principal Performance Contributors**

In the SHIP guidance system under consideration, the reentry systems errors consist of the navigated position and velocity plus the 93 SHIP error sources, while the navigation aid, the NS-20, is modeled by 78 error source states in a filter state vector because of correlations from measurement to measurement. The SEAP state vector is shown in Figure F-4.

The system sensitivities were calculated by perturbing the error source magnitude by a factor of 10 (making the magnitude larger) and calculating the resulting change in CEP.

The system sensitivities were first evaluated in groups to eliminate possible error sources from contention. The groups were formed based upon the results of linear error analyses of the SHIP over the boost and reentry phases of the mission. For those groups not eliminated, the contributing error sources were determined using subdivisions of the groups and finally individual system CEP sensitivities were determined. For the system and a priori error budget under consideration, the system sensitivity magnitudes are dominated by 13 error sources. The 13 error sources with the largest sensitivities and their sensitivities are given in Table F-1. These significant sensitivities arise during the reentry phase since the effects during boost are estimated by the inflight measurements. Error sources, such as azimuth alignment which might be expected to appear among the largest contributors do not because they are estimated by the inflight measurements.

**F-3.2     DINS Principal Performance Contributors**

In the DINS guidance system, the reentry system errors consist of navigated position and velocity, initial misalignment and 96 DINS error sources. The NS-20 errors are modeled as for SHIP. The SEAP state vector is as shown in Figure F-4 except for an added random walk gyro drift, which is modeled as described earlier.

$$\begin{aligned}
 \underline{S} &= \begin{bmatrix} \underline{\delta P} \\ \underline{\delta V} \end{bmatrix} && \text{ECI Position Error} \\
 \underline{E}_{\text{RIMU}} &= \begin{bmatrix} \underline{\delta \phi} \\ \underline{R} \\ \underline{E} \quad \underline{A} \\ \underline{R} \quad \underline{E} \quad \underline{G} \end{bmatrix} && \begin{array}{l} \text{RIMU Alignment Errors} \\ \text{RIMU Accelerometer Errors} \\ \text{RIMU Gyro Errors} \end{array} \\
 \underline{E}_{\text{NS20}} &= \begin{bmatrix} \underline{\delta \phi} \\ \underline{N} \\ \underline{E} \quad \underline{A} \\ \underline{N} \quad \underline{E} \quad \underline{G} \end{bmatrix} && \begin{array}{l} \text{NS20 Alignment Errors} \\ \text{NS20 Accelerometer Errors} \\ \text{NS20 Gyro Errors} \end{array} \\
 \underline{E}_{\text{G\&G}} &= \begin{bmatrix} \underline{\delta GM} \\ \underline{\text{ETC}} \end{bmatrix} && \text{G\&G Errors}
 \end{aligned}$$

$$\underline{X} = \begin{bmatrix} \underline{S} \\ \underline{E}_{\text{RIMU}} \\ \underline{E}_{\text{NS20}} \\ \underline{E}_{\text{G\&G}} \end{bmatrix} \quad \text{Error States}$$

Figure F-4. System State Vector

Table F-1. SHIP Principal Performance Contributors

Source Number	Description	CEP Contribution (% of System CEP)
1	Gimbal Mass Imbalance about Z by Y	139
2	Y-Gyro $D_{11}$	95
3	X-Accelerometer Bent to Y by Y	84
4	Z-Gyro $D_{55}$	78
5	Z-Gyro $D_{15}$	56
6	X-Accelerometer Bent to Y by X	40
7	X-Gyro $D_{10}$	39
8	Gimbal Mass Imbalance About X by Y	35
9	Y-Gyro $D_{10}$	35
10	X-Accelerometer Bent to Z by Z	35
11	Y-Gyro $D_{00}$	34
12	Z-Gyro $D_{11}$	27
13	Z-Gyro $D_{05}$	27

\*1000% increase in uncertainty

## LOGICON

---

As with SHIP, the significant system error contributions of the DINS platform arise after the boost phase. The principal DINS error contributor is the gyro scale factor which causes a misalignment at reentry. This misalignment is substantial because of the many revolutions of the reentry vehicle during free flight. Thus a small gyro scale factor error will produce a large misalignment at reentry.

This misalignment is oriented principally along the average direction of the roll axis during free flight. Since this direction is approximately along the roll axis at reentry, the effect on CEP at impact is less for the trajectories considered here than if the misalignment were about the pitch or yaw axes. Consequently, the initial pitch and yaw misalignments, though much smaller than the roll misalignment, have a comparable miss contribution. The initial platform misalignments at reentry contribute 96% of the total DINS reentry CEP for the operational yaw-maneuvering trajectory. Thus, the principal performance contributors considered for the DINS guidance system are only the three initial platform misalignments at reentry.

F-4. FLIGHT TEST REENTRY TRAJECTORY DESIGN

F-4.1 Flight Test System

The system assumed for the flight test experiment is the flight test reentry vehicle deployed from a Minuteman I booster on a SAMTEC to Kwajalein trajectory. For this analysis the reentry vehicle impact is assumed to be in the lagoon where adequate ground sensor coverage is possible. The flight test boost trajectory has a -26.7 degree reentry angle.

The boost guidance system is the NS-10 guidance set and each RIMU is a less mature version of the operational RIMU. (Some of the error source magnitudes are budgeted larger than those for the operational version.) The flight test RIMU error model form is identical to the operational model described earlier. Except, the SHIP platform axes are in a down-range, crossrange, and down orientation at launch, and the DINS platform axes are along roll, pitch, and yaw at reentry.

A set of three sensors has been chosen. Figure F-5 shows the locations of the sensors and the assumed impact point. The three sensors are each assumed to be a composite of a radar (for range measurement) and a camera (for angle measurements) located at the sites shown. Ground sensor measurement accuracy is assumed to be 20 ft ( $1\sigma$ ) in range and  $0.003^\circ$  ( $1\sigma$ ) in azimuth and elevation. (In addition, the radars have bias and scale factor modeled errors and the cameras have bias errors for azimuth and elevation each with the equivalent corresponding  $1\sigma$ 's at a range of 100,000 ft.) The initial estimate of the reentry vehicle state at reentry is assumed to be derived from this ground sensor data.

The assumed vehicle is a bank-to-turn vehicle so that the controls available are normal acceleration,  $a_n$ , and the bank angle,  $\phi$ . The acceleration due to aerodynamic drag on the vehicle is partially a function of the normal acceleration. The vehicle is subject to constraints on normal acceleration magnitude, integral of acceleration, and impact Mach number.

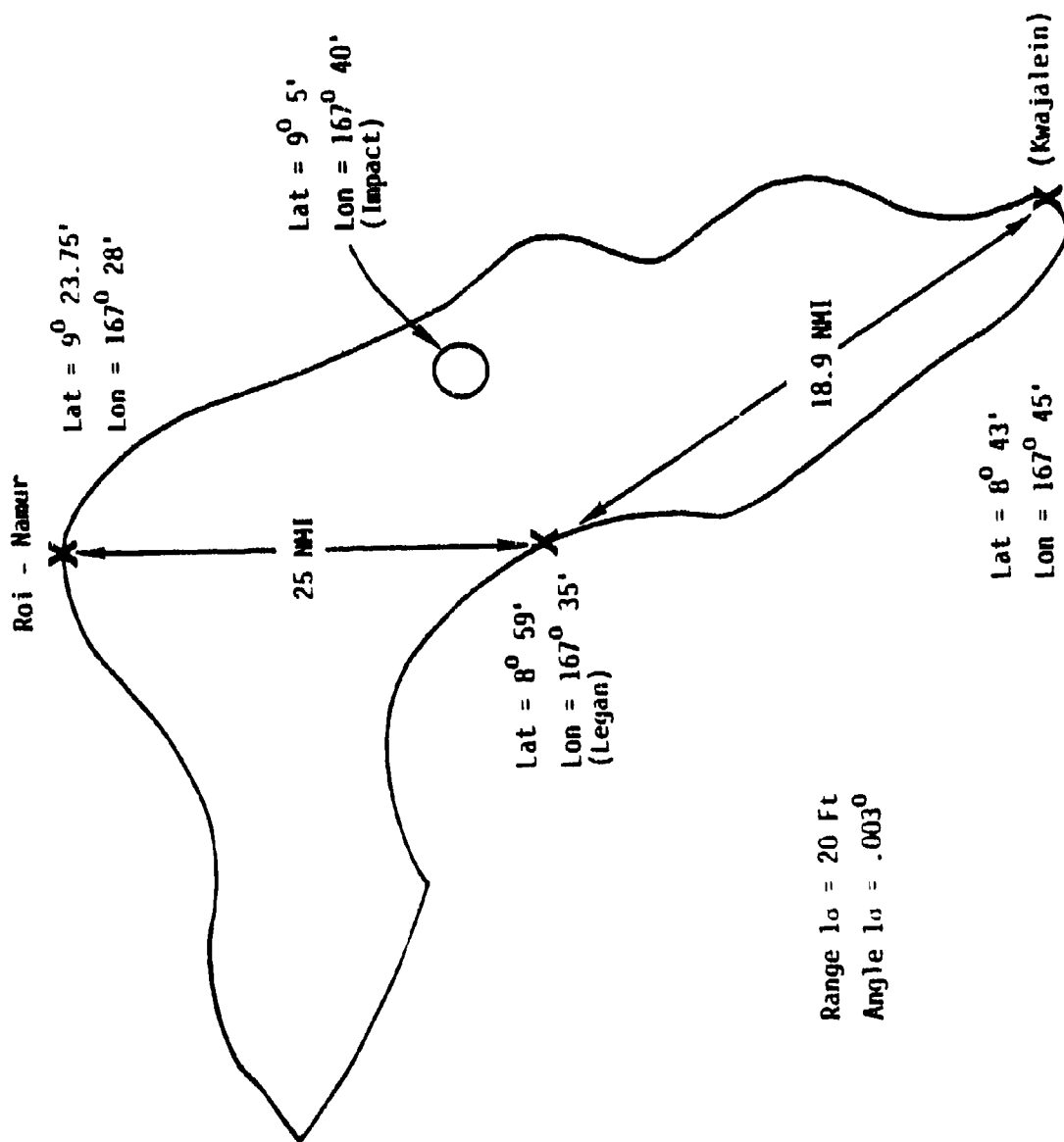


Figure F-5. Ground Sensor Geometry

## LOGICON

---

### F-4.2 The Identification Problem

The RIMU and ground sensor state error variables are taken to be of the bias form, i.e.

$$\bar{\theta} = \begin{pmatrix} \theta_{\text{RIMU}} \\ \theta_{\text{SENSOR}} \end{pmatrix}, \quad \dot{\bar{\theta}} = 0$$

where the vector  $\theta_{\text{RIMU}}$  contains the RIMU error parameters to be identified and the vector  $\theta_{\text{SENSOR}}$  contains the ground sensor non-random error parameters.

The measurement equation is

$$Z(t) = H(t, u) \bar{\theta} + v(t)$$

where

$$E(v(t)v^T(t')) = R(t) \delta(t - t')$$

#### F-4.2.1 Observability of SHIP Error Sources

It is instructive to examine the form of the SHIP errors. The SHIP error sources can be divided into gyro and non-gyro errors. In platform coordinates, the SHIP acceleration errors can be shown to be of the following forms.

##### Non-Gyro Errors

$$N_1: \Delta \bar{A}_i(t) \approx \theta_i$$

$$N_2: \Delta \bar{A}_i(t) \approx \theta_i A_k(t)$$

$$N_3: \Delta \bar{A}_i(t) \approx \theta_i A_k(t) A_g(t)$$

## LOGICON

### Gyro Errors

$$G_1: \Delta \bar{A}_1(t) = \theta_1 t B_1 \bar{A}(t)$$

$$G_2: \Delta \bar{A}_1(t) = \theta_1 \int_0^t A_1(\tau) d\tau B_1 \bar{A}(t)$$

$$G_3: \Delta \bar{A}_1(t) = \theta_1 \int_0^t A_k(\tau) A_l(\tau) d\tau B_1 \bar{A}(t)$$

where  $A_k$  and  $A_l$  are the  $k$  and  $l$  components of the acceleration  $\bar{A}$  and

$$B_1 = \begin{bmatrix} 0 & \delta_{j3} & -\delta_{j2} \\ -\delta_{j3} & 0 & \delta_{j1} \\ \delta_{j2} & -\delta_{j1} & 0 \end{bmatrix}$$

is a misalignment matrix corresponding to a rotation about a predefined  $j$ th axis for the  $i$ th error source.

If a velocity measurement is to be made, the observable for the  $i$ th SHIP error source is

$$\Delta \bar{V}_i(t) = \int_0^t \Delta \bar{A}_i(\tau) d\tau$$

and for a position measurement

$$\Delta \bar{R}_i(t) = \int_0^t \int_0^\tau \Delta \bar{A}_i(s) ds d\tau$$

The non-gravitational acceleration in platform coordinates is a function of the normal acceleration and bank angle control.

At the time of maneuver initiation on the flight test trajectory, the vehicle drag is nearly along the platform negative z-axis and yaw maneuvers will produce platform y-accelerations while pitch maneuvers produce x-accelerations.

Figure F-6 depicts the non-gravitational acceleration in platform coordinates for the flight test trajectory equivalent to the assumed operational trajectory (a yaw-maneuvering trajectory). For the yaw-maneuvering trajectory, drag and the yaw-accelerations produce primarily  $a_y$  and  $a_z$  inputs to the SHIP error dynamics. It can be seen that for nine of the error sources, including the five most important, little separation in the output channel can be achieved by the yaw-maneuvering trajectory. On this trajectory error sources 6 and 13 have virtually no output. In contrast, for a combined  $a_x$ ,  $a_z$  (pitching maneuver), a three-way channel separation can be achieved for five of the error sources. This observation, coupled with the realization that a pitch-up maneuver tends to extend flight time and thus the number of measurements, suggests that pitching maneuvers may be advantageous. It is also clear that more output channel separation would be achieved by the use of maneuvers which induce accelerations along all three platform axes. Thus high acceleration and "zig-zag" type maneuvers are desirable for SHIP error source observability.

#### F-4.2.2 Observability of DINS Error Sources

To enhance the observability of the principal DINS error sources, namely the initial platform misalignments at reentry, by using radar/camera measurements, a trajectory with a large dispersion from the ballistic impact point is desired. This can be accomplished by a large yaw maneuver in one direction. Thus the DINS principal error sources, in contrast to those of SHIP, are easily observable.

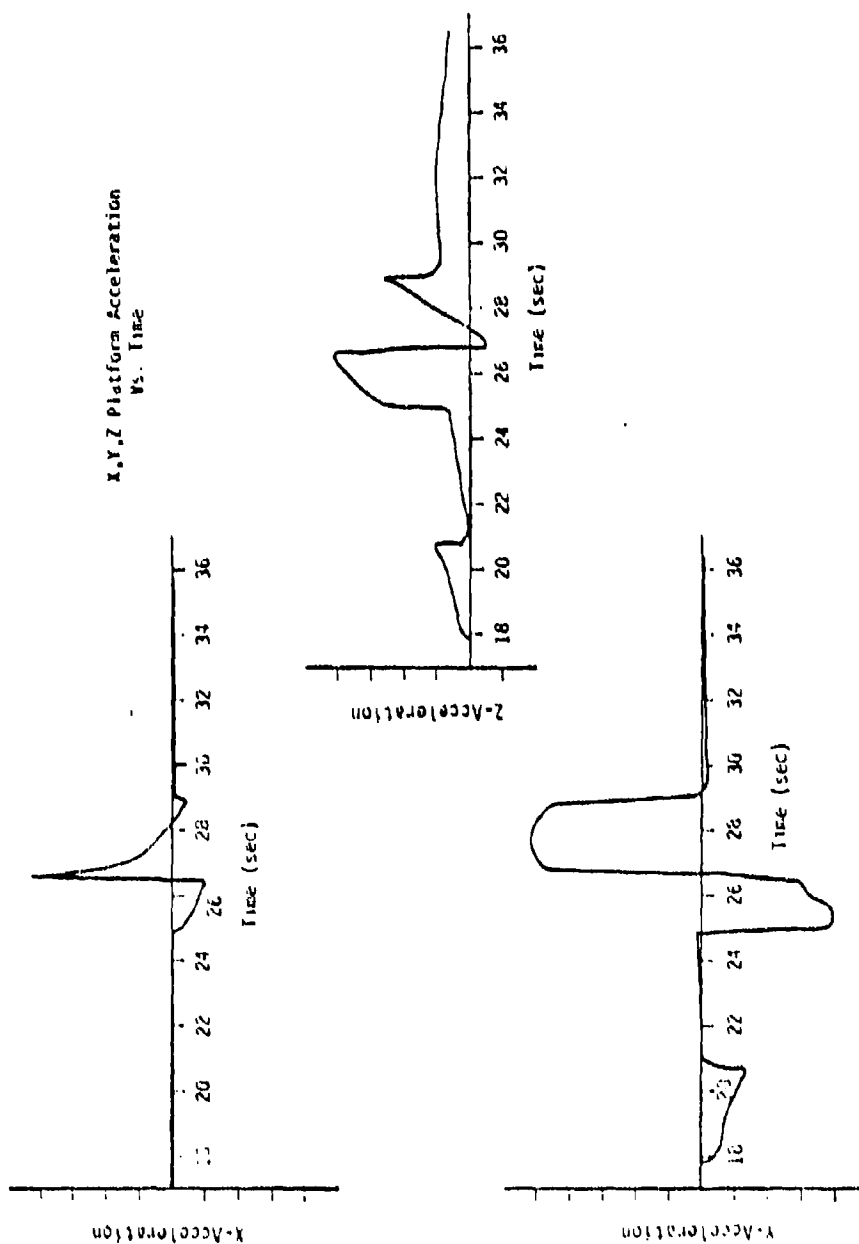


Figure F-6. Accelerations in Platform Coordinates  
Yaw-Maneuvering Trajectory

F-4.3      Input Design Techniques

The problem under investigation here is to improve the identification of the RIMU error sources by varying the test flight trajectory, and as such, is an input design problem. This problem area has been the subject of much statistical and engineering literature. A common approach, which is somewhat independent of the estimator invoked, is to use the Fisher information matrix,  $M$ , as a measure of the information on  $\theta$  provided by a feasible input. The reason for its use is that it is computationally attractive and its inverse, termed the Cramer-Rao lower bound, provides a "good" lower bound on the covariance of  $\theta$  for all regular unbiased estimators. (Here, regular refers to certain modest regularity assumptions on the distribution of the observations, Rao (1965).) The solution sought optimizes some objective functional of  $M$  or  $M^{-1}$ , for example a weighted trace or determinant, Mehra-Gupta (1974).

The general problem considered in the literature is of the form

$$\dot{X} = F(t, \theta) X + G(t, \theta) u \quad ; \quad Y = H(t, \theta) X + v \quad (F-1)$$

where

- $X$  is the state vector
- $u$  is the input control vector
- $\theta$  is the vector of unknown parameters
- $v$  is a white noise vector with zero mean and covariance  $R$ .

Making use of the additive type control, various objective functionals can be expressed as

$$J(u) = | \langle Tu, u \rangle |$$

where  $u$  belongs to some Hilbert space  $H$ ,  $\|u\| \leq 1$  and  $T$  is some normal, compact bounded linear operator on  $H$ . An optimal input  $u$  then is  $\max_{u \in H} J(u)$ , which is satisfied by the  $u$  corresponding to the largest eigenvalue (in absolute value) of  $T$  (see p.313 of Rudin (1973), Gupta and Hall (1975)).

The problem considered here does not fall into the form of (F-1) since it is not linear in the control  $u$ . Consequently, it cannot be solved by applying the above technique. In fact, here  $H$  is a function of  $u$  and is sufficiently nonconvex in  $u$  so as not to guarantee convergence to an optimal input of any general optimization algorithm. As a result, optimization techniques, based on certain necessary conditions for solution, are used in the present problem.

Commonly, a linear functional of the information matrix  $M$  is chosen for the objective functional, since for the general problem (F-1),  $M$  is a quadratic function of  $u$ . The drawback with maximization of diagonal elements of  $M$  is that the off-diagonal elements can become large, in which case the diagonal elements of  $M^{-1}$  can increase. This fact, in conjunction with the nonconvexity of  $H$  in  $u$  for the problem here caused the choice of a linear functional of the covariance matrix as the objective functional to be minimized. This function is defined next.

#### F-4.4 Trajectory Performance Criterion

The performance function chosen for the trajectory design problem here is

$$J = \text{tr}(W^T W P_f) = W P_f W^T = E(W \theta \theta^T W^T)$$

where  $P_f$  is the final covariance of the RIMU error parameters after estimation.

W is a row vector of sensitivities of the candidate operational system error contributions with respect to error source uncertainty. Table F-2 gives these weights for SHIP when multiplied by the initial error source uncertainties and normalized to 1.0. The normalized weights used for the initial roll, pitch, and yaw misalignments of the DINS platform when multiplied by their initial uncertainties are 0.5, 0.25, 0.25 respectively.

**F-4.5      The Trajectory Design Problem**

The flight test trajectory design problem formulated above is

Min WPFWT  
uEU

**Table F-2. SHIP Performance Criterion Weights\***

<u>Error Source</u>	<u>Weights</u>
1	0.192
2	0.132
3	0.116
4	0.108
5	0.077
6	-0.055
7	0.053
8	0.048
9	-0.048
10	0.048
11	0.047
12	0.038
13	0.038

\*Normalized to 1.0

## LOGICON

---

where

- U is the set of autopilot of control commands satisfying vehicle and instrumentation constraints, and yielding reentry trajectories with a sufficiently high velocity at impact
- W is a vector of weights based on the contribution of  $\theta$  to the operational trajectory CEP
- $P_f$  is the covariance of the RIMU error sources after estimation using the measurements

The form of the measurement is:

$$Z(t) = H(t, u) \bar{\theta} + v(t)$$

where

- $Z(t)$  is the difference between the telemetered RIMU output and radar/camera ground measurements
- $H(t, u)$  is the matrix of sensitivities to the RIMU and radar/camera error sources,
- $v(t)$  is the measurement white noise with covariance  $R(t)$

This problem is a "highly" nonlinear optimization problem over the Banach space of continuous control functions  $u \in U$  and is too unwieldy to solve. Consequently, an approximate solution is sought. First, a finite dimensional approximation to the space of control functions is defined by considering only step function control commands which are defined over the following six time intervals.

$$\left( \begin{array}{l} 19.0 \rightarrow 22.0 \\ 22.0 \rightarrow 24.0 \\ 24.0 \rightarrow 26.0 \\ 26.0 \rightarrow 28.0 \\ 28.0 \rightarrow 30.5 \\ 30.5 \rightarrow 34.5 \end{array} \right)$$

## LOGICON

---

The control commands are specified as a normal acceleration and a bank angle during each time interval. So, the allowable control command space has been reduced to a twelve dimensional euclidean space. Second, in order to decrease the cost of the reevaluation of  $P_f$ , the number of error sources considered is decreased from the full model to the principal operational error sources plus the three initial misalignments. Third, an efficient reentry trajectory generator was developed to approximate the more costly complete 3 DOF flight test trajectory simulator.

This reduced trajectory design problem is still a highly nonlinear constrained optimization problem, but the number of variables have been dramatically cut to make the problem manageable.

The procedure herein is to apply the simplicial pivoting algorithm to the reduced trajectory design problem for SHIP and for DINS and then determine the improvement of this designed trajectory over two current candidate flight test trajectories using the full model estimator and trajectory generator.

**F-5. THE SIMPLICIAL PIVOTING ALGORITHM**

In this section the rational behind the selection of the simplicial pivoting algorithm to solve the reduced trajectory design problem is given and the development of the algorithm to the problem is described. The rational used here is the same as would be used in attacking a variety of optimization problems.

**F-5.1 Selection of an Optimization Algorithm**

The methods available to solve constrained optimization algorithms can be classified into gradient-type and direct-search methods. The characteristics of the problem at hand are used to determine the appropriate type of algorithm to apply.

**F-5.1.1 The Two Classes of Algorithms**

Gradient-type algorithms are those which require the use of a derivative, or an increasingly accurate "approximate" derivative, of the objective or constraint functionals. These algorithms require more computations per iteration than the direct-search algorithms, but for "well-behaved" problems they have a faster convergence rate as well as conditions for "optimality" of the solution. Gradient-type algorithms are divided into two classes - those which solve a sequence of unconstrained problems formed by adding a sequence of penalty functions and those which generate a sequence of feasible-descent steps.

Penalty functions are added to the objective functional or to the Lagrangian of the problem in an effort to increasingly penalize candidate solutions which are near the constraints or infeasible. Feasible-descent directions are commonly generated by using a minimum norm projection onto the feasible set of a descent direction such as  $-\nabla J$  or  $-H^{-1}\nabla J$ . In the case of non-linear constraints the projection is frequently performed onto the intersection of the tangent hyperplanes of the " $\epsilon$ -active" constraints at the point.

## LOGICON

---

In many optimization problems analytical derivatives are not available and finite difference approximations involve excessive computational cost. Consequently, direct-search algorithms based only on the values of the objective functional and the constraints have been widely used. These algorithms are easy to implement and are applicable to a broad class of problems. They are aimed at finding "good" solutions since optimality conditions are usually sacrificed for improved efficiency. Though the rate of convergence is generally slower than for a gradient-type method, the lower computational cost per iteration, which is indicative of direct-search methods, provides for better overall efficiency in many problems.

### F-5.1.2 Trajectory Design Problem Characteristics

The choice of the type of algorithm to use depends on the properties of the problem at hand.

The characteristics of the reduced trajectory design problem which are important in algorithm selection are the following:

- 1) The objective functional  $J_p(u)$  and the trajectory constraints are "highly" nonlinear in the trajectory control variable  $u$ .
- 2) The gradients of  $J_p(u)$  are costly to compute.
- 3) Due to inflight perturbations in the commanded trajectory a "precise" solution is not necessary.
- 4) The dominant cost of solution is the functional evaluation of  $J_p(u)$ .
- 5) The trajectory control solution space is twelve dimensional euclidean space.

Properties 1, 2, and 3 of this problem indicate that a direct-search algorithm will perform better here than a gradient-type algorithm. Properties 4 and 5 will help in determining which type of direct-search algorithm to choose.

## F-5.1.3 Direct-Search Algorithms

The first type of direct-search algorithm to be considered is the method of local variations, see Banitchouk (1966). This method is based on a progressively finer partitioning of the feasible set. From  $x^K$  the algorithm samples adjacent vertices of the partition,  $x^K + \alpha_i^K p_i^K$ , until for  $i = j$ ,  $J(x^K + \alpha_j^K p_j^K) < J(x^K)$ . Then  $x^{K+1} = x^K + \alpha_j^K p_j^K$ . When such an improvement is no longer possible, the  $\alpha_i^K$ 's are reduced (i.e., the mesh of the partition is reduced) and the algorithm pivots on a finer partition (see Figure F-7 for an example). For the unconstrained problem, the accumulation points  $x^*$  of these  $\{x^K\}$  are shown, under reasonable assumptions, to satisfy  $\nabla J(x^*) = 0$ .

The standard partition is an orthogonal one, but, if possible, it is better to choose a partition where there are  $p_i$ 's along the constraint boundaries. When the constraints are nonlinear a penalty function technique should be added. The purpose of this is to help avoid a "jamming" of the algorithm at a boundary point which is not near a solution.

The DSC method (see Swann (1972)) is like the above method except that mutually orthogonal search directions are rotated according to the progress made after trying all the search directions. For example, in the case of a linear constraint violation, the boundary point is estimated and the normal to the constraint is taken as one of the search directions with the others chosen orthogonal to it. (This is usually called self-bounding.) Such methods which change the search directions sacrifice the partitioning and the corresponding convergence proof of local variations for a more efficient boundary following search scheme. Since there is no longer a partition to ensure no cycling, the DSC method uses a single-step parameter for its search and it is reduced when it is greater than the total progress made after a full cycle of search directions.

A simpler approach is a Monte Carlo method (see Luus and Jaakola (1973)) where  $m$  search directions are selected at random. The algorithm pivots

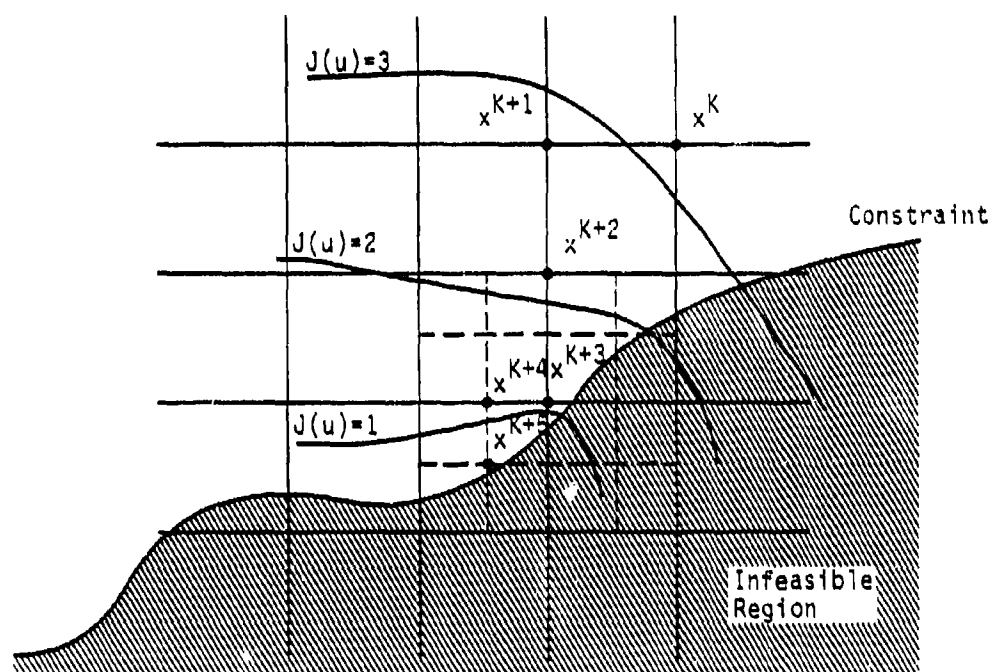


Figure F-7. Method of Local Variations

## LOGICON

---

to the best feasible of these and then a new set of reduced size is again selected at random. This method, however, seems to require an excessive number of function evaluations.

Powell's (1964) conjugate direction method searches on a set of directions which are updated each iteration using the total progress vector  $P$ , only if exchanging it with a current search direction increases the value of  $\Delta$  which is characteristic of a conjugate direction with respect to a quadratic approximation of  $J$ . Namely, if  $J = 1/2 x^T H x + a^T x$  and if the search directions  $\{P_i: i = 1, \dots, n\}$  satisfy  $1/2 P_i^T H P_i = 1$ , then the determinant,  $\Delta$ , of the matrix  $P$  composed of  $P_i$ 's takes its maximum when the  $P_i$  are mutually conjugate (i.e.,  $P_i^T H P_j = 0$ ). Simple tests can be derived to determine which  $P_i$  to replace by  $P$  for maximum increase in  $\Delta$ . The generation of the search directions  $P_i$  is based on  $n$ -dimensional minimizations and the following easily-derived fact.

If the minimum of a quadratic  $J$  in a direction  $P$  from  $y_1$  is at  $x_1$  for  $i = 1, 2$  then  $x_2 - x_1$  is a conjugate direction to  $P$ . A basic iteration for an initial guess  $x_0$  and  $(P_1, \dots, P_n)$  is

- 1) Define  $x_i = x_{i-1} + \alpha_i P_i$  where  $\alpha_i$  minimizes  $f(x_{i-1} + \alpha_i P_i)$  for  $i = 1, \dots, n$ .
- 2) Define  $P_i = P_{i+1}$ ,  $P_n = x_n - x_0$ , and replace  $x_0$  by  $x_0 + \alpha P_n$ .

The purpose of evaluating  $\Delta$  is to help avoid the directions  $P_i$  from becoming linearly dependent. A simpler way to avoid this is to reinitialize every  $n+1$  iterations.

A method which does not require the 1-dimensional minimizations as described above is the pattern search method (see Hooke and Jeeves (1961)). This method searches from  $x^K$  along  $x^K - x^{K-1}$  a distance  $\|x^K - x^{K-1}\|$  to obtain a point  $y^K$ , from which  $n$ -iterations of a local variation-type pivoting is performed to obtain  $x^{K+1}$ . An example is shown in Figure F-8 for  $n = 2$ .

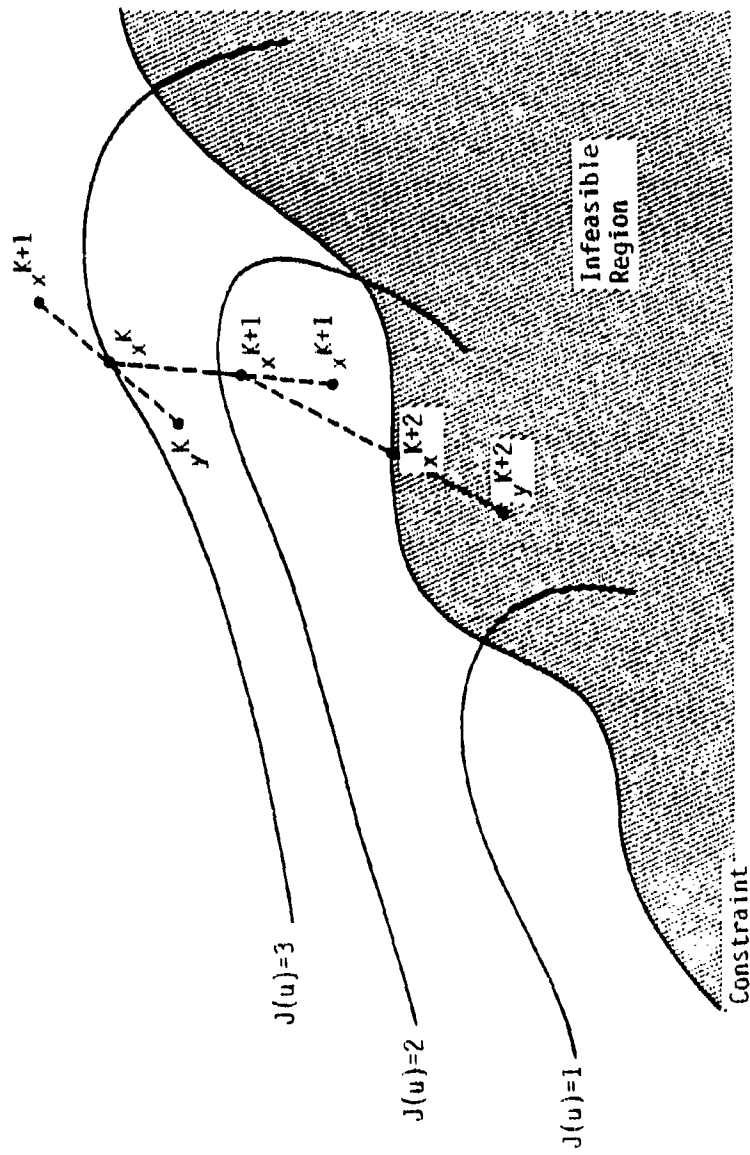


Figure F-8. Pattern Search Method

## LOGICON

---

There are many constraint-following schemes (see Glass and Cooper (1965)) the purposes of which are to avoid "jamming." Some of these include: searching along a pattern direction as long as there is improvement, local variations along tangent hyperplanes to active constraints, and gradient projection techniques.

The probes  $y^K$  are allowed to be nonfeasible in the hope that local variations pivoting will produce a feasible point, if not, local variations are performed around  $x^K$ . If these variations fail the step size is reduced. As an additional aid, penalty functions have been used as described earlier. Nevertheless, in higher dimensional problems, pattern search is not as effective in determining appropriate pattern directions and seems to be more prone to "jamming."

Some of the methods which are more flexible in selecting search directions are the simplicial pivoting methods (see Spendley, Hext, and Himsworth (1962), Box (1965), and Keefer (1973)).

To approximate solutions to minimization problems on an  $n$ -dimension euclidean space,  $R^n$ , simplicial pivoting algorithms store the value of the objective functional,  $J$ , at  $n+1$  points  $\{V_i : i, \dots, n+1\}$ . Pivoting from these points is accomplished by dropping the point  $V_j$  with the largest value of  $J$  and adding the point  $V_j^*$  obtained by reflecting  $V_j$  through the centroid,  $c$ , of the remaining points. Namely,

$$V_j^* = 2c - V_j$$

where

$$c = \sum_{\substack{i=1 \\ i \neq j}}^{n+1} V_i / n$$

## LOGICON

---

The convex hull of  $\{V_i : i = 1, \dots, n + 1\}$  forms a closed  $n$ -simplex. The simplicial pivoting just defined is depicted for  $n=2$  in Figure F-9.

In the algorithm this pivoting continues until  $V_j^*$  is infeasible or  $J(V_j^*)$  is also the largest value of  $J$  when compared with the other vertices of the  $n$ -simplex. When this occurs a new vertex is generated by reflecting  $V_j$  through the vertex  $V_k$  with the best value of  $J$ , namely  $V_j' = 2V_k - V_j$ . If  $J(V_j')$  is again the largest, then  $V_j$  is dropped and simplicial pivoting is performed on the remaining  $n-1$ -simplex. The purpose of this is to cause the algorithm to follow the valley or constraint which is assumed to be approximately orthogonal to  $V_j^* - V_j$ .

To help avoid "jamming" on the constraint boundaries a penalty function is added to the objective functional which increasingly penalizes points near the constraints. The penalty function is chosen so as to form a valley between the constraints on the interior which the algorithm can follow. To aid in this and thereby increase the rate of convergence, mesh expansion logic can be included to increase the size of the pivoting steps along directions "locally" parallel to the constraints.

### F-5.1.4 A Comparison of Direct-Search Algorithms

The direct-search algorithm to be applied to the reduced trajectory design problem is chosen based on the characteristics of the problem. The Monte Carlo method is ruled out since information on previously evaluated trajectories should be used to aid in selecting a new trajectory in order to cut down on the prohibitive cost of trying to cover the space of feasible trajectories. Also, the conjugate directions method does not seem appropriate due to the nonquadratic nature of  $J$  and the cost of 1-dimensioned minimizations.

The methods of local variations, pattern search and simplicial pivoting can be compared on the basis of the amount of memory of previously evaluated trajectories that each possesses. The method of local variations

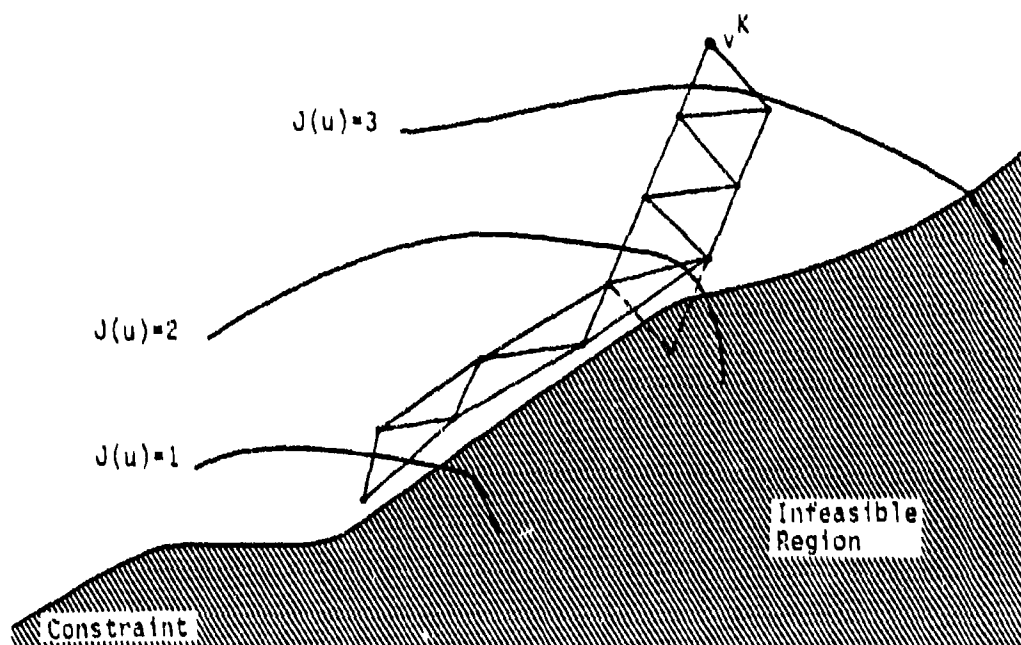


Figure F-9. Simplicial Pivoting Method

and pattern search have 1 and 2 point memories respectively. Whereas, simplicial pivoting has a  $n+1$  point memory where  $n$  here is twelve. Due to the dominant cost of functional evaluation, the relative cost of this memory is negligible. Thus, since the simplicial pivoting method provides a better current local approximation of  $J(u)$  without noticable additional cost, it should better select a new pivoting direction in which to proceed. Also, the improvement techniques (i.e. penalty functions, constraint following, and mesh variation) of local variations and pattern search have their counterparts in the simplicial pivoting algorithm. Consequently, a simplicial pivoting algorithm was selected to be applied to the reduced trajectory design problem.

#### F-5.2 The Simplicial Pivoting Algorithm

In this section the application of the simplicial pivoting algorithm to the reduced trajectory design problem is described. The pivoting is performed with twelve dimensional simplices where each dimension represents a commanded normal acceleration or bank angle over one of the six trajectory time intervals specified above. The initial simplex is generated using a method of local variations from the starting trajectory comprised of 10% max  $g$ 's changes in the yaw commands and 5% max  $g$ 's changes in the pitch commands. The objective functional  $J_r$  was evaluated for each of the thirteen vertices and a penalty function based on the velocity at impact was added to each  $J_r$ . More precisely the total cost  $C_r$  for the trajectory specified at each vertex was evaluated as follows:

$$C_r(i) = [1 + 10/(V(i) - V_B)] J_r(i)$$

where

$V(i)$  is the velocity at impact of the  $i$ th vertex

and  $V(i) > V_B + 10$ .

$V_B$  is the smallest allowable velocity at impact in ft/sec

If  $V(i) \leq V_B + 10$  then  $C_r(i)$  is assigned a large number.

The vertex  $V_j$  of the simplex with the largest  $C_r$  is dropped. If this vertex is an allowable trajectory a new vertex is added by reflecting it through the centroid,  $C$ , (i.e., center of mass) of the remaining vertices. Namely, the new vertex,  $V_j^*$ , is  $C + (C - V_j)$ . On the other hand, when  $V_j$  is not an allowable trajectory or it was the last to be added, it is replaced first by the reflection of it through the vertex with the smallest  $C_r$  with the step cut in half. Namely,  $V_j^* = V_k + 1/2(V_k - V_j)$ . If this last replacement  $V_j^*$  is not an allowable trajectory then it is dropped and pivoting is resumed on the remaining simplex of one lower dimension.

Mesh expansion is incorporated whenever the newly added vertex,  $V_j^*$ , has the smallest  $C_r$  and the decrease in the velocity at impact is not too large. Namely,  $V_j^* = C + 2(C - V_j)$  whenever  $V(V_j) - V(V_j^*) \leq V(V_j^*) - (V_B + 100)$  where  $V(V_j^*)$  is the velocity at impact of the trajectory  $V_j^*$ . These mesh reduction and expansion schemes help, respectively, to flatten the simplex along directions which cause  $V(i)$  to decrease too rapidly and lengthen the simplex along directions which improve  $C_r(i)$  while not decreasing  $V(i)$  too rapidly.

In addition to computing the performance criteria  $J_r = WPW^T$ , the algorithm also computes the weighted trace  $T_r = \sum_{i=1}^{13} W_i^2 p_{ii}$  as a measure of performance independent of any correlations set up between the error sources. When desired, the algorithm will optimize with respect to  $T_r$  instead of  $J_r$ .

## F-6. RIMU PARAMETER ESTIMATION PERFORMANCE

In this section the performance of the estimation of the principal RIMU error sources, after comparing RIMU data and radar/camera ground sensor data, is described for various simulated flight test trajectories. Results are presented for SHIP and for DINS. The estimator used in this analysis is a version of the USAF/ABRES post-flight data reduction Extended Kalman Filter estimator operating in a covariance-only mode so that synthetic data is not required. Estimation performance is first evaluated for the principal error model state used in the reduced trajectory design problem and then for the full error model state. The measure of performance used is the trajectory performance criterion  $J = WP_p W^T$  defined earlier.

In addition the value of the weighted trace  $T = \sum_{i=1}^{13} W_i^2 P_{ii}$  is given for

each trajectory as an alternate measure of performance which disregards correlations.

F-6.1 SHIP Parameter Estimation Performance

The results of the SHIP flight test trajectory design for the purpose of improving the estimation of the principal performance contributors are presented in two parts. First, the trajectories designed by the simpli-  
cial pivoting algorithm using the 16 state reduced order model are compared with the two candidate flight test trajectories. Second, the full SHIP and radar/camera error models are applied to determine the error source parameter estimation performance of each trajectory. The results show a designed trajectory with 66% and 78% improvement in the full model weighted performance criterion over the two candidate flight test trajectories, respectively.

## F-6.1.1 SHIP Trajectory Design Results

This section gives the results of applying the simplicial pivoting algorithm to the reduced trajectory design problem. The algorithm was initiated from the operational yaw maneuvering trajectory, on which the performance weightings are based, the two candidate AMarV flight test trajectories, and a ballistic trajectory. The commanded normal acceleration and bank angles as a function time for these trajectories are given in Tables F-3, F-4, and F-5. Forty simplicial pivots were made from each of these trajectories. The performance results using the 16 state vector are summarized in Table F-6. Tables F-7, F-8, F-9, and F-10 give the resulting designed trajectories from the simplicial pivoting algorithm.

Of the four initial simplicial pivoting results, the trajectory designed from the candidate operational yaw maneuvering trajectory performed the best. Consequently, the algorithm was applied from this trajectory two more times at 40 pivots each. The first application yielded a trajectory with a  $J_r = 0.035$  and the next application yielded the trajectory called Design A, described in Table F-11, with a  $J_r = 0.018$  and a  $T_r = 0.80$ . To check for an approximate local solution the algorithm was applied again for 40 steps from this Design A trajectory. The resulting Design B trajectory defined in Table F-12 had  $J_r = 0.016$  and  $T_r = 0.80$ . Since the additional improvement in  $J_r$  was minimal, the minimization was stopped here with a 97% improvement of  $J_r$  over the yaw maneuvering trajectory.

Next, the simplicial pivoting algorithm was applied to the minimization of the weighted trace  $T_r$  for the reduced trajectory design problem which was defined above. As expected, the improvement in  $T_r$  is not as dramatic as that for  $J_r$  since correlations set up in the measurements do not affect the value of  $T_r$ . The minimization of  $T_r$  was initiated at the Design A trajectory. The resulting trajectory after forty pivots is described in Table F-13 and has  $T_r = 0.76$ . This trajectory is similar to the Design A

Table F-3. Yaw Maneuvering Trajectory

<u>T (seconds)</u>	<u>A (% maximum)</u>	<u><math>\phi</math>(deg)</u>
17.7	67	90
20.4	0	90
24.5	100	90
26.0	100	-90
28.5	0	-90

Table F-4. Flight Test Trajectory #1

<u>T (seconds)</u>	<u>A (% maximum)</u>	<u><math>\phi</math>(deg)</u>
19.8	67	90
24.8	0	-75
26.8	67	-75
29.8	0	180
31.8	67	180
33.9	0	180

Table F-5. Flight Test Trajectory #2

<u>T (seconds)</u>	<u>A (% maximum)</u>	<u><math>\phi</math>(deg)</u>
17.8	47	180
21.3	0	0
26.3	100	0
27.6	0	90
28.5	100	90
30.	67	180

**LOGICON**Table F-6.  $J_r$  SHIP Optimization Results After 40 Steps

	Initial		After 40 Pivots	
	$J_r$	$T_r$	$J_r$	$T_r$
Yaw Maneuvering	0.525	1.07	0.103	0.875
Flight Test #1	0.85	1.15	0.44	0.86
Flight Test #2	0.60	1.52	0.256	1.24
Ballistic	2.22	2.24	0.17	1.07

Table F-7. Trajectory Designed With Initialization at Yaw-Maneuvering

<u>T (seconds)</u>	<u>A (% maximum)</u>	<u><math>\phi</math> (deg)</u>
18.0	13	61
20.5	11	-45.6
22.0	20	-39
24.0	100	91
26.0	97	-98
28.0	38	-153
29.0	43	128
30.5	27	76.5
34.5	0	76.5

Table F-8. Trajectory Designed from Flight Test #1

<u>T (seconds)</u>	<u>A (% maximum)</u>	<u>φ(deg)</u>
19.0	23	83.6
22.0	31	87.5
23.0	61	90.3
25.5	7	-81
27.0	97	-86.8
30.0	25	97
32.0	74	159
34.0	0	140

Table F-9. Trajectory Designed from Flight Test #2

<u>T (seconds)</u>	<u>A (% maximum)</u>	<u>φ(deg)</u>
18.0	15	176
20.0	37	178
21.5	10	-33.8
24.0	11	5.6
26.0	100	93.6
30.0	67	176.5

Table F-10. Trajectory Designed from Ballistic Trajectory

<u>T (seconds)</u>	<u>A (% maximum)</u>	<u>φ(deg)</u>
19.	0.9	3
22	75.	- 60
24	67.	90
26	50.	100
28	33.	-112
30.5	11.	96.6
34.5	0.	96.6

Table F-11. SHIP Design A Trajectory

<u>T (seconds)</u>	<u>A (% maximum)</u>	<u><math>\phi</math> (deg)</u>
19	4	-53
22	31	-34
24	100	98.3
26	100	-96
28	94	133
30.5	6	91
34.5	0	180

Table F-12. SHIP Design B Trajectory

<u>T (seconds)</u>	<u>A (% maximum)</u>	<u><math>\phi</math> (deg)</u>
19	5	-42.6
22	36	-35.2
24	100	96.4
26	100	-93.8
28	100	138.2
30.5	26	92.9
34.5	0	76.

Table F-13. Trajectory Design Using  $T_r$ 

<u>T (seconds)</u>	<u>A (% maximum)</u>	<u><math>\phi</math> (deg)</u>
19	10	-63
22	30	-26
24	97	101.5
26	99	-96
28	100	129
30.5	23	90.2

trajectory and, as will be seen, its performance with the full error model is expected to be nearly the same as that for the Design A trajectory. The reason for this is the significant degradation in the final covariance  $P_f$  of the significant error sources caused when the error sources neglected in the reduced design problem are added. The extent of this degradation from the 97% and 29% improvements in  $J_p$  and  $T_p$  respectively for the reduced design problem will be described next.

#### F-6.1.2 SHIP Parameter Estimation Results

In this section the SHIP parameter estimation performance using the full filter model is determined for the yaw maneuvering trajectory, the two candidate flight test trajectories, and for the Design A and Design B trajectories described above. Each reentry trajectory is simulated with a detailed 3 DOF AMaRV vehicle simulator initialized with the nominal flight test reentry state. The full filter state vector includes 90 RIMU error sources, 12 ground sensor error sources, and 9 states for initial position, velocity, and misalignment. The full state estimator results measured in terms of J and T are given in Table F-14. A comparison of the improvement in the SHIP principal performance parameter 1σ's for the trajectories is summarized in Table F-15. In terms of the trajectory performance criterion J, the Design A trajectory represents a 49% improvement in the yaw-maneuvering trajectory and a 66% and 78% improvement in the flight test #1 and #2 trajectories respectively.

Table F-14. Full State Estimator Results

	J	T	Velocity at Impact (% of Minimum)
Yaw Maneuvering	0.731	1.40	132
Flight Test #1	1.11	1.62	137
Flight Test #2	1.70	2.04	152
Design A	0.376	1.27	116
Design B	0.394	1.26	112

Table F-15. SHIP Principal Parameter Estimation

Percent change in  $\sigma$  Values from initial values

<u>Error Source</u>	<u>Yaw Maneuvering</u>	<u>AMaRV #1</u>	<u>AMaRV #2</u>	<u>Design A</u>	<u>Design B</u>
1	19.0	13.7	6.3	34.2	34.3
2	47.0	26.2	3.8	34.4	32.5
3	6.3	5.1	1.7	9.0	8.6
4	30.5	22.0	2.2	28.7	29.8
5	16.5	21.5	13.2	16.5	17.7
6	4.6	6.2	4.1	8.9	10.1
7	51.6	23.8	1.9	32.4	27.2
8	38.3	27.1	7.2	46.8	45.3
9	2.4	4.2	3.3	2.9	2.7
10	3.5	5.5	6.3	5.9	7.3
11	6.0	6.2	12.4	7.3	10.1
12	3.4	5.3	7.9	5.0	4.3
13	2.7	11.1	0.6	6.8	4.7
$\phi_x$	57.0	57.5	66.0	46.5	48.5
$\phi_y$	33.6	36.3	69.1	52.4	54.5
$\phi_z$	34.0	47.0	58.8	51.4	54.1

**F-6.2     DINS Parameter Estimation Performance**

The results of the DINS flight test design for improving principal parameter estimation performance are presented in two parts. First, the trajectory design by the simplicial pivoting algorithm using the three state reduced order model is compared with the two candidate flight test trajectories. Second, the full DINS and radar/camera error models are applied to determine the error source parameter estimation performance of each trajectory. The results show a 49% and an 80% improvement in the performance criterion over the flight test #1 and #2 trajectories, respectively.

**F-6.2.1     DINS Trajectory Design Results**

The simplicial pivoting algorithm was applied to the DINS trajectory design problem with the reduced model consisting of the initial misalignments. The algorithm was started with the ballistic trajectory. After forty pivots the trajectory performance criterion,  $J$ , was reduced to 0.096 with a 1 directional yaw-type trajectory. From here forty more pivots were made to decrease  $J$  to 0.066. The resulting DINS design trajectory is described in Table F-16. A value of  $J$  and the weighted trace  $T$  for this designed trajectory and the other selected trajectories are compared in Table F-17. No further minimization of  $J$  was performed because the misalignments are very observable with almost all non-ballistic trajectories. The degree with which the observability varies is depicted in the following section for the above trajectories.

**F-6.2.2     DINS Parameter Estimation Results**

The full 110 state DINS error model, the twelve radar/camera error states, and a detailed 3 DOF trajectory simulation were used to drive the Kalman filter which determined the parameter estimation performance. The values of the velocity at impact, the performance criterion  $J$ , and the weighted

Table F-16. DINS Design Trajectory

<u>T (seconds)</u>	<u>A (% maximum)</u>	<u><math>\phi</math> (deg)</u>
19.	25.	65.
22.	59.	57.
24.	32.	76.
26.	37.	134.
28.	35.	91.
30.5	64.	93.
34.5	0.	96.

Table F-17. DINS Reduced State Trajectory Design Performance

	<u>Yaw Maneuvering</u>	<u>Ballistic</u>	<u>Flight Test #1</u>	<u>Flight Test #2</u>	<u>DINS Design</u>
J	0.096	795.	0.24	0.76	0.066
T	0.099	906.	0.16	0.33	0.037

## **LOGICON**

---

trace of the covariance matrix of the error at impact for the selected trajectories are given in Table F-18. A comparison of the accuracy of the DINS platform misalignment estimates derived for each trajectory using the full model is given in Table F-19. As a result, DINS design trajectory exhibits a 49% and 80% improvement in J over the flight test #1 and #2 trajectories, respectively.

Table F-18. DINS Full State Estimator Results

	<u>Yaw Maneuvering</u>	<u>Flight Test #1</u>	<u>Flight Test #2</u>	<u>DINS Design</u>
Velocity at Impact (% of minimum)	132	137	152	101
J	35.5	14.9	39.0	7.6
T	29.1	14.5	38.6	19.4

Table F-19. DINS Principal Parameter Estimation  
(% change in  $\sigma$  values from initial)

	<u>Yaw Maneuvering</u>	<u>Flight Test #1</u>	<u>Flight Test #2</u>	<u>Design</u>
Roll	91.3	93.4	92.6	97.4
Pitch	76.4	85.2	73.9	84.5
Yaw	80.6	85.0	72.8	76.4

## F-7. SUMMARY

An approach to the design of flight test trajectories for the observation of RIMU guidance system errors has been formulated. The approach entailed a determination of the principal operational performance contributors and the design of a flight test trajectory to increase the observability of these principal error sources. A simplicial pivoting algorithm has been developed to perform this and trajectories have been designed with SHIP and with DINS as the RIMU. The results show a 66% and 78% improvement of the SHIP performance criterion and a 49% and 80% improvement of the DINS performance criterion over the flight test #1 and #2 trajectories, respectively. Also, the full covariance of the error in estimating the RIMU and ground sensor errors has been generated for each RIMU and for each of the selected trajectories.

## REFERENCES

1. Archer, S. M., Bowman, C. L. and Gurwell, N. N. (1977). "Designing Weapon System Test Trajectories for Guidance Error Source Observability," Eighth Biennial Guidance Test Symposium.
2. Banitchouk, N. V., Petrov, V. M. and Chernousko, R. L. (1966). "Numerical Solution of Problems with Variational Limits by the Method of Local Variations," Zh. Kychil. Mat. Fiz. 6(6), 947-961.
3. Box, M. J. (1965). A new method of constrained optimization and a comparison with other methods. Comput. J. 8, 42-52.
4. Glass, H. and Cooper, L. (1965). "Sequential Search: A Method for Solving Constrained Optimization Problems," JACM 12, 71-82.
5. Gupta, N. K. and Hall, W. E., Jr. (1975). "Input Design for Identification of Aircraft Stability and Control Derivatives," NASA CR-2493, Systems Control Inc., Palo Alto, California, February.
6. Hooke, R. and Jeeves, T. A. (1961). "Direct Search Solution of Numerical and Statistical Problems," JACM 8, 212-229.
7. Keefer, D. L. (1973). "Simpat: Self-Bounding Direct Search Method for Optimization," Ind. Eng. Chem. Process Des. Develop. 12, No. 1.
8. Luus, R. and Jaakola, T. H. I. (1973). "Optimization by Direct Search and Systematic Reduction of the Size of Search Region," A.I. Ch.E. Journal 19, 70-766.
9. Mehra, R. K. and Gupta, H. K. (1974). "Status of Input Design for Aircraft Parameter Identification," AGARD Specialists Meeting NASA Langely Research Center, Hampton, Virginia, November.
10. Powell, M. J. D. (1964). "An Efficient Method of Finding the Minimum of a Function of Several Variables Without Calculating Derivatives," Comput. J. 7, 155.
11. Rao, C. R. (1965). Linear Statistical Inference and Its Applications, Wiley.
12. Rudin, W. (1973). Functional Analysis, McGraw-Hill Book Company.

13. Spendley, W., Hext, G. R. and Himsworth, F. R. (1962). "Sequential Application of Simplex Designs in Optimization and Evolutionary Design," *Technometrics* 4, 441-461.
14. Swann, W. H. (1972). Direct search methods. In "Numerical Methods for Unconstrained Optimization," (W. Murray, ed.). Academic Press, London and New York.

APPENDIX G  
FREE-FLIGHT FILTERINGG-1. Measurement Equations

In order to improve alignment using free-flight filtering, the attitude and sensed velocity obtained from the DINS gyros and accelerometers must be compared with the attitude and sensed velocity calculated from body dynamics. Using state space notation, the measurement at time  $i$  is expressed as

$$\delta \underline{z}_i = H_i \delta \underline{x}_i + \underline{v}_i \quad (G-1)$$

where the measurement  $\delta \underline{z}$  and the state vector  $\delta \underline{x}$  are given in differential notation to indicate that these quantities are errors about the nominal values.

In Figure G-1, the free-flight filtering state vector is given. By treating the position, velocity, and alignment errors as initial errors, the entire free-flight state vector consists entirely of bias states, thus eliminating the need for performing a time propagation between measurement updates. At the end of free-flight filtering, the contribution of DINS errors to the present position, velocity, and alignment errors is easily calculated and added to the state vector. In practice, the G&G errors of Figure G-1 are not included in the free-flight state vector since they do not contribute to alignment or sensed velocity errors. Their contribution to the total position and velocity errors is calculated independently and is then added directly to the position and velocity errors at the appropriate time.

For the case of a combined angle and sensed velocity update, the free-flight filtering measurement vector is the difference between the DINS calculated values and the body dynamics calculated values and is given by

$$\delta \mathbf{x} = \begin{bmatrix} \mathbf{s}_0 \\ \delta \phi_0 \\ \mathbf{E}_A^{\text{DINS}} \\ \mathbf{E}_G^{\text{DINS}} \\ \mathbf{E}_{BD} \\ \mathbf{E}_{G\&G} \end{bmatrix} \begin{array}{l} \text{Initial ECI position and velocity error} \\ \text{Initial DINS alignment errors} \\ \text{DINS accelerometer errors} \\ \text{DINS gyro errors} \\ \text{Body dynamics errors} \\ \text{G\&G errors} \end{array}$$

Figure G-1. Freeflight Filtering State Vector

# LOGICON

$$\delta z = \begin{bmatrix} V_{DINS} - V_{BD} \\ \theta_{DINS} - \theta_{BD} \end{bmatrix} \quad (G-2)$$

Each individual term can be expressed as the sum of the actual value plus an error term:

$$\begin{aligned} V_{DINS} &= V_{Actual} + \delta V_{DINS} + \delta V_{Quant} \\ V_{BD} &= V_{Actual} + \delta V_{BD} \\ \theta_{DINS} &= \theta_{Actual} + \delta \theta_{DINS} + \delta \theta_{Quant} \\ \theta_{BD} &= \theta_{Actual} + \delta \theta_{BD} \end{aligned} \quad (G-3)$$

The quantization errors, which are due to the finite instrument scale factors, are separated from the other errors in these equations. Substituting equation (G-3) into equation (G-2), the measurement equation becomes

$$\delta z = \begin{bmatrix} \delta V_{DINS} - \delta V_{BD} + \delta V_{Quant} \\ \delta \theta_{DINS} - \delta \theta_{BD} + \delta \theta_{Quant} \end{bmatrix} \quad (G-4)$$

Since all error states are treated as bias errors here, the velocity and alignment errors as a function of time are given by

$$\begin{aligned} \delta V_{DINS} &= \frac{\partial V}{\partial E_A^{DINS}} E_A^{DINS} + \frac{\partial V}{\partial E_G^{DINS}} E_G^{DINS} \\ \delta V_{BD} &= \frac{\partial V}{\partial E_{BD}} E_{BD} \\ \delta \theta_{DINS} &= \frac{\partial \theta}{\partial E_A^{DINS}} E_A^{DINS} + \frac{\partial \theta}{\partial E_G^{DINS}} E_G^{DINS} \\ \delta \theta_{BD} &= \frac{\partial \theta}{\partial E_{BD}} E_{BD} \end{aligned} \quad (G-5)$$

# LOGICON

Substituting these expressions for the velocity and alignment errors into equation (G-4), we obtain

$$\delta \underline{z} = \begin{bmatrix} \frac{\partial \underline{V}}{\partial \underline{E}_A} \underline{E}_A^{DINS} + \frac{\partial \underline{V}}{\partial \underline{E}_G} \underline{E}_G^{DINS} - \frac{\partial \underline{V}}{\partial \underline{E}_{BD}} \underline{E}_{BD} + \delta \underline{V}_{Quant} \\ \frac{\partial \theta}{\partial \underline{E}_A} \underline{E}_A^{DINS} + \frac{\partial \theta}{\partial \underline{E}_G} \underline{E}_G^{DINS} - \frac{\partial \theta}{\partial \underline{E}_{BD}} \underline{E}_{BD} + \delta \theta_{Quant} \end{bmatrix} \quad (G-6)$$

Comparing equations (G-1) and (G-6), the measurement matrix H is seen to be

$$H = \begin{bmatrix} 0 & 0 & \frac{\partial \underline{V}}{\partial \underline{E}_A} & \frac{\partial \underline{V}}{\partial \underline{E}_G} & - \frac{\partial \underline{V}}{\partial \underline{E}_{BD}} \\ 0 & 0 & \frac{\partial \theta}{\partial \underline{E}_A} & \frac{\partial \theta}{\partial \underline{E}_G} & - \frac{\partial \theta}{\partial \underline{E}_{BD}} \end{bmatrix} \quad (G-7)$$

and the measurement noise  $\underline{v}$  is seen to be

$$\underline{v} = \begin{bmatrix} \delta \underline{V}_{Quant} \\ \delta \theta_{Quant} \end{bmatrix} \quad (G-8)$$

This measurement matrix and the covariance of this measurement noise are incorporated into a Kalman filter (Appendix C) to update the state vector.

G-2. Body Dynamics

In order to calculate the free-flight filter H matrix, the sensitivity of velocity and angle errors to the error state vector must first be calculated. The sensitivity to the DINS error state is obtained from the DINS error equations (Section 3.2.3). To obtain the sensitivity to the body dynamics errors, body dynamics error equations are needed. Before deriving the body dynamics error equations, the nominal equations for calculating attitude and sensed velocity will be presented.

Euler's equation, modified to the case of zero external torque, can be used to compute the RV attitude during free-flight. The equation is written as

$$[\bar{I}_p] \dot{\bar{\omega}}_p + [\bar{\omega}_p \times] [\bar{I}_p] \bar{\omega}_p = 0 \quad (G-9)$$

The subscript p indicates that these quantities are to be calculated in the coordinate frame of the principal axes of the RV. Brackets are used to denote matrix (or tensor) operations, and the symbol  $[\bar{\omega}_p \times]$  corresponds to the matrix which results in the indicated cross product operation.

The equation for sensed velocity is given by

$$\dot{\bar{V}}_b = \bar{\omega}_b \times (\bar{\omega}_b \times \bar{r}_b) + \dot{\bar{\omega}}_b \times \bar{r}_b \quad (G-10)$$

where the subscript b indicates that these quantities are to be calculated in a coordinate frame fixed with respect to the body. The first term on the right hand side of the equation is the centripetal acceleration. As a result of the coning motion,  $\dot{\bar{\omega}}_b$  is nonzero, and both terms on the right hand side of the equation therefore contribute to the sensed velocity.

In the computer simulation, error equations for body dynamics are used to compute angle and sensed velocity errors directly. The error equations

## LOGICON

are obtained by taking small perturbations about the nominal body dynamics equations (G-9) and (G-10). The resulting equations are:

$$\begin{aligned} \delta \dot{\bar{\omega}}_I = & \left\{ [I \rightarrow P]^T [\zeta_p] [I \rightarrow P] - [\bar{\omega}_I \times] \right\} \delta \bar{\omega}_I + [I \rightarrow P]^T [\lambda] \delta I_p \\ & + \left\{ [I \rightarrow P]^T [\zeta_p] [I \rightarrow P] [\bar{\omega}_I \times] - [\dot{\bar{\omega}}_I \times] \right\} [I \rightarrow P]^T \delta \bar{\phi}_p \\ \delta \dot{\bar{\theta}}_I = & \delta \bar{\omega}_I \end{aligned} \quad (G-11)$$

$$\begin{aligned} \delta \dot{\bar{v}}_b = & 2 [I \rightarrow B] [(\bar{r}_I \times \bar{\omega}_I) \times] \delta \bar{\omega}_I - [I \rightarrow B] [\bar{r}_I \times] \delta \dot{\bar{\omega}}_I \\ & + [I \rightarrow B] \left\{ [\bar{\omega}_I \times] [\bar{\omega}_I \times] + [\dot{\bar{\omega}}_I \times] \right\} \delta \bar{r}_I \end{aligned}$$

where

$\delta \bar{\omega}_I$  = rate error in inertial coordinates

$\delta \bar{\theta}_I$  = alignment error in inertial coordinates

$\delta \bar{v}_b$  = sensed velocity error in body coordinates

$[I \rightarrow P]$  = coordinate transformation from inertial to principal axis coordinates

$[I \rightarrow B]$  = coordinate transformation from inertial to body coordinates

$\delta I_p$  = error in magnitude of moment inertia about principal axes

$\delta \bar{\phi}_p$  = alignment error of principal axes

$[\lambda] = \frac{\partial \dot{\bar{\omega}}_p}{\partial I_p}$  = sensitivity of rate error derivative about principal axes to  $\delta I_p$

$[\zeta_p] = \frac{\partial \dot{\bar{\omega}}_p}{\partial \bar{\omega}_p}$  = sensitivity of rate error derivative about principal axes to  $\delta \bar{\omega}_p$

# LOGICON

The quantities  $[\lambda]$  and  $[\zeta_p]$  can be calculated in a straightforward manner from equation (G-9). First, we write the equation for each component of the vector equation separately:

$$\dot{\omega}_{p1} = \frac{I_{p2} - I_{p3}}{I_{p1}} \omega_{p3} \omega_{p2}$$

$$\dot{\omega}_{p2} = \frac{I_{p3} - I_{p1}}{I_{p2}} \dot{\omega}_{p1} \omega_{p3}$$

$$\dot{\omega}_{p3} = \frac{I_{p1} - I_{p2}}{I_{p3}} \omega_{p2} \omega_{p1}$$

Then,  $[\zeta_p]$  is seen to be

$$[\zeta_p] = \begin{bmatrix} 0 & \frac{I_{p2} - I_{p3}}{I_{p1}} \omega_{p3} & \frac{I_{p2} - I_{p3}}{I_{p1}} \omega_{p2} \\ \frac{I_{p3} - I_{p1}}{I_{p2}} \omega_{p3} & 0 & \frac{I_{p3} - I_{p1}}{I_{p2}} \dot{\omega}_{p1} \\ \frac{I_{p1} - I_{p2}}{I_{p3}} \omega_{p2} & \frac{I_{p1} - I_{p2}}{I_{p3}} \omega_{p1} & 0 \end{bmatrix} \quad (G-12)$$

$[\lambda]$  is given by

$$[\lambda] = \begin{bmatrix} \frac{I_{p3} - I_{p2}}{I_{p1}^2} \omega_{p2} \omega_{p3} & \frac{1}{I_{p1}} \omega_{p2} \omega_{p3} & -\frac{1}{I_{p1}} \omega_{p2} \omega_{p3} \\ -\frac{1}{I_{p2}} \dot{\omega}_{p1} \omega_{p3} & \frac{I_{p1} - I_{p3}}{I_{p2}^2} \omega_{p1} \omega_{p3} & \frac{1}{I_{p2}} \omega_{p1} \omega_{p3} \\ \frac{1}{I_{p3}} \omega_{p1} \omega_{p2} & -\frac{1}{I_{p3}} \omega_{p1} \omega_{p2} & \frac{I_{p2} - I_{p1}}{I_{p3}^2} \omega_{p1} \omega_{p2} \end{bmatrix} \quad (G-13)$$

## LOGICON

Since the matrix  $[A]$  is singular, there is some linear combination of the moment of inertia states that is nonobservable. To improve the filter stability, it is desirable to choose a different basis in which one of the states is explicitly nonobservable. While there are many possible choices for such a basis, the one that was chosen is the following:

$$\delta I_{m1} = \frac{\delta \left( \frac{I_{p1}}{I_{p2}} \right)}{\frac{I_{p1}}{I_{p2}}}$$

$$\delta I_{m2} = \frac{\delta \left( \frac{I_{p2}}{I_{p3}} \right)}{\frac{I_{p2}}{I_{p3}}}$$

$$\delta I_{m3} = \frac{\delta I_{p2}}{I_{p2}}$$

where the subscript  $m$  indicates that the state vector has been modified. The new sensitivity  $[\lambda_m]$  becomes

$$[\lambda_m] = \begin{bmatrix} \frac{I_{p3} - I_{p2}}{I_{p1}} \omega_{p2} \omega_{p3} & \frac{I_{p3}}{I_{p1}} \omega_{p2} \omega_{p3} & 0 \\ -\frac{I_{p1}}{I_{p2}} \omega_{p1} \omega_{p3} & -\frac{I_{p1}}{I_{p2}} \omega_{p1} \omega_{p3} & 0 \\ \frac{I_{p1}}{I_{p3}} \omega_{p1} \omega_{p2} & \frac{I_{p1} - I_{p2}}{I_{p3}} \omega_{p1} \omega_{p2} & 0 \end{bmatrix} \quad (G-14)$$

## LOGICON

---

It is apparent from equation (G-14) that  $\delta I_{m3}$  is nonobservable. This is not surprising since a change in the value of  $\delta I_{m3}$  ( $\delta I_{m1}$  and  $\delta I_{m2}$  remaining constant) corresponds to the same proportional change in each of  $\delta I_{p1}$ ,  $\delta I_{p2}$ , and  $\delta I_{p3}$ . Since Euler's equation does not depend on the total magnitude of the moment of inertia but only on the relative sizes of the individual components, the state  $\delta I_{m3}$  does not affect body dynamics and is thus nonobservable.

## LOGICON

---

### G-3. Computer Organization

A flow diagram indicating the computer programs used in free-flight filtering is shown Figure G-2. The free-flight simulation program FFSIM uses quaternions to calculate the body attitude as a function of time. To calculate the vehicle position and velocity, FFSIM employs a spherical harmonic expansion of the earth's gravitational field. The body dynamics program BODYN uses the error equations of Section G-2 to calculate the body dynamics measurement matrices as a function of time, while the linear error analysis program LEAP uses the DINS error model of Section 3.2.3.1 to calculate the DINS transition and measurement matrices as a function of time. The system error analysis program SEAP incorporates the LEAP and BODYN outputs into a Kalman filter to obtain several measures of the system performance, including inflight alignment performance and inflight calibration performance of the DINS and body dynamics error sources.

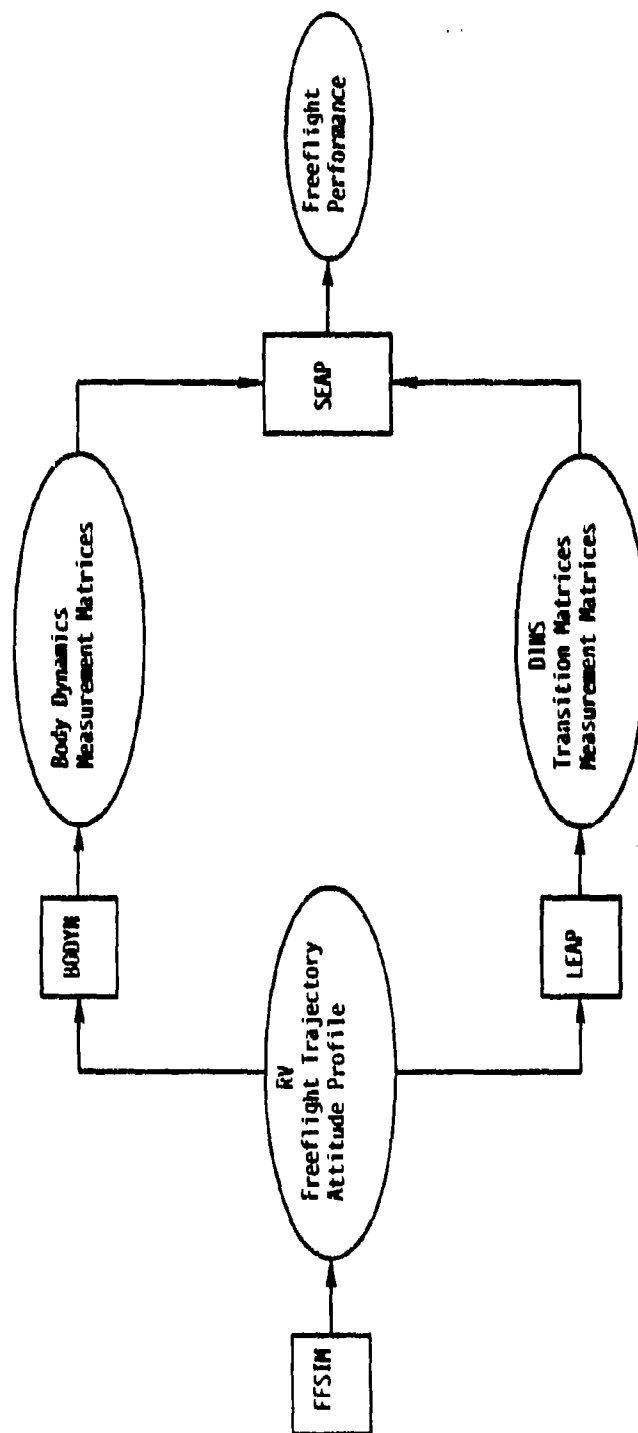


Figure G-2. Freeflight Filtering Computer Program Organization